UNIVERSITÀ DEGLI STUDI
DI GENOVA

DEPARTMENT OF EXPERIMENTAL MEDICINE (DIMES)

PhD Course in

EXPERIMENTAL MEDICINE curriculum BIOCHEMISTRY

XXX cycle

MiRNA-mediated KHSRP silencing rewires distinct post-transcriptional programs during TGFβ-induced Epithelial-to-Mesenchymal Transition

Scientific Sector **Bio/10**

PhD Candidate
Margherita PUPPO

Tutor
Roberto GHERZI, M.D.
Prof. Michela TONETTI

PhD Course Coordinator
Prof. Franca SALAMINO

A.A. 2017/2018

Index

Summary

Epithelial-to-Mesenchymal Transition (EMT) is a reversible trans-differentiation process that confers to cancer cells several traits required for malignant progression and metastatization.

In this thesis I report that the silencing of the RNA-binding protein KHSRP, mediated by the microRNA miR-27b-3p, is required for Transforming Growth Factor β (TGF-β)-induced EMT in mammary gland cells. We found that sustained KHSRP expression limits TGF-β-dependent induction of EMT factors and cell migration, whereas its knockdown in untreated cells mimics TGF-β-induced EMT. Genome-wide sequencing analyses revealed that KHSRP affects the expression of select genes at two distinct post-transcriptional levels by controlling:

1. the levels of mature miR-192-5p (a microRNA that targets a group of EMT factors);
2. the alternative splicing of a cohort of microRNA precursors related to cell adhesion and motility including CD44, ENAH and FGFR2.

KHSRP belongs to a ribonucleoprotein complex that includes hnRNPA1, and the two proteins cooperate in promoting epithelial-type exon usage of select pre-mRNAs. The importance of the KHSRP/hnRNPA1 complex in regulating the alternative splicing of factors critical to cell adhesion and migration is highlighted by the fact that Resveratrol (RESV), a natural polyphenolic compound, increases the expression of both KHSRP and hnRNPA1. We also show that, as a consequence of KHSRP and hnRNPA1 increased expression, RESV counteracts the TGF-β-induced EMT phenotype in mammary gland cells and affects the alternative exon usage of pre-mRNAs that encode crucial factors in adhesion and migration (including CD44, ENAH, and FGFR2) in a panel of immortalized and transformed mammary gland cells. RESV causes a shift from the mesenchymal-specific forms of these factors to the respective epithelial forms and the combined silencing of KHSRP and hnRNPA1 prevents the RESV-dependent inclusion of the epithelial-type exons in the *Cd44* pre-mRNA.

In conclusion, our findings support the evidence that KHSRP plays a central role in the complex process that leads to the changes induced by TGF-β in mammary gland cells.

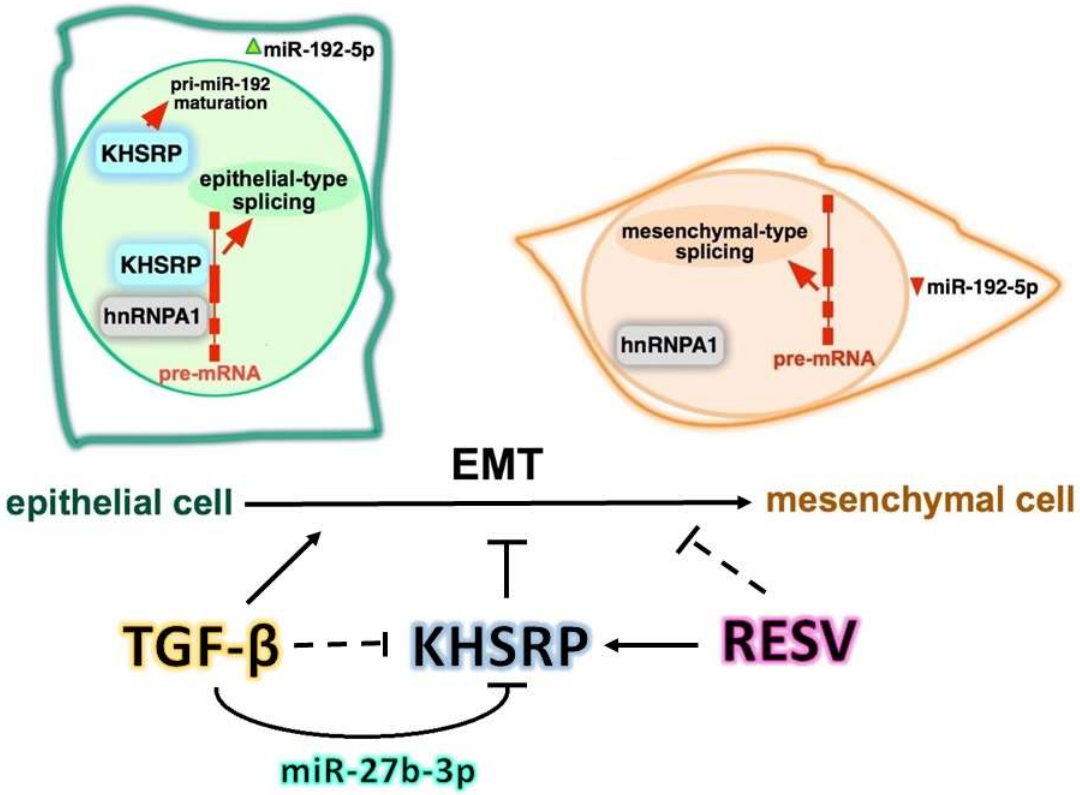

Image modified from: **Puppo et al., 2016**

Abbreviation List

Abbrevation	Definition
3' UTR	3' Untranslated Region
ACTA2	Actin
AKT	RAC-serine/threonine-protein kinase
ARE	AU-rich element
ARE-BP	ARE-binding protein
AS	Alternative Splicing
ATM	ATM serine-protein kinase
BMP	Bone Morphogenetic Protein
BRF1	Butyrate Response Factor 1
CDH1	Cadherin 1
CDH2	Cadherin 2
Cdk1	Cyclin-dependent kinase 1
CPM	Count Per Million
CSC	Cancer Stem Cell
DEXSeq	Differential Exon usage
Dis3	Ribonuclease chromosome Disjunction 3
DSP	Desmoplakin
ECM	Extracellular matrix
EGF	Epidermal Growth Factor
ELAVL1	ELAV-like protein 1
EMT	Epithelial-to-Mesenchymal Transition
ERK	Extracellular signal-regulated kinase
ESRP1	Epithelial Splicing Regulatory proteins 1
ESRP2	Epithelial Splicing Regulatory proteins 2
FGFR	FGF-Receptor
FN1	Fibronectin
FSTL1	Follistatin-like 1
GAP43	Growth Associated Protein 43
Gly	Glycine
GO	Gene ontology
GSK-3β	Glycogen Synthase Kinase-3 β
hnRNP	Heterogeneous nuclear Ribonucleoprotein Particle
JNK	c-Jun N-terminal kinase
KH domain	Heterogeneous nuclear ribonucleoprotein K homology domain
KHSRP	KH-type Splicing Regulatory Protein
LIN28	Protein lin-28 homolog A
lncRNA	Long non-coding RNA
MAPK14	p38 mitogen-activated protein kinase

MET	Mesenchymal-to-Epithelial Transition
miRNA	MicroRNA
MMP	Matrix Metalloproteinase
Myog	Myogenin
NF-κB	Nuclear Factor-κB
NMP	Nucleophosmin
NOS2	Nitric Oxide Synthase 2
OCLN	Occludin
ORF	Open reading frame
PARN	poly(A)-Rnase
PDGF	Platelet Derived Growth Factor
Per2	Period Circadian Clock 2
PI3K	Phosphatidyl Inositol 3-Kinase
PRC2	Polycomb repressor complex 2
pre-miRNA	Precursor microRNA
pri-miRNA	Primary microRNA
RESV	Resveratrol
RIP	Ribonucleoprotein Immunoprecipitation
RISC	RNA-Induced Silencing Complex
RNA Pol II	RNA polymerase II
RNA-seq	RNA sequencing
RPB	RNA-binding protein
RT-qPCR	Retro Transcription- quantitative Polymerase Chain Reaction
Ser	Serine
SIRT1	Sirtuin-1
TGF-β	Transforming Growth Factor β
Thr	Threonine
TL	Terminal loop
TNF	Tumor Necrosis Factor
TRIM33	Tripartite Motif Containing 33
TTP	Tristetraprolin
UTRN	Utrophin
VIM	Vimentin
VTN	Vitronectin

Introduction

EPITHELIAL-TO-MESENCHYMAL TRANSITION

Epithelial-to-Mesenchymal Transition (EMT) is a reversible trans-differentiation program that plays a central role in both physiological and pathological processes, such as embryogenesis, development, wound healing, fibrosis, and tumor progression (Thiery, 2003; Kalluri & Weinberg, 2009; Lim & Thiery, 2012; Jolly et al, 2017). During EMT process, a polarized epithelial cell undergoes multiple biochemical changes and acquires a mesenchymal phenotype which includes enhanced migratory capacity, invasiveness, elevated resistance to apoptosis, increased production of extracellular matrix (ECM) components as well as the potential to enter a stem cell-like state (Kalluri & Neilson, 2003; De Craene & Berx, 2013; Ye & Weinberg, 2015).

The concept of EMT emerged many years ago from initial observations that both embryonic and adult epithelial cells have the potential to convert to fibroblast-like cells with migratory and invasive properties in 3D collagen gels (Greenburg & Hay, 1982).

EMT has been classified into three different subtypes (*Figure 1*) based on the biological contexts in which it occurs (Kalluri & Weinberg, 2009):

- *Type I:* associated with implantation, embryo formation, and organ development;
- *Type II*: associated with wound healing, tissue regeneration, organ fibrosis, and the presence of inflammation;
- *Type III*: associated with cancer progression in which neoplastic cells invade other tissues and metastasize.

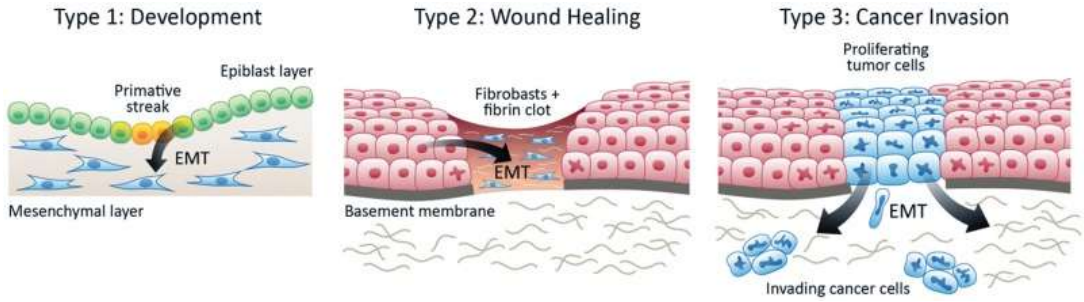

Figure 1; Different types of EMT processes (Scanlon et al, 2013).

EMT is reversible and the opposite trans-differentiation process is called Mesenchymal-to-Epithelial Transition (MET) (De Craene & Berx, 2013; Ye & Weinberg, 2015). In tumor progression, cancer cells undergo EMT to escape from the primary tumor, invade adjacent tissues, intravasate in blood or lymphatic vessels, travel through the circulation system, extravasate, and finally colonize distant organs to form metastasis (Tam & Weinberg, 2013). In the last step, cells that had acquired mesenchymal features can revert to the epithelial state through MET (Tam & Weinberg, 2013) (*Figure 2*).

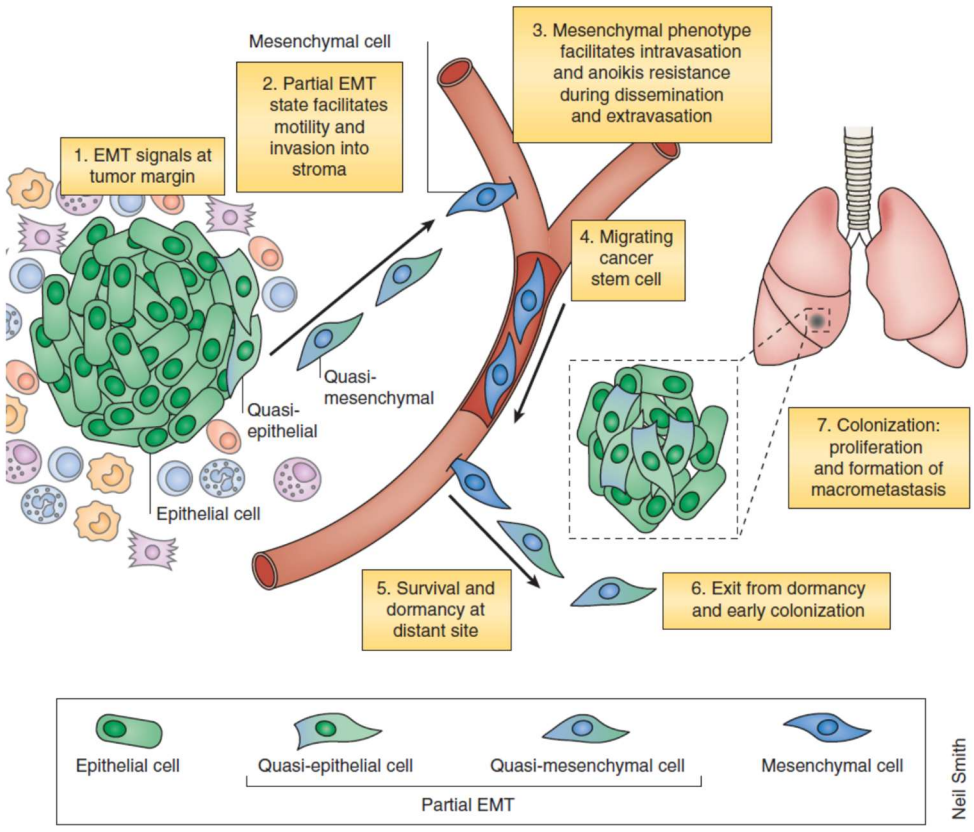

Figure 2; EMT and MET processes during metastasis formation (Tam & Weinberg, 2013).

The contribution of EMT to cancer cell invasion and metastasis has been well documented in many types of carcinoma, and clinical evidence support the idea that high-grade tumors associated to poor prognosis often contain cells that express molecular signatures of EMT (Tam & Weinberg, 2013). However, some tumors contain neoplastic cells that, even if have acquired mesenchymal markers, retained certain epithelial characteristics showing a 'partial EMT' (Sarrió et al, 2008; Grigore et al, 2016). Sometimes cells enter an intermediate state where mesenchymal and epithelial features coexist, and in some cases (e.g. the absence of pro-EMT signals) they may naturally revert to an epithelial state (Tam & Weinberg, 2013). The idea that 'partial EMT' refers to an intermediate state between EMT and MET has been recently changed with the concept of a stable hybrid Epithelial/Mesenchymal phenotype (Jolly et al, 2015). Moreover, the connection between carcinoma cells that have undergone EMT and the acquisition of stem-like properties have been described extensively in multiple tumor types, and cells that have only undergone a 'partial EMT' have more chances to acquire stem-like properties, while several studies have reported that in certain tumors the mesenchymal cells, after completing the EMT program, lack the ability to behave as stem cells (Prieto-Garcìa et al, 2017; Grosse-Wilde et al, 2015; Jolly et al, 2015; Andriani et al, 2016).

Although EMT is commonly believed to contribute to metastasis, two recent studies challenged this idea suggesting that EMT is instead a prerequisite for acquisition of chemoresistance (Fischer et al, 2015; Zheng et al, 2015). Fischer and colleagues engineered cancer cell in order to track reversible EMT *in vivo* and showed that EMT is not required for metastasis, whereas it confers chemoresistance to cancer cells (Fischer et al, 2015). In addition, Zheng and colleagues demonstrated that suppression of EMT leads to enhanced expression of nucleoside transporters in tumors, contributing to enhanced sensitivity to gemcitabine treatment and increased overall survival of mice (Zheng et al, 2015). Nonetheless, the two alternative views can be reconciled and it is possible to propose that pro-metastatic properties of EMT may originate from its ability to induce chemoresistance enabling cells to survive therapeutics and cause metastasis (Qi et al, 2016). The above described debates highlight the concept that EMT is not a stereotypical program and various versions of this process are expressed under different conditions in a variety of carcinomas (Pattabiraman & Weinberg, 2016).

The conversion from an epithelial to a mesenchymal cell requires changes in cell morphology and cell/matrix adhesion as well as the acquisition of migratory abilities (Prieto-Garcìa et al, 2017). Phenotypical hallmarks of EMT include morphological changes from a cobblestone-like epithelial shape to a spindle-like fibroblast phenotype, loss of epithelial Cadherin 1 (CDH1; also known as E-Cadherin) expression at cell junctions, decreased expression of the desmosome protein Desmoplakin (DSP) as well as the tight junction protein Occludin (OCLN), with increased expression of mesenchymal Cadherin 2 (CDH2; also known as N-Cadherin), Vimentin (VIM) and Matrix Metalloproteinases (MMPs) (Kalluri & Neilson, 2003; Kalluri & Weinberg, 2009; Lee et al, 2006; Nieto et al, 2016). A group of EMT-inducing transcription factors, including SNAI1, SNAI2, ZEB1, ZEB2, TWIST1, and TWIST2, are activated during EMT and co-operate in orchestrating the molecular changes (Kalluri & Weinberg, 2009; Nieto et al, 2016). Some of the transcripts whose expression is modified during EMT are listed in *Figure 3*.

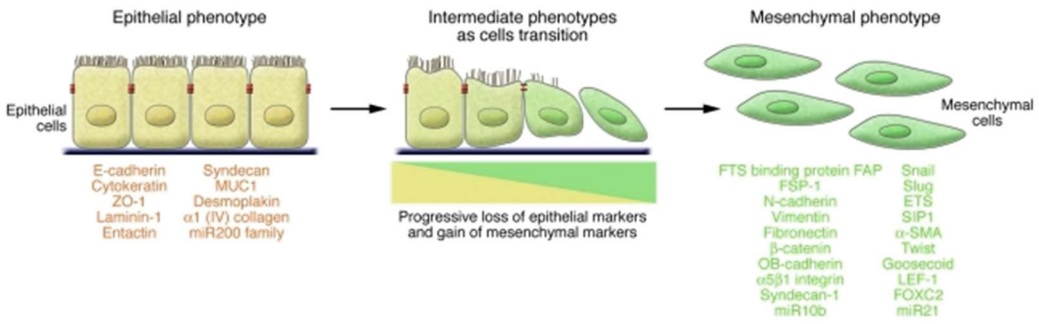

Figure 3; Factors involved in EMT (Kalluri & Weinberg, 2009).

The expression of CDH1 at the cell surface contributes to maintain intact cell/cell interactions and stabilizes the cytoskeleton preventing cell mobility, whereas its downregulation causes adherents junctions breakdown leading to a mesenchymal phenotype with migratory abilities (Tam & Weinberg, 2013; Prieto-Garcìa et al, 2017). CDH1 down-regulation and inactivation of the *Cdh1* gene have been described during tumor cell progression (Acs et al, 2001; Guilford et al, 1998; Pharoah et al, 2001). It has been reported that *Cdh1* transcription is repressed by transcription factors such as SNAI1, SNAI2, ZEB1, ZEB2, TWIST1 and TWIST2, Homeobox proteins (GSC and SIX1), bHLH factor E2.2 (TCF4), and Forkhead-Box protein (FOXC2) (Bolos et al, 2003; Canel

et al, 2013; Serrano-Gomez et al, 2016). Additional genes encoding tight junction proteins (e.g. Claudins and OCLNs) are subject to transcriptional repression, thus allowing tumor invasiveness (Ikenouchi et al, 2003; Martinez-Estrada et al, 2006).

SNAI1/2 proteins have a central role in EMT determining overexpression of mesenchymal markers such as Fibronectin (FN1) and Vitronectin (VTN), and suppression of various epithelial markers (Zeisberg & Neilson, 2009). SNAI1 is also known to upregulate the expression of several *MMP* genes including MMP9 which degrades the basement membrane stimulating tumor cell invasion (Kessenbrock et al, 2010). In addition, SNAI1 blocks cell-cycle progression, contributes to cell survival, and regulates the expression of genes related to the apoptosis pathway (Scanlon et al, 2013). Further, SNAI1 and SNAI2 are involved in the acquisition of stem-like traits (Zeisberg & Neilson, 2009; Kurrey et al, 2009). As a critical regulator of multiple signaling pathways leading to EMT, the expression of SNAI1 is closely associated with cancer metastasis (Wang et al, 2013).

TWIST1/2 proteins modulate the expression of many target genes through E-box-responsive elements (Scanlon et al, 2013). The two TWIST genes, *Twist1* and *Twist 2*, are well-conserved in Vertebrates, and TWIST1/2 proteins can act as either transcriptional repressors of epithelial markers, such as CDH1, or activators of mesenchymal markers, such as CDH2 and FN1 (Scanlon et al, 2013). Like SNAI1, TWIST1/2 proteins are upregulated in many cancer (Zeisberg & Neilson, 2009).

Also epigenetic regulation and post-translational modification can regulate EMT process (Prieto-Garcìa et al, 2017; Serrano-Gomez et al, 2016; Nieto et al, 2016). It has been demonstrated that EMT program is activated by epigenetic regulation (e.g. modification of histone tails, global hypomethylation of genome, and specific hypermethylation of cytosine residues in CpG islands in the DNA promoter regions) that either promotes or represses the expression of EMT-related genes (Prieto-Garcìa et al, 2017; Kouzarides, 2007). Post-translational modifications involved in EMT program include acetylation, methylation, phosphorylation, ubiquitination, sumoylation, proline isomerization, and deamination (Serrano-Gomez et al, 2016). For example, SNAI1 expression is controlled by Glycogen Synthase Kinase-3 β (GSK-3β) phosphorylation that regulates its ubiquitination and its subcellular localization: the inhibition of GSK-3β causes SNAI1 upregulation and can induce the EMT program (Zhou et al, 2004).

Various signals that cells receive from their microenvironment can initiate the EMT process (Teng et al, 2007; Kalluri & Weinberg, 2009; Polyak & Weinberg, 2009; Nisticò et al, 2012; Nieto et al, 2016). In the context of the natural history of carcinoma cells important extracellular signals like WNT, NOTCH, and Transforming Growth Factor β (TGF-β) modulate EMT (Tam & Weinberg, 2013).

TGF-β is considered to act as a primary inducer of EMT via activation of the SMAD family of transcription factors (Moustakas & Heldin, 2012; Ikushima & Miyazono, 2010; Katsuno et al, 2013). TGF-β belongs to a large family of structurally related factors, including Activins and Bone Morphogenetic Proteins (BMPs), which regulate cell growth, survival, differentiation, and migration (Shi & Massagué, 2003). TGF-β is structurally characterized by a specific three-dimensional fold and by a conserved number and spacing of cysteine residues in the C-terminus of the mature polypeptide (Derynck & Miyazono, 2008). All TGF-β ligands bind to *Type I* (seven in humans) and *Type II* (five in humans) Receptors (TGF-βRI and TGF-βRII, respectively) to generate heterotetrameric complexes in the presence of the dimeric ligand that transmit biological information into the cells (Wrana et al, 2008). Both types of receptors are characterized by a dual specificity cytoplasmic kinase domain: a strong serine/threonine (Ser/Thr) kinase activity and a weaker tyrosine (Tyr) kinase activity (Dijke & Heldin, 2006). Phosphorylation of TGF-βRI by the Ser/Thr kinase activity of TGF-βRII creates a docking site in the Gly/Ser (GS)–rich domain of TGF-βRI that recruits, and consequently phosphorylates, the transcription factors SMAD2 and SMAD3 (Gonzalez & Medici, 2014). Phosphorylated SMADs form a complex with the common SMAD4 which then translocate into the nucleus to regulate gene expression by modulating gene transcription as well as promoting maturation of select microRNAs (miRNAs) from precursors (Tam & Weinberg, 2014; Blahna & Hata, 2012) (*Figure 4*). In addition to SMAD-dependent signaling, TGF-β receptor complexes are involved in a number of SMAD-independent pathways (Gonzalez & Medici, 2014). TGF-β can directly activate the Phosphatidyl Inositol 3-Kinase (PI3K) machinery through its own receptors or can trans-activate Epidermal Growth Factor (EGF) and Platelet Derived Growth Factor (PDGF) receptors (Gonzalez & Medici, 2014). Moreover, TGF-β is a potent activator of various other kinase pathways including extracellular signal-regulated kinase (ERK), c-Jun N-terminal kinase (JNK), and p38 mitogen-activated protein kinase (MAPK14), whose activation can be SMAD-dependent or SMAD-independent (Gonzalez & Medici, 2014).

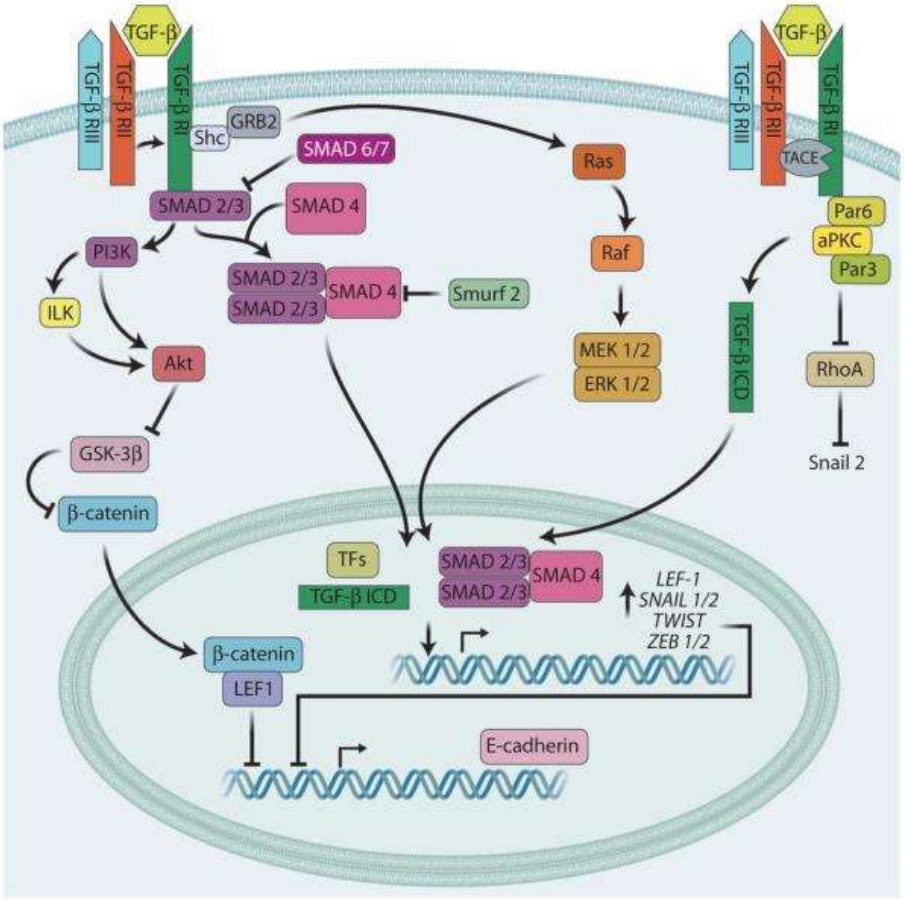

Figure 4; The complex network of TGF-β signaling in EMT (Gonzalez & Medici, 2014).

Whereas in normal epithelial cells TGF-β suppresses cell proliferation, in the advanced stages of cancer TGF-β signaling is commonly hyper-activated and promotes invasion and metastasis (Kim et al, 2007; Saitoh, 2015). TGF-β can promote tumor progression by modifying tumor microenvironment since it regulates cell viability and function of immune cells, endothelial cells, and fibroblasts, as well as facilitates proliferation and motile properties of tumor cells (Bierie & Moses, 2006). Further, TGF-β can cooperate with other growth factors in the cancer microenvironment (Tam & Weinberg, 2014; Ehata et al, 2007). Hence, TGF-β signaling inhibition has the potential to block EMT induction and, therefore, disease progression (Tam & Weinberg, 2014).

TGF-β signaling can control also the epigenetic regulation of downstream target genes (Tam & Weinberg, 2014). SMAD2 and SMAD3 can associate with epigenetic regulators, such as Tripartite Motif Containing 33 (TRIM33), and cell exposure to TGF-β increases the amount of the H3K4me3 and H3K36me3 chromatin marks (Xi et al, 2011;

McDonald et al, 2011). Experimental evidences suggest that TGF-β signaling can indirectly affect the alternative splicing of a number of mRNAs by regulating the expression of splicing factors (Tripathi et al, 2016; Horiguchi et al, 2012; Saitoh, 2015). For example, it has been demonstrated that TGF-β downregulates the expression of the Epithelial Splicing Regulatory proteins 1 (ESRP1) and 2 (ESRP2) that bind directly the *FGF-Receptor* (FGFR) mRNA and subsequently switches the epithelial *IIIb* isoforms of *FGFRs* to mesenchymal *IIIc* isoforms (Horiguchi et al, 2012). Importantly, aggressive breast cancer cells express only *IIIc* isoforms of *FGFR*, whereas non-aggressive cells express *IIIb* isoforms (Horiguchi et al, 2012).

In the laboratory where I conducted my thesis, it has been demonstrated that the single-strand RNA binding protein KHSRP is a component of the TGF-β/BMP signaling pathway in multipotent mesenchymal C2C12 cells (Pasero et al, 2012). TGF-β/BMP-activated SMAD proteins associate with KHSRP and block its ability to promote maturation of myogenic miRNAs from precursors, thus orienting C2C12 cells toward osteoblastic differentiation (Pasero et al, 2012). Accordingly, KHSRP silencing in C2C12 cells produces effects that largely coincide with those induced by TGF-β/BMP signaling activation (Pasero et al, 2012). Further, it has been recently reported that TGF-β regulates wound healing by controlling KHSRP levels and determining a switch between miR-198 and Follistatin-like 1 (FSTL1) protein expression (Sundaram et al, 2013). The human exonic miR-198 belongs to the protein-coding *Fstl1* gene and it is expressed in normal epidermis, while upon injury, its levels early plummet and remain low for at least 24 hours after wounding (Tan et al, 2011; Sundaram et al, 2013). In contrast to miR-198, *Fstl1* mRNA and FSTL1 protein are expressed in the wound-edge epidermis 24 hours after injury, but not in normal epidermis (Sundaram et al, 2013). It has been shown that KHSRP has an essential role in miR-198/FSTL1 expression-switch since the processing of miR-198 is dependent on its *trans*-action (Sundaram et al, 2013). Sundaram and colleagues have demonstrated that KHSRP is physiologically expressed in normal epidermis but, upon injury, TGF-β1 downregulates its expression with the consequent switch-off of miR-198 expression and the promotion of FSTL1 expression (Sundaram et al, 2013).

I will describe in detail the structure and the functions of KHSRP in the following section.

KHSRP, A MULTIFUNCIONAL PROTEIN

KHSRP (KH-type Splicing Regulatory Protein, also known as KSRP or FBP2) is a single-stranded nucleic acid-binding protein independently discovered by the Levens and Black laboratories (Briata et al, 2016). KHSRP is ubiquitous and its nucleo/cytoplasmic distribution varies in distinct cell types (Gherzi et al, 2014).

KHSRP was initially described as a factor interacting with an enhancer element upstream of the *c-myc* oncogene promoter, as a component of a multi-protein complex that binds to a splicing enhancer element of *c-src* pre-mRNA, and as part of the Apolipoprotein-B editing complex (Davis-Smyth et al, 1996; Min et al, 1997; Lellek et al, 2000). Upon these initial discoveries, additional roles of KHSRP in the post-transcriptional control of gene expression have been investigated in greater detail, specifically two distinct functions (Gherzi et al, 2014):

1. the ability to favor degradation of labile mRNAs via AU-rich element (ARE)-mediated decay;
2. the ability to promote maturation from precursors of select miRNAs.

In general, KHSRP is considered a regulator of gene expression that can modulates diverse cellular functions including cell differentiation/proliferation, innate immunity, and lipid metabolism (Briata et al, 2016).

1. KHSRP STRUCTURE

The *Khsrp* gene maps to human chromosome 19p13.3 and to mouse chromosome 17 (Ring et al., 1999). The human KHSRP protein has a length of 711 amino acids and a mass weigh of 73115 Dalton (data from UNIProtDataBase, 2017). KHSRP protein is organized in three distinct regions: a mainly structured central region that includes four KH domains (KH1 to 4) responsible for nucleic acid binding, and two low

complexity terminal regions that contain several sites for post-translational modifications as well as protein-interaction motifs (Gherzi et al., 2010) (*Figure 5*).

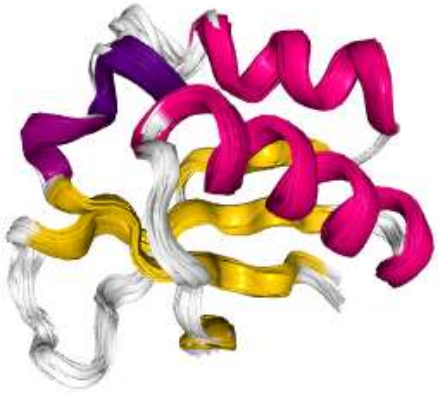

Figure 5; Solution structure of KH4 domain of KHSRP (from http://www.rcsb.org/pdb/protein/Q92945).

The heterogeneous nuclear ribonucleoprotein K (hnRNPK) homology (KH) domain, first identified in the hnRNPK protein, consists of approximately 70 amino acids and it has been recognized as a nucleic acid recognition motifs able to bind RNA or single-strand DNA with varying degrees of affinity and specificity (Valverde et al., 2008). KH domains are found in multiple copies which can function independently or cooperatively (Valverde et al., 2008). They are present in proteins with various cellular functions including transcriptional and translational regulation (Chen & Varani, 2013). Interestingly, several diseases (e.g. Fragile X Mental Retardation Syndrome, Paraneoplastic Disease and some cancers) are associated with the loss of function of the KH domain (Valverde et al., 2008). Analysis of available spatial structures revealed that two different KH domains, *Type I* and *Type II*, exist (Valverde et al., 2008). They belong to different protein folds, but share a single KH motif (βααβ): in addition to the motif core, *Type I* KH domains (e.g. hnRNPK) contain C-terminal extension βα and *Type II* KH-domains (e.g. ribosomal protein S3) include N-terminal extension αβ (Grishin, 2001) (*Figure 6*). The *Type I* fold is typically found in eukaryotic proteins, whereas the *Type II* fold is typically found in prokaryotic proteins (Grishin, 2001). The highly conserved 'GXXG loop' of the KH domain directly interacts with the nucleobases of either DNA or RNA targets to make

specific contacts with protein moieties (Lewis et al., 2000). The KH domain can recognize specifically up to four nucleobases: of these, the nucleobases in positions 2 and 3 are normally recognized with a higher degree of specificity by moieties from the protein side chains (for position 2) and backbone (for position 3) (Hollingworth et al., 2012). Along with the interaction with the KH domain canonical recognition surface, the nucleic acid molecule can make non-specific contacts with protein groups outside the groove (Braddock et al., 2002).

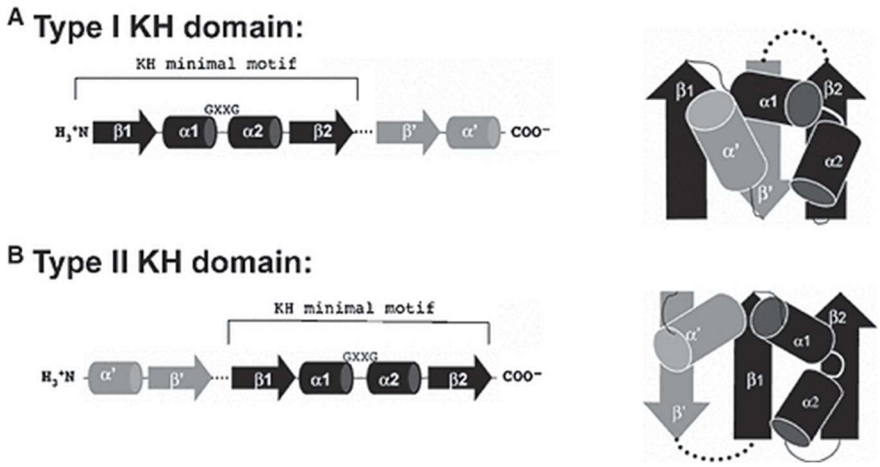

Figure 6; Structure of *Type I* and *Type II* KH domains (Valverde et al., 2008).

The solution structure of the four KH domains of KHSRP has been solved and it was shown that the KH1 and KH4 can re-orient freely in solution respect to a central core formed by KH2 and KH3 thus allowing the protein to adapt to the structural context of different protein-RNA regulatory particles (García-Mayoral et al., 2008; Dìaz-Moreno et al., 2010). The RNA-binding specificity of each KH-domains of KHSRP has been established by Scaffold Independent Analysis (SIA), and the different specificities of the domains of KHSRP as well as their affinity for the AREs ('UAUUUA' and 'UAUUAU') have been extensively explored (García-Mayoral et al., 2008). More recently, it has been found that individual KH domains of KHSRP have different sequence specificities (Briata et al., 2013). While KH1, KH2 and KH4 bind to a broad range of sequences within a small range of affinities, KH3 interacts with a set of G-rich sequences, with an unusual affinity that is 100-fold higher than the affinity for AU-rich targets (García-Mayoral et al., 2008). Importantly, the *in vitro* interaction of KHSRP with the RNA target is combinatorial, with each KH domain providing a fraction of the RNA binding affinity

(Hollingworth et al., 2012). Indeed, the *Kd* of isolated domains in complex with short AREs (derived from the target TNF-AREs) ranges between 10^{-4} and 10^{-3} M, while the *Kd* of the whole protein for the full TNF-AREs is 5 orders of magnitude lower (~$4x10^{-9}$ M) (Hollingworth et al., 2012). KHSRP is also able to interact with high affinity with the terminal loop (TL) of both primary and precursor of miR-let-7a as well as of other miRNA precursors (Trabucchi et al, 2009). Structural and biophysical analyses revealed that the contribution of KH3 to KHSRP/miR-let-7a precursor interaction is 50 fold higher than the one provided by KH2 and KH4 (Nicastro et al., 2012). Further, NMR analysis of the interaction confirms that KH3 defines the binding frame of KHSRP on the miRNA precursors TL (Díaz-Moreno et al., 2009).

Proteins, including RNA-binding proteins (RBPs), are often subject to post-translational modifications like phosphorylation, which is a mechanism used by cells to link extracellular signals to different gene regulation pathways (Brivanlou & Darnell, 2002; Wilson et al., 2003; Gherzi et al., 2014). Two different signaling pathways, MAPK14 and the RAC-serine/threonine-protein kinase (AKT; also known as PKB) have been shown to target decay-promoting ARE-BPs including Tristetraprolin (TTP), Butyrate Response Factor 1 (BRF1), and KHSRP (Sandler & Stoecklin, 2008; Schmidlin et al., 2004; Ruggiero et al., 2007). KHSRP function is regulated by a number of post-translational modifications including phosphorylation by AKT on *Ser 193*, by ATM serine-protein kinase (ATM) on *Ser 132*, *Ser 274* and *Ser 670*, and by MAPK14 on *Thr 692* (Gherzi et al., 2006; Briata et al., 2005; Zhang et al., 2011) (*Figure 10*).

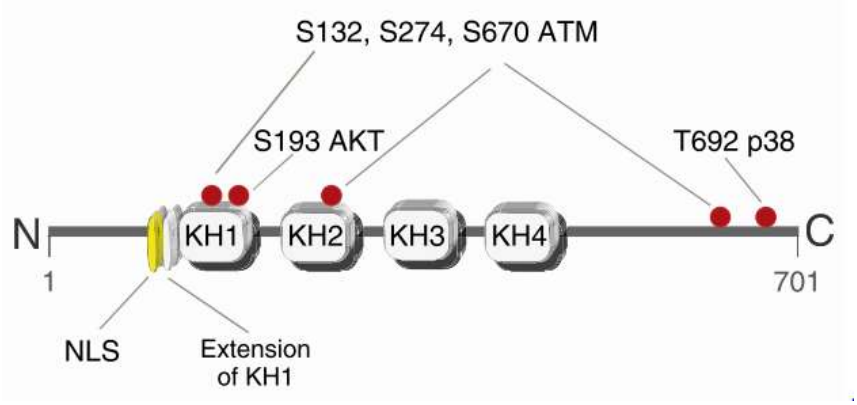

Figure 10; Schematic representation of phosphorylation sites on KHSRP (Briata et al., 2005).

A consequence of AKT-phosphorylation on the unique serine residue is the association of KHSRP with the multifunctional protein 14-3-3 (Gherzi et al., 2010). This association prevents the interaction of KHSRP with the exoribonucleolytic complex RNA exosome and impairs its ability to promote rapid mRNA decay (Gherzi et al., 2010). Instead, the KHSRP phosphorylation operated by MAPK14 compromises KHSRP binding to ARE-containing transcripts and KHSRP fails to promote their rapid decay, although the ability to interact with the mRNA degradation machinery is retained (Briata et al., 2005). Further, direct binding and phosphorylation of ATM on serine residues enhance KHSRP interaction with primary miRNAs and its miRNA-processing activity (Zhang et al., 2011).

2. KHSRP FUNCTIONS

The molecular functions of KHSRP in mRNA decay, alternative splicing, and miRNA biogenesis have been extensively investigated.

2.1 Implication of KHSRP in mRNA decay

In eukaryotes, productive expression of a gene involves multiple steps including gene transcription into mRNA in the nucleus, mRNA export into the cytoplasm upon 5' capping and polyadenylation, mRNA translation and, finally, mRNA degradation in specific cytoplasmic location (Das et al., 2017; Bicknell & Ricci, 2017). Degradation of mRNAs is a highly regulated process and mRNA stability, whose variability from one mRNA species to another is well known, plays a central role to define levels of gene expression (Houseley & Tollervey, 2009). Modulation of mRNA stability has been largely investigated and important advances in the characterization of the *cis*-acting RNA elements and the *trans*-acting cellular proteins that control mRNA decay have been made (Schoenberg & Maquat, 2012).

AREs are landmark of *cis*-acting motifs responsible for rapid mRNA decay in mammalian cells and they can be found in the 3' Untranslated Regions (3' UTRs) of many short-lived transcripts encoding cytokines, cell-cycle regulators, cell type-specific transcription factors, and proto-oncogenes (Briata et al., 2012). AREs can differ in both length and AU content, and it does not exist a real consensus motif (Chen et al.,1994).

However, an intensive genome-wide bioinformatics approach was used to classify ARE-containing transcripts into 5 clusters based on the number of overlapping AUUUA pentamers (Vlasova-St. Louis & Bohjanen, 2017). Numerous proteins have been described to bind to AREs, and called ARE-binding proteins (ARE-BPs) (Vlasova-St. Louis & Bohjanen, 2017). ARE-PBs compete with each other for ARE-binding and they have different functions: some of them, such as TTP and KHSRP, mediate transcript degradation, while others, such as ELAV-like protein 1 (ELAVL1; also known as HuR), mediate transcript stabilization, possibly by preventing binding by ARE-BPs that promote decay (Vlasova-St. Louis & Bohjanen, 2017). In addition, in the case of some ARE-BPs such as the heterogeneous nuclear Ribonucleoprotein D (hnRND; also known as AUF1), the mRNA destabilizing or stabilizing function is dependent on the cellular context and/or the expressed protein isoforms (Garneau et al., 2007).

Most eukaryotic mRNA decay events are initiated by deadenylation and/or decapping, followed by 5'-exonucleolytic degradation operated by Xrn1 (Bicknell & Ricci, 2017). Several eukaryotic deadenylases (including PAN2-PAN3, CCR4-NOT, and PARN) as well as decapping enzyme such as Dpc1/2 have been described (Das et al., 2017; Zhang et al., 2015). Less commonly, endonucleases can initiate decay by internal cleavage thus leading to exonucleolytic decay in both directions from the cleavage site (Bicknell & Ricci, 2017). 3'- 5' mRNA decay is also possible since unprotected 3' end can be degraded by a large complex of 3'-to-5' exonucleases known as the RNA exosome (Das et al., 2017) (*Figure 7*). The RNA exosome is a multi-protein complex formed by 10 ($Exo10^{Dis3}$) or 12 ($Exo12^{Dis3/Rrp6/C1D}$) distinct subunits: the EXO9 core, which comprises the 'cap' structure (formed by Rrp4, Rrp40 and Csl4) and the 'ring' complex (formed by RNase PH-like proteins and Mtr3), is catalytically inactive and associates with the processive 3′-to-5′ ribonuclease chromosome disjunction 3 (Dis3; also known as Rrp44) in cytoplasm and with the distributive 3′-to-5′ exonuclease Rrp6 and its obligate binding partner C1D in the nucleus (Kilchert et al., 2016; Zinder & Lima, 2017).

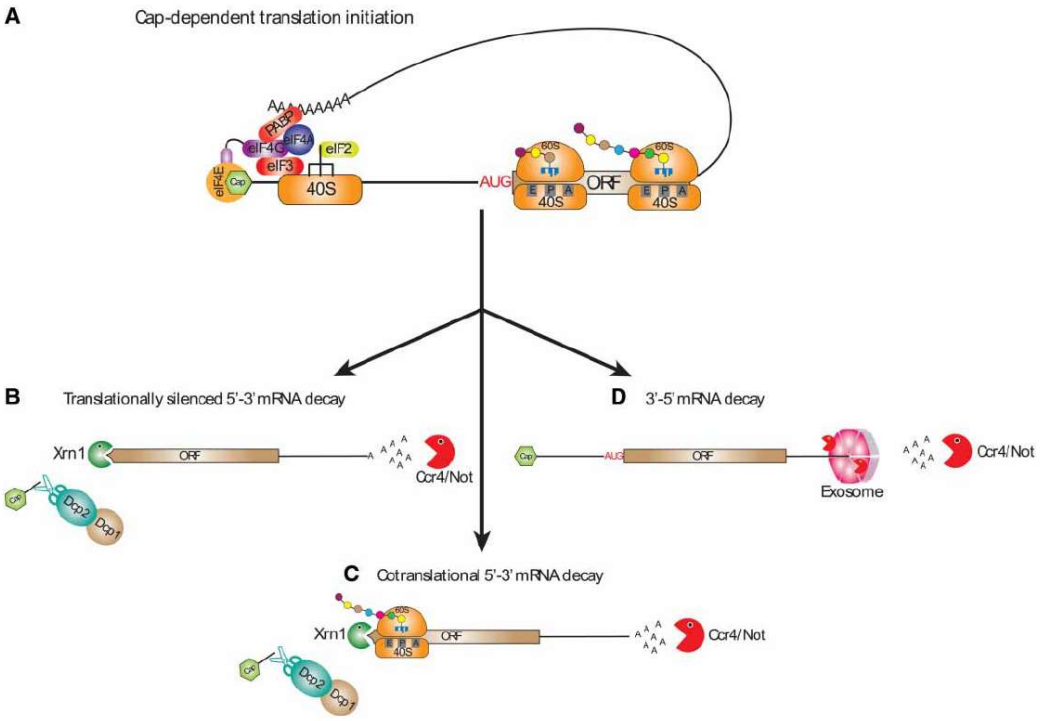

Figure 7; Translation initiation and mRNA degradation (Bicknell & Ricci, 2017).

During the years, many laboratories have been studying the role of KHSRP in the rapid decay of inherently labile transcripts as well as its ability to bind to AREs and to recruit the enzymatic complexes required for mRNA degradation (Chen et al., 2001; Gherzi et al., 2004; Chou et al., 2006; Gherzi et al., 2010; Briata et al., 2013). KHSRP binds to ARE-containing mRNAs and forms a complex with mRNA decay enzymes including the poly(A)-RNase (PARN), the RNA exosome component Rrp4, and the decapping enzyme Dcp1/Dcp2 (Chen et al., 2001; Gherzi et al., 2004; Chou et al., 2006). A global study has identified one hundred mRNAs that are physically associated with KHSRP and it was not surprising that many cytokines that contains AREs were identified as KHSRP targets and up-regulated upon its down-regulation, such as IL-8, IFN-α and IFN-β (Winzen et al., 2007; Lin et al., 2011; Gherzi et al., 2014). In addition, KHSRP promotes the decay of a number of regulators of cell identity and fate, such as Myogenin (Myog), Cyclin-dependent kinase 1 (Cdk1) and Utrophin (UTRN) in myogenesis, Nitric Oxide Synthase 2 (NOS2) and Tumor Necrosis Factor (TNF) in inflammatory response, Growth Associated Protein 43 (GAP43) in axonal outgrowth, Period Circadian Clock 2 (Per2) in non-alcoholic liver steatosis (Briata et al., 2016).

2.2 Implication of KHSRP in pre-mRNA alternative splicing

Alternative splicing (AS) is an important and versatile mechanism of gene expression control through which a pre-mRNA is processed into multiple mRNA isoforms differing in their combination of exon sequences thus allowing functional and genetic variability (Black & Grabowski, 2003). It is estimated that 95% of human genes are alternatively spliced (Pan et al., 2008). Although the regulation of splice site usage is still unclear, it is well known that numerous RBPs are involved in the control of AS (Black & Grabowski, 2003). The interaction of *cis*-sequence elements and *trans*-acting RBPs modulate the splicing process that can be highly variable as these interactions are transient and of relatively low specificity. Importantly, both changes in *cis*-sequence and levels of *trans*-factors can alter mRNA splicing and cause disease (Fredericks et al., 2015). A major group of splicing factors is represented by the heterogeneous nuclear ribonucleoprotein particles (hnRNPs) (Chaudhury et al., 2010). Among them, hnRNPA1 whose association with KHSRP in different cell type has been demonstrated (Ruggiero et al., 2007; Michlewski & Càceres, 2010).

KHSRP has been initially described as an essential component of a multiprotein complex that binds specifically to a G+U-rich intronic splicing enhancer element downstream of the neuron-specific *c-src N1* exon (Min et al., 1997). In detail, KHSRP induces the assembly of five other proteins, including hnRNPF, hnRNPH and PTB, to the splicing enhancer (Min et al., 1997). Min and colleagues suggested that KHSRP is involved in the splicing of other transcripts besides *c-src* (Min et al., 1997). Indeed, it was observed both *in vivo* and *in vitro* that KHSRP associates with hnRNPH1 and Nucleophosmin (NMP), and that complex interacts with *intron 3* of human *RPL3* gene thus promoting the expression of an alternative isoform of RPL37 (Russo et al., 2011).

2.3 Implications of KHSRP in miRNA biogenesis

MiRNAs are short non-coding RNAs (~21-nucleotide in length) that exert key roles in the post-transcriptional regulation of gene expression. It has been predicted that miRNAs control the expression of about 50% of all protein-coding genes in mammalian cells (Krol et al., 2010). Many studies revealed that miRNAs regulate nearly every aspect of cell life interacting with specific mRNA targets, inhibiting their translation and favoring

their decay (Krol et al., 2010). Importantly, a single miRNA can modulate the expression of multiple target mRNAs to rapidly modify complex cellular functions, while one gene may be targeted by more than one miRNA (Hashimoto et al., 2013).

The transcription of the precursors of miRNAs is carried out by RNA polymerase II (RNA Pol II) and it is controlled by RNA Pol II-associated transcription factors as well as by epigenetic regulators (Ha & Kim, 2014). Primary mi-RNAs (pri-miRNAs) typically consist of a double-stranded stem of 33–35 bp, a terminal loop, and single-stranded RNA segments at both the 5′ and 3′ sides undergo several steps of maturation (Ha & Kim, 2014). A complex that includes the nuclear RNase III Drosha co-transcriptionally initiates pri-miRNA maturation process by cropping the stem–loop to release a small hairpin-shaped RNA of ~65 nucleotides called precursor mi-RNA (pre-miRNA) (Ha & Kim, 2014). The dsRNA-binding domain of Drosha is necessary but not sufficient for substrate interaction, thus additional RNA-binding activity is provided by DGCR8 recruited through the middle region of Drosha (Ha & Kim, 2014). Drosha cleaves the hairpin at approximately 11 bp away from the 'basal' junction between single-stranded RNA and dsRNA, and approximately 22 bp away from the 'apical' junction linked to the terminal loop (Ha & Kim, 2014). Next, pre-miRNA is exported into the cytoplasm where it is cleaved near the terminal loop by a second ribonuclease Dicer-containing complex generating a small RNA duplex (the two RNA-filament have been historically called 'guide' and 'passenger', respectively) (Ha & Kim, 2014). Subsequently, the RNA duplex is loaded onto an AGO protein (four distinct AGO proteins exist in humans) to form an effector complex called RNA-Induced Silencing Complex (RISC) that quickly removes one of the two strands holding the other filament to generate a mature RISC (Ha & Kim, 2014; Nakanishi, 2016) (*Figure 8*). MiRNAs are highly stable once they enter the RISC because both ends are protected by AGO proteins (Ha & Kim, 2014). RISC recognizes its target mRNA based on the miRNA-target sequence complementarity and the accessibility of the target site (Jo et al., 2015). Once bound the target, the RISC complex inhibits protein synthesis by either repressing translation or promoting mRNA deadenylation and decay (Bartel, 2009; Jo et al., 2015).

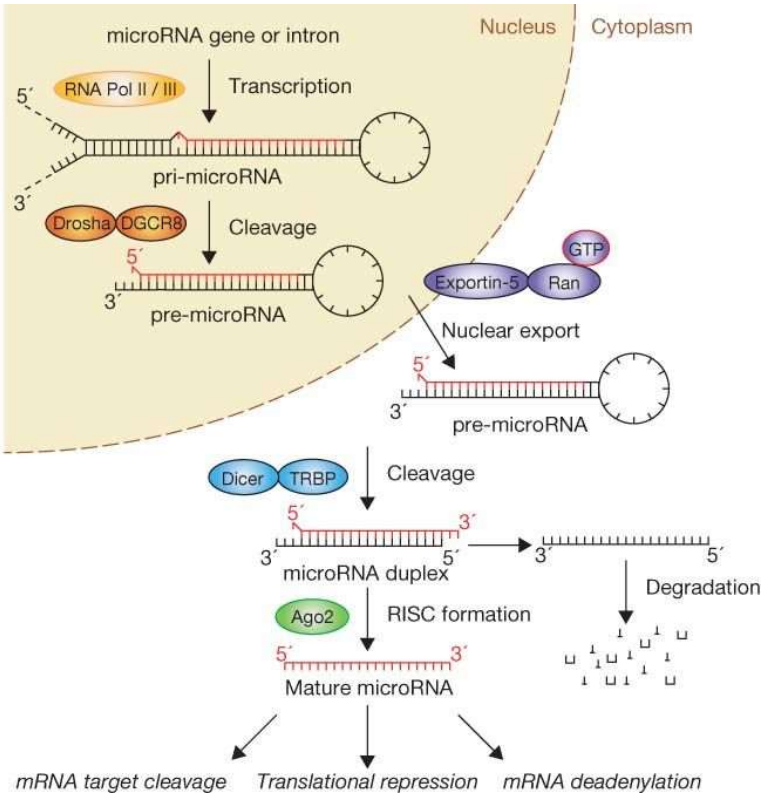

Figure 8; MicroRNA biogenesis (Winter et al., 2009).

Changes in the expression of miRNAs are associated with a number of human pathologies and, over the last decade, it has become clear that miRNAs are widely dysregulated in cancer (Krol et al., 2010; Calin & Croce, 2006; Visone & Croce, 2009). MiR-200 family members (miR-200s), often highly expressed in epithelial cells compared to mesenchymal cells, are downregulated during EMT (Bullock et al., 2012; Ding, 2014). MiR-200 family is composed of five different members (miR-200a, miR-200b, miR-200c, miR-141 and miR-429) that have been classified into two functional groups based on the seed sequence (Senfter et al., 2016). It has been shown that the miR-200 family is able to target and downregulate ZEB1 and ZEB2 thus promoting *Cdh1* expression and the epithelial phenotype (Senfter et al., 2016). Conversely, the expression of miR-21 (a TGF-β-induced miRNA in solid cancers) and miR-155 (that, among others, targets RhoA GTPase, a key regulator of cell polarity and tight junction formation) is increased during EMT (Volinia et al., 2006; Kong et al., 2014).

In the laboratory where I conducted my thesis, it has been discovered that KHSRP binds to the TL of a cohort of pre-miRNAs and interacts with both Drosha and Dicer complexes to promote pre-miRNAs maturation (Trabucchi et al., 2009).

Further studies have confirmed the role of KHSRP in miRNA biogenesis in different cell lines (Liu & Liu, 2011; Michlewski & Càceres, 2010; Castilla-Llorente et al., 2013) (*Figure 9*). MiRNAs whose biogenesis is favored by KHSRP exert important functions in various biological processes as cell proliferation, immune response, metabolic homeostasis, and cell fate determination in response to extracellular stimuli (Gherzi et al., 2010; Briata et al., 2016).

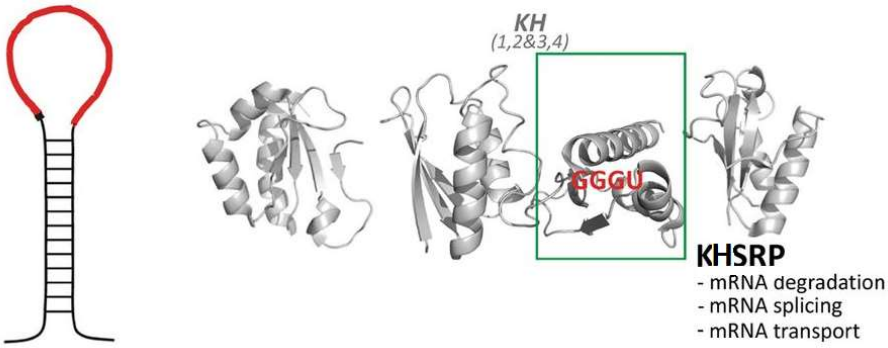

Figure 9; Recognition of the pre-miRNA TL by KHSRP (image modified from Castilla-Llorente et al., 2013).

KHSRP can interact and/or compete with other proteins to regulate the biogenesis of specific miRNAs in different contexts and cell types (Rüegger & Großhans, 2012; Repetto et al., 2012). Lin-28 homolog A (LIN28) protein is able to repress the maturation of let-7 family members by interacting with the TL of let-7 precursors and by interfering with the Drosha and Dicer cleavage (Viswanathan & Daley, 2010). Moreover, LIN28 promotes 3'-uridylation of pre-let-7 that inhibits Dicer cleavage leading to degradation of the pre-let-7 itself (Heo et al., 2008). In different cell contexts, LIN28 and hnRNPA1 compete with KHSRP for pri-let-7a processing (Trabucchi et al., 2009; Michlewski et al., 2010). Since KHSRP also controls the decay of hnRNPA1 mRNA (Ruggiero et al., 2007), it is possible to hypothesize that KHSRP functions in mRNA decay and in miRNAs maturation are connected (Ruggiero et al., 2007; Michlewski & Càceres, 2010).

2.4 Novel functions: KHSRP can interact with long non-coding RNAs

Long non-coding RNAs (lncRNAs) are a numerous and loosely classified group of long transcripts with no apparent protein-coding potential (Quinn & Chang, 2016). By convention, lncRNAs are defined as non-coding transcripts longer than 200 nucleotides (Rinn and Chang, 2012). Even if the function of the majority of lncRNAs is still unknown, some lncRNAs (e.g. XIST, HOTAIR, TERC, etc.) have been extensively investigated and characterized (Quinn & Chang, 2016).

LncRNAs are involved in important biological events and specific patterns of their expression coordinate cell state, differentiation, development, and disease (Ponting et al., 2009; Rinn & Chang, 2012; Batista & Chang, 2013; Flynn & Chang, 2014). Accordingly, deregulations of lncRNA expression or mutations of the relative genes have been implicated in numerous human diseases (Esteller, 2011). Aberrant expression of lncRNAs plays a considerable role also in tumorigenesis, with several hundred dysregulated lncRNAs which have been recorded in human cancers so far (Gibb et al., 2011; Prensner & Chinnaiyan, 2011). Potentially, dysregulation of lncRNAs may contribute to each of the hallmarks of cancer cells: *(I)* sustained proliferative signaling, *(II)* evasion of growth suppressors, *(III)* replicative immortality, *(IV)* invasion and metastasis, *(V)* induction of angiogenesis, *(VI)* and resistance to cell death (Gutschner et al., 2012). An increasing number of lncRNAs have being implicated in the regulation of EMT through various molecular mechanisms that include their function as competing endogenous RNAs (ceRNAs) for miRNAs involved in EMT regulation, and the epigenetic silencing of gene expression via the recruitment of the polycomb repressor complex 2 (PRC2) (Heery et al., 2017).

A further layer of complexity has been provided by recent evidences that a number of lncRNAs potentially include short open reading frames (ORF). Some annotated lncRNAs are found associated with ribosomes and they code for short functional peptides (Dinger et al., 2008; Ingolia et al., 2011). For example, in Drosophila the tarsal-less/polished rice transcript is currently known to code for very short functional peptides (Tupy et al., 2005; Kondo et al., 2010). However, the ability to recruit the ribosome and be translated would not preclude the non-coding function of these transcripts (Ulitsky & Bartel, 2013).

Considering its versatility and ability to interact with different RNA species, it is not surprising that KHSRP associates with lncRNAs. It has been recently reported that the oncogenic H19 lncRNA directly interacts with KHSRP in undifferentiated multipotent mesenchymal C2C12 cells thus favoring KHSRP-mediated destabilization of labile myogenin mRNA (Giovarelli et al., 2014). In the early steps of myogenesis, AKT1 and AKT2 are activated and directly phosphorylate KHSRP inducing its dismissal from H19 with the consequent stabilization of myogenin mRNA (Giovarelli et al., 2014). Further, KHSRP translocates to the nucleus of differentiating C2C12 cells where it promotes myogenic-miRNAs maturation favoring myogenic differentiation (Giovarelli et al., 2014). It is likely that regulatory mechanisms involving lncRNAs and KHSRP might exist in other cell types.

RESVERATROL

Currently, cancer is treated by diverse therapeutics tools, such as surgery, radiotherapy, chemotherapy, hormonal therapy, immunotherapy, and targeted therapies (Palumbo et al., 2013). However, the genetic heterogeneity of cancer evades these treatment pathways and continuously deters clinical efforts (Block et al., 2015). To overcome the limitations and provide more effective cancer treatment, the development of low-toxicity broad-spectrum therapies that can collectively impact important mechanism and pathways for the genesis and spread of cancer has been pursued (Block et al., 2015). Consequently, the interest in chemopreventive activities of phytochemicals on cancer have been continuously growing.

Stilbenes are molecules that contribute to flavor and color of many fruits and plants, as well as to growth, development, and defense from pathogens and herbivores (Dewick, 2002; Chong et al., 2009). Structurally, stilbenes are formed by two phenolic rings connected by an ethene molecule (Rocha-González, 2008). Resveratrol (RESV; also known as 3,4',5-trihydroxystilbene) is the main stilbene generated in the skin of grapes, raspberries, mulberries, pistachios and peanuts, and by at least 72 medicinal and edible plants species (Rocha-González, 2008). From a chemical point of view, RESV is a polyphenolic phytoalexin that exists in two isomers, *cis*-(Z) and *trans*-(E) RESV, both with biological activity, although *trans*-RESV seems to have a more potent activity than *cis*-RESV (Orallo, 2006).

RESV exerts a number of biological activities, as anti-inflammatory, anti-proliferative, and anti-oxidant effects, and both basic and preclinical studies have assigned to the molecule health-promoting effects in cardiovascular and neurodegenerative diseases, in diabetes, and also in cancer (Weiskirchen & Weiskirchen, 2016; Baur & Sinclair, 2006; Latruffe et al., 2015; Han et al., 2015) (*Figure 11*). RESV affects different steps of carcinogenesis, such as tumor initiation, tumor promotion and progression, neo-angiogenesis and metastasis formation (Ferraz da Costa et al., 2017). In addition, in various cancer types, RESV behaves as a chemo-sensitizer by lowering the threshold of

cell death induction by classical anticancer agents and counteracts tumor cell chemoresistance (Ferraz da Costa et al., 2017).

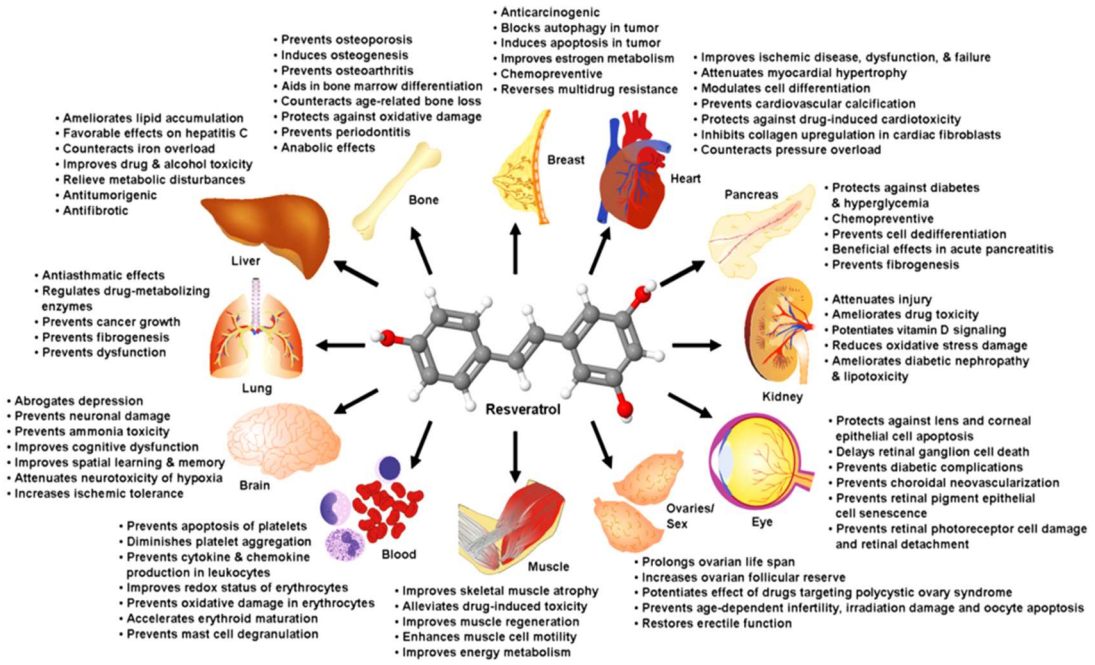

Figure 11; Some of the reported beneficial effects of RESV on organ function (Weiskirchen & Weiskirchen, 2016).

Although there are still unsolved mechanistic questions to be faced, RESV holds promising anti-tumor potential through its ability to induce apoptosis as well as to suppress both proliferation and invasion in a number of cell lines (Han et al., 2015; Xu et al., 2015). It has been suggested that the anti-proliferative properties of RESV are related to its capacity to block DNA synthesis as well as to interfere with various stages of cell progression by regulating the machinery of proteins involved in cell cycle control (Ferraz da Costa et al., 2017). In some cases, the induction of cell cycle arrest by RESV is followed by apoptotic cell death with activation of pro-apoptotic molecules and inhibition of anti-apoptotic molecules (Lin et al., 2011). Independent studies showed that RESV can also induce p53-dependent cell death in a variety of cancer cell lines (She et al., 2001; Hsieh et al., 2011; Ferraz da Costa et al., 2017). Furthermore, a functional wild-type p53 protein is required to increase the RESV-sensitivity of tumor cells (Ferraz da Costa et al., 2017) (*Figure 12*).

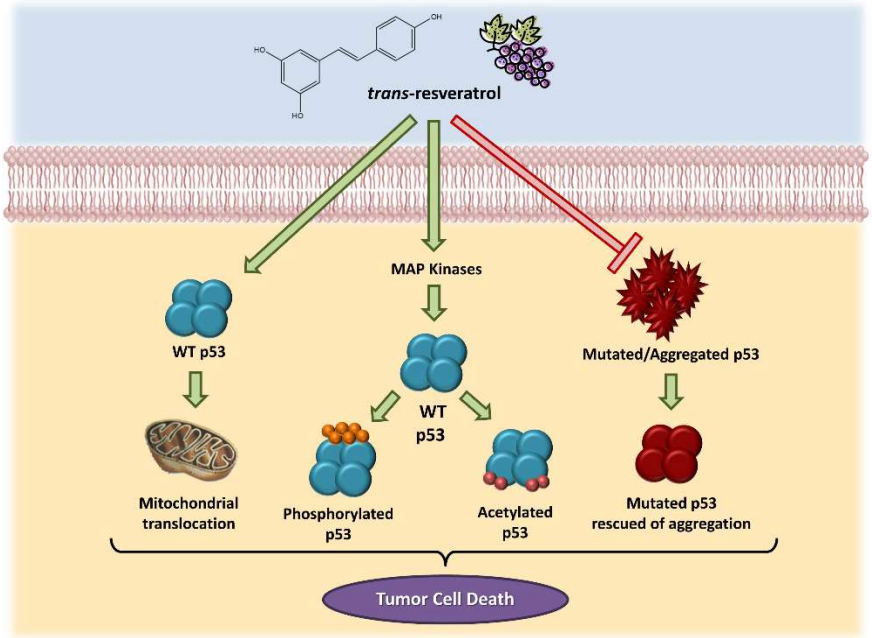

Figure 12; Effects of RESV on p53 pathway in cancer cells (Ferraz da Costa et al., 2017).

The capacity of RESV to interact with numerous proteins and biomolecules could explain why it acts upon various different signaling and can modulate gene expression (Britton et al., 2015). RESV can directly bind to its targets, altering their activity, structure and/or stability (Britton et al., 2015). Some examples are reported below.

1) It has been postulated that RESV produces a neuroprotective activity against Alzheimer's Disease since it indirectly stimulates the proteosomal degradation of *β*-amyloid peptides (Marambaud et al., 2005). Chen and colleagues have reported that the microglial Nuclear Factor-*κ*B (NF-*κ*B) signaling mediates *β*-amyloid peptides-dependent neurodegeneration and that this pathway is inhibited by RESV through Sirtuin-1 (SIRT1) modulation (Chen et al., 2005). Accordingly, RESV strikingly reduces the expression of genes modulated by NF-*κ*B (Chen et al., 2005). Further, RESV allosterically binds to SIRT1 and lowers the *Km* of SIRT1 for acetylated substrate (Canto et al., 2012). As a consequence, RESV, activating SIRT1, regulates different downstream targets through deacetylation (Canto et al., 2012). A recent study has demonstrated a new role for RESV in limiting TGF-β2-induced EMT through SIRT1 activation that lead to SMAD4 deacetylation, which in turn modulates the expression of target molecules, such as CDH1 and Actin (ACTA2) (Ishikawa et al., 2015).

2) Not all RESV effects are SIRT1-dependent. It has been reported that RESV can directly bind to both DNA and RNA, and it is also involved in alternative splicing regulation (Usha et al., 2005; Markus et al., 2011). RESV can promote exon inclusion in an RNA-specific manner and can influence the levels of a group of splicing factors, including ASF/SF2, hnRNPA1 and HuR (Markus et al., 2011).

3) Target-fishing and drug responsive target stability experiments showed selective, direct binding of RESV to KHSRP pointing out a KHSRP role for the post-transcriptional effect of RESV (Bollmann et al., 2014). RESV/KHSRP interaction prevents KHSRP phosphorylation by MAPK14 thus enhancing KHSRP ability to bind to its target mRNAs as well as KHSRP association with the RNA exosome (Bollmann et al., 2014) As a result, TNF, IL8 and NOS2 mRNA half-life decreased with the consequent reduction of their steady-state levels (Bollmann et al., 2014). This observation could explain, at least in part, the anti-inflammatory effect of RESV (Bollmann et al., 2014).

Aims of the Study

Metastases are formed when cancer cells break away from where they first originated (primary tumor), travel through the blood or lymphatic system, and form new tumors (metastatic tumors) in other parts of the body (Tam & Weinberg, 2013). EMT active role during metastasis is suggested by several experimental and clinical lines of evidence (Trimboli et al., 2008; De Craene & Berx, 2013). The activation of EMT program depends on the convergence of multiple signals from the surrounding microenvironment with TGF-β being recognized as a major inducer (Xu et al., 2009). Although transcriptional regulation of factors involved in EMT has been established, post-transcriptional regulation has been addressed more recently (Lamouille et al., 2009; Aparicio et al., 2013).

Since 1996, multiple roles of the single-strand RNA-binding protein KHSRP have been studied (see Briata et al., 2016 for a recent review). In the last decade, in the laboratory where I conduct my thesis, a role for KHSRP as a negative regulator of gene expression at a post-transcriptional level has been investigated (Trabucchi et al., 2009). It has been demonstrated that KHSRP operates by promoting decay of unstable mRNAs and favoring maturation from precursors of select miRNAs (Trabucchi et al., 2009). More recently, it was shown that KHSRP is a component of the TGF-β/BMP signaling pathway in multipotent mesenchymal C2C12 cells (Pasero et al., 2012). Based on these previous data, the aims of this study were:

1. to investigate KHSRP role in TGF-β-dependent EMT in mammary gland cells;
2. to search for compounds able to interfere with KHSRP function.

Experimental Procedures

Cell cultures and treatments

Murine immortalized NMuMg cells (obtained from ATCC) were cultured in DMEM plus 10% FBS and 10 mg/ml bovine insulin (Sigma-Aldrich). HEK293 cells (obtained from ATCC) were cultured in DMEM plus 10% FBS. Py2T cells, a kind gift of Dr. G. Christofori (University of Basel), were cultured in DMEM plus 10% FBS as described (Waldmeier et al, 2012). The immortalized HMLE cells, a kind gift of Dr. R. Weinberg (Whitehead Institute), were cultured as described (Elenbaas et al, 2001). Human mammary gland adenocarcinoma cells MDA-MB-231 and MCF7 were cultured in DMEM plus 5% FBS; human non-tumorigenic epithelial cell line MCF 10A were cultured in DMEM/F12 plus 5% horse serum, 10 mg/ml bovine insulin (Sigma-Aldrich), EGF (20 ng/ml, Sigma-Aldrich), hydrocortisone (0.5 mg/ml, Sigma-Aldrich), and cholera toxin (100 ng/ml, Sigma-Aldrich). 4T1 and TS/A mouse mammary gland cancer cells (obtained from Dr. C. Bagni, VIB Center for the Biology of Disease) were cultured in DMEM/F12 plus 10% FBS.

NMuMg and Py2T cells were maintained in DMEM supplemented with 2% and 1% FBS, respectively, for 8h–16h prior to the addition of 10 ng/ml human recombinant TGF-β1 purchased from R&D Systems.

Resveratrol was purchased from Sigma (R5010), dissolved in DMSO at a 100mM concentration, and used at a 75 μM concentration in the majority of the experiments.

Cell transfections and adenoviral infections

The adenoviral vectors pAdCMVnull (AdNull) and pAdKHSRP (full-length human KHSRP cDNA cloned into an Adenoviral-Type 5 backbone) were purchased from Vector Biolabs (Eagleville, PA, USA). HEK-293 cells were transfected using

Attractene transfection Reagent (Qiagen) while NMuMg, Py2T and 4T1 cells were transfected with Lipofectamine 2000 (ThermoFischer). Stable KHSRP knock-down was obtained using previously described silencing sequences cloned in pSuper-Neo (Oligoengine) for NMuMg and in pSuper-Puro (Oligoengine) for Py2T and 4T1. Stable NMuMg transfectants were obtained using G418 (Sigma) selection (800 μg/ml) while stable Py2T transfectants were obtained using Puromycin (ThermoFischer) selection (4.5 μg/ml). Either stable hnRNPA1 knock-down (generated transfecting cells with hnRNPA1 shRNA plasmid [sc-35,576-SH, Santa Cruz Biotechnologies]) or stable KHSRP knock-down were obtained using Puromycin selection (5.0 μg/ml, ThermoFischer) in 4T1 cells. Double knock-down (shKHSRP/shhnRNPA1) was obtained transfecting cells with pSuper-Neo-shKHSRP and hnRNPA1 shRNA plasmid. Then transfected 4T1 cells were selected in both G418 (100 μg/ml) and Puromycin (5.0 μg/ml). A minigene splicing reporter construct that contains the *Cd44v8* exon and its flanking introns (kindly provided by Dr. Chonghui Cheng) was transfected into HEK-293 cells using Attractene transfection Reagent (Qiagen). siRNAs utilized to knock-down human KHSRP (5'—GAUCAACCGGAGAGCAAGA—3') and human hnRNPA1 (5'—AACUUUGGUGGUGGUCGUGGA—3') were purchased from Sigma. Mouse miR-27b-3p mimic and anti-mmu.miR-27b-3p miScript miRNA inhibitor were from Qiagen. siRNAs utilized to knock-down murine hnRNPA1 were purchased from Santa Cruz (sc-35576). miRCURY LNA mmu-miR-192-5p and mmu-miR-194-5p Inhibitors were from Exiqon.

It is noteworthy that miR-27b-3p targets the 3'UTR region of *Khsrp* transcript that has not been included in our adenovirus-based vector and that the hairpin sequence cloned into the pSuper vector in order to stably silence KHSRP has been designed on the basis of the mouse sequence while the adenoviral vector overexpressing KHSRP includes the human cDNA that diverges from the mouse cDNA in the region targeted by the hairpin.

Phalloidin staining

Mock and shKHSRP NMuMg cells were fixed in 3.7% formaldehyde, stained using Alexa Fluor 568 Phalloidin, and imaged with the Imager M2 microscope (Zeiss).

Scratch wound closure assay

For TGF-β studies, cells were cultured in six-well plates up to sub-confluence and maintained in 2% FBS-containing medium for 16h. After starvation, a wound was scratched into confluent monolayers, and cultures were either maintained in 2% FBS containing medium for 48h or treated with 10 ng/ml TGF-β in the same medium for different times. For RESV studies, NMuMg and 4T1 cells were cultured in six-wells plates up to confluence. A wound was scratched into monolayers and cultures were treated for 40h with either RESV or DMSO.

Images were taken using Olympus CKX41 microscope at different time post-wounding and analyzed using the ImageJ package (http://imagej.nih.gov/ij/index.html). Average distance of wound obtained from six microscopic fields was used for calculation of percent wound healed. Experiments were performed three times.

Immunofluorescence

Cells were grown on chamber-slides, fixed with 3% paraformaldehyde in PBS and permeabilized with 0.5% Triton X-100 for 5 minutes at room temperature. Subsequently, cells were blocked with 3% bovine serum albumin for 30 minutes and incubated with affinity-purified anti-KHSRP antibody for 1h at room temperature and then incubated with Dylight 488-labeled secondary antibody (Abcam) for 1h at room temperature. Cells were imaged with the Imager M2 microscope (Zeiss).

Antibodies

Affinity-purified rabbit polyclonal anti-KHSRP antibody and the corresponding pre-immune serum were previously described (Pasero et al, 2012); rabbit polyclonal anti-HDAC1, mouse monoclonal anti-ACTB (also known as β-actin), mouse monoclonal anti-hnRNPA1 (4B10), and mouse monoclonal anti-TUBA1 (also known as α-tubulin) antibodies were from Sigma; anti-CDH2 rabbit polyclonal antibody was from Abcam; anti-FN1 (IST9) monoclonal antibody, anti-CDH1 (S-17) goat polyclonal antibody, and anti-14-3-3ξ goat polyclonal antibody (L-15) were from Santa Cruz; monoclonal antibody

to ESRP1/ESRP2 was from Rockland; rabbit polyclonal antibody to ESRP2 was from Abcam. Immunoblots were quantitated using ImageJ 1.49r software.

RNA preparation, RT-PCR, and quantitative RT-PCR

Total RNA was isolated using either the miRNeasy mini kit (Qiagen) or QIAzol Lysis Reagent (Qiagen) and retro-transcribed (50–100 ng) using either miScript reverse transcription kit (Qiagen) or Transcriptor Reverse Transcriptase (Roche) according to manufacturers' instructions. PCR analysis was performed using the GO-Taq system (Promega) and PCR products were analyzed by agarose (2% in TAE) gel electrophoresis. Quantitative PCR was performed using either the miScript SYBR green PCR kit (Qiagen) or the Precision 2× QPCRMasterMix (Primer Design), and the Realplex IIMastercycler (Eppendorf). For some experiments the end-points of the qPCR reactions were analyzed by agarose gel (2% in TAE buffer) electrophoresis. The sequence-specific primers utilized for PCR reactions are listed in *Table 1*.

TRANSCRIPT	FORWARD	REVERSE
mmu.Adamtsl2	CCTGGATTTGACAGCTCCGT	GACATCTCCCACTGTGGTCC
mmu.CD44	ATCCTCGTCACGTCCAACAC	TCTTCTTCAGGAGGGGCTGA
mmu.CD44s	CACCTTGGCCACCACTAAGA	CCCATTTTCCATTGTGTCTGGG
mmu.CD44v	CAACCACCAGGATGGCTGAT	GCATGTGGGGTCTCCTCTTC
mmu.Cdh1	GTGAGGACGACTAGGGGACT	CACACTCAGGGAAGGAGCTG
mmu.Cdh2	CGAGAGGCCTATCCATGCTG	CCCAATATCCCCAGGGTGTG
mmu.Cdkn2b	GCAGCTGGATCTGGTCCTTGAGC	CCCCTGCAGCAGCAGCTTGT
mmu.Chst1	CCACCAGGTAACTGCTGTGT	CAGGCCTTCAGGTGGAGAAG
mmu.Col12a1	TGGTTAACGAACTGGGTCGG	GAAAAGCATCAGGCGGACAC
mmu.Col6a2	GGGGGTGGTCAACTTCGCCG	CGGATGCCCTCTTCACGGGC
mmu.Enah5+6C	GAATGTCCAATGCTGCTGCC	GGAAGCAGAGGAGTCTCCCA
mmu.Enah5+6L	TGTCCAATGCTGCTCCATCT	CGGCTGGCAACTGGAATACT
mmu.Ext1	GGACAGACTTCCCGAGCATC	CTGAGAATGGATCAGCGGCA
mmu.Ext2-001	GGAGAGAGCAAACCTGCCAT	TGTGCTCTGCTGTGGATCTG
mmu.Ext2-012	AGGCATTTTGTCACAGTCCCA	AGCCTGCTCATCATTTGCCT
mmu.Fn1	GCAGGAAAGTCACCCAGACA	CTGTGGGAGGGGTGTTTGAA
mmu.Fstl1	ACGCTCCCACCTTCGCCTCT	GTCACCAGCGAGAGCGCCAG
mmu.Fstl1	CCTCAGACAGAAGCCACAGG	TGAGCGTCCATCCTTGGAAC
mmu.Gpc6	CACGAACGCTGTAGTCCTGT	GTGCTATAGTCGGGGATGGC
mmu.IIIbFgfr2	CACGTGGAAAAGAACGGCAG	AGAGCCAGCACTTCTGCATT
mmu.IIIcFgfr2	AATATACGTGCTTGGCGGGT	CTCCTTCTCTCTCACAGGCG
mmu.Isg20-001	AAAGGGAGGAGTAGGGCAGG	CTCAAGGCTGGCCAGGTAAG

mmu.Isg20-002	GCTGCTGTTTGTCAACTCTCC	CACTCACCCTTTGAGGCCC
mmu.Itga9	GGGTGGAGCATTGTCTTGGA	TGATCCCTGGAGGGAGACTG
mmu.Khsrp	CCTGATTTTGGCTTTGGGGG	CCAGTTTCTTGCTGTCTGGC
mmu.Khsrp	CCTGATTTTGGCTTTGGGGG	CCAGTTTCTTGCTGTCTGGC
mmu.Lrrd1-e1	ACAGCTTTGCCCAGTGGTAT	TTCCATTGGCGGTCTCATCA
mmu.Lrrd1-e2	GCTAAGCCCAGGCTAGGTTC	ACACCTCTACAGTTGTTGCGA
mmu.Mbp7-e7	GTGGTATGTGAGCACAGGCT	GGATAGCTGGCCTGGAAGTG
mmu.Mbp-e1-2	CATAGTATCCGCGCCCCAG	CGACCCAATGGGGTGTTCAA
mmu.miR-192-5p	CTGACCTATGAATTGACAGCC	
mmu.miR-194-5p	TGTAACAGCAACTCCATGTGGA	
mmu.miR-27b-3p	TTCACAGTGGCTAAGTTCTGC	
mmu.Mmp9	AGGCTCTCTACTGGGCGTTA	AGGAGTCTGGGGTCTGGTTT
mmu.Plod2	GTTCCTCCAGGGCAAGTCTC	ACTTGGAGCTGACGCTTGAA
mmu.pri-194-1	CACCAGGCTCCAGGTTCAAT	GTTTGCCGGATGGGTCCTTA
mmu.pri-194-1	ATTTCTGGGTGGGCTCTTGG	TCCTCTGCTGACCTAGCACT
mmu.pri-miR-192	CGGCTAGTACCAGCAGAGGAAG	ATGCCTGAAGACTGCTGTGTAGG
mmu.pri-miR-194-1	CACCAGGCTCCAGGTTCAAT	GTTTGCCGGATGGGTCCTTA
mmu.pri-miR-194-2	GACTTCGCTCAGGGAGGTTG	CGGCTCCAAGTCCACACTTT
mmu.Rarres1	GCATGCGCACTTTCCTGATT	GACGAAACCTTTTCCCAAAGCA
mmu.Rpl32	CTGGCCATCAGAGTCACCAA	TGCACACAAGCCATCTACTCA
mmu.Runx2	GTACCCGGGGGAGACCGGTC	TGCTGTGGCTTCCGTCAGCG
mmu.Snai1	CAGGACTCCTTCCAGCCTTG	CGGGTACAAAGGCACTCCAT
mmu.sno234	TTCGTCACTACCACTGAGA	
mmu.Zeb1	AGCCTTAAGGAAGCAGCCAG	ACATCAACACTGGTCGTCCC
mmu.Zeb2	GTCTCTGCAAGTGCCATCCT	ACTGACACGGGTGCTTCAAA
qPCRskipv8	GAGGGATCCGGTTCCTGCCCC	CAGTTGTGCCACTTGTGGGT
qPCRv8inc	CAATGACAACGCTGGCACAA	CCAGCGGATAGAATGGCGCCG

Table 1; List of primers used in the present study.

In order to analyze gene expression changes among the pool of nascent mRNAs, we adopted the Click-iT Nascent RNA Capture kit (ThermoFischer) and performed experiments according to manufacturer's instructions. NMuMg cells were pulsed with 0.5 mM 5-ethynyl Uridine for 1 hour.

Exon-level quantification and splicing analysis

To test differences in exon usage, we followed the procedure described for DEXSeq (v 1.14.2, R 3.2.2) (Anders et al, 2012) adapting linear model design to test for differential usage induced by TGF-β in the presence or absence of KHSRP overexpression (cells infected with either AdKHSRP or AdNull, respectively). In brief, we first created a GFF file from the Ensembl GRCm38.74 GTF with the provided script

dexseq_prepare_annotation. Reads counts were then collected from the sorted_by_name BAM, with dexseq_count.py on the previously created GFF reference in "unstranded" "paired" mode. Exons with log2 fold change greater than j1.2j (linear FC 2.3), showing an adjusted p value <0.01 (FDR <1%, Benjamin-Hochberg corrected) were selected for downstream analysis.

Electrophoretic mobility shift assays

Electrophoretic mobility shift assays (EMSA) were performed as detailed in Trabucchi et al. (2009). Production and purification of recombinant KHSRP and GST-hnRNPA1 have been described previously in Briata et al., 2005 and in Ruggiero et al., 2007 respectively. The labeled RNA was transcribed using Sp6 polymerase from a template generated by inserting into pCY vector (Chen et al., 2000) a PCR product (forward primer: ATGCTGCAGTCCAGTACCAGTAAGA ATAC; reverse primer: AT GTCTAGACTCATCAGAATGGAATTAAGG). RNAs corresponding to ARETNF and E3 have been previously described (Gherzi et al., 2004; Giovarelli et al., 2014).

Ribonucleoprotein complexes immunoprecipitation assays

Ribonucleoprotein complexes immunoprecipitation (RIP) assays were performed as previously described (Giovarelli et al., 2014) with minor modification. Briefly, total cell lysates were immunoprecipitated with Dynabeads (Invitrogen, Carlsbad, CA) coated with protein A/protein G and pre-coupled to specific antibodies at 4ºC overnight. Pellets were washed three times with a buffer containing 50mM Tris-HCl [pH 8.0], 150mM NaCl, 0.5% Triton X-100, 1X Complete (Roche). Total RNA was prepared from immunocomplexes using either the miRNeasy mini kit (Qiagen) or QIAzol Lysis Reagent (Qiagen), retro-transcribed, and amplified by qPCR as described above. The primer sequences are detailed in *Table 1* (see before).

Deep sequencing of small RNAs

Twelve small RNA libraries were generated from total RNA samples (biological triplicates for each experimental condition) using the Illumina TruseqTM Small RNA

Preparation kit according to Illumina's TruSeqTM Small RNA Sample Preparation Guide at LC Sciences (Houston, TX). The purified cDNA libraries were used for cluster generation on Illumina's Cluster Station and then sequenced on Illumina GAIIx following vendor's instructions. Raw sequencing reads (40 nts) were obtained using Illumina's Sequencing Control Studio software version 2.8 (SCS v2.8) following real-time sequencing image analysis and base-calling by Illumina's Real-Time Analysis version 1.8.70 (RTA v1.8.70). The extracted sequencing reads were further analyzed. First, the "impurity" sequences due to sample preparation, sequencing chemistry and processes, and to the optical digital resolution limits of the sequencer detector were removed. Those remaining *sequ seqs* (filtered *sequ seqs* with lengths between 15 and 32 bases) were grouped by families (*unique seqs*) and were used to map with the reference database files. The filtered *unique seqs* were aligned against mirs of mammals in miRbase. The mapped *unique seqs* were grouped as "*unique seqs* mapped to selected mirs in miRbase", while the remaining ones were grouped as "*unique seqs* un-mapped to selected miRs in miRbase". Bioinformatic data analysis was performed at LC Sciences. Raw data are available on the SRA archive under the BioProject ID PRJNA312753 (http://www.ncbi.nlm.nih.gov/bioproject/312753).

Other experimental procedures

Bioinformatic analysis and statistical evaluation of RNA-seq data have been performed by Dr. Gabriele Bucci at the '*Department of Functional Genomics of Cancer*' (San Raffaele Hospital, Milan).

- ***RNA deep-sequencing***

High-quality RNA was extracted from NMuMg cells (biological triplicates for each experimental condition), and a total of twelve libraries were prepared using standard Illumina TrueSeq SBS PE 200 cycles protocol and sequenced on HiSeq2500. Image analysis and base calling were performed using the HiSeq Control Software and RTA component from Illumina. This approach yielded between 33 and 69 millions of reads that were further processed. Raw data have been published on the SRA archive under the BioProject Accession PRJNA312702 (http://www.ncbi.nlm.nih.gov/bioproject/312702).

- ***RNA-seq preprocessing and alignment***

Illumina 100bp Paired-End FASTQ files were quality checked with FASTQC (http://www.bioinformatics.bbsrc.ac.uk/projects/fastqc). Low quality bases and adapters sequences were trimmed with FASTX (http://hannonlab.cshl.edu/fastx_toolkit). Preprocessed reads were aligned to mouse mm10/GRCm38 reference genome using STAR version 2.3.0 (Dobin et al., 2013) in paired end, unstranded mode. After alignment, putative PCR and optical duplicates were flagged with Picard MarkDuplicates version 1.128 (http://broadinstitute.github.io/picard).

- ***RNA-seq analysis and differential expression gene analysis***

To quantify expression levels mapped reads were counted from BAM files with HTSeq-counts version 1.2.1 (Anders et al., 2015), in "intersection-strict" mode, feature type "exon" and id attribute "gene_name" against reference annotation Ensembl GRCm38.74. We tested for differential gene expression, at transcript level, with a custom R script following the DESeq2 (Anders, 2010) Bioconductor package. We considered as significantly regulated, those transcripts with a Benjamini-Hochberg adjusted p value < 0.01 and an absolute log2 fold change > 1.2.

- ***Gene ontology and pathway enrichment***

Gene lists were tested for enrichment in GO categories, protein-protein interactions networks and known pathways using EnrichR (Chen et al., 2013) and Cluego+Clupedia (Bindea et al., 2009) Cytoscape (Shannon et al., 2003) plugin. Enrichment were selected when p-value < 0.01 (EnrichR, Fisher exact test) or p-value < 0.05 (ClueGO, two sided hypergeometric test, Bonferroni corrected).

- ***RIP-seq peak detection and annotation***

Raw FASTQ reads were trimmed at the ends to remove low quality calls with FASTX (http://hannonlab.cshl.edu/fastx_toolkit). Paired reads were aligned to indexed mm10 genome with bowtie2 (Langmead et al., 2012) allowing for gapped pair-end

alignments. After-alignment statistics and metrics were collected and analyzed using samtools (Li et al., 2009) and Picard (https://github.com/broadinstitute/picard) suites. Peak calling on TGF-β treated and untreated RIP was done using MACS2 in absolute mode with the 'no lambda' 'no model' options set true. To keep only high scoring peaks the p-value filter was fixed to 0.01. We further discarded pileup regions with less than 3 reads at summit. The resulting putative binding regions were annotated with mouse genome annotation Ensembl GRCm38.74. Bedtools (Quinlan et al., 2010) and custom scripts were used to differentially intersect peaks/genes position from the two dataset.

Statistical methods

Quantitative RT-qPCR: averaged CTs among replicates were tested for mean difference between conditions with Student's T-test, and considered significant when nominal $p < 0.01$.

Differential Expression Analysis: sample triplicates were processed and analyzed as described in the DESeq2, bioconductor manual. Genes having less than 1 CPM (Count Per Million) reads were excluded from the analysis. DESeq2 implements a method for differential analysis of count data, using shrinkage estimation for dispersions and fold changes to improve stability and interpretability of estimates. P-values are estimated using Wald-Test corrected by Benjamini and Hochberg (BH) multiple test. Genes were defined as significantly regulated when the tested coefficient p-values were below 0.01 and the mean, log2, absolute fold change per gene was higher than 1.2.

Differential Exon Usage Analysis: the estimation of the isoform expression levels was achieved using DEXseq. Sample were processed and analyzed as described in the DEXseq bioconductor manual. The method uses a generalized linear model (negative binomial GLM) to estimate an overall expression level for each exon, then infers differential expression among genes and between condition triplicates. We adapted the model to fit our design's condition (transfection) and treatment (TGF-β):

formulaFullModel = ~ sample + exon + condition:exon + treatment:exon

formulaReducedModel = ~ sample + exon + condition:exon

DexSeq calculates the probability of each exon within a gene, to be differentially expressed between condition, taking in to account the biological variability and experimental conditions. Using these p-values, a rejection threshold is chosen according to a multiple testing correction method (BH) at $p < 0.01$.

RIP-Seq Peak Detection: low quality bases at the end of reads were trimmed with a threshold of Q30 (phred 33). Quality is assigned by the Illumina sequencer software and is expressed as the -10*log10 of the probability that the corresponding base call is incorrect. Aligned reads were analyzed using MACS2 and peaks were filtered at nominal $p < 0.01$. MACS2 employs a Poisson distribution to accurately approximate a binomial distribution model and test dynamic Poisson parameters for each genomic region.

Gene Ontology and Pathway Enrichment: Gene Ontology enrichment were obtained from EnrichR web-application and ClueGO using p-value threshold of nominal $p < 0.01$ and corrected $p < 0.05$ respectively. The EnrichR p-values used in the present works refer to the Fisher Exact Test statistics, which is a proportion test that assumes a binomial distribution and independence for probability of any gene belonging to any set. ClueGO enrichment probabilities are calculated as a Bonferroni-Corrected, two-sided hypergeometric test.

Deep sequencing of small RNAs: a proprietary pipeline script, ACGT101-miR v4.2 (LC Sciences), was used for sequencing data analysis and preprocessing. Two-way ANOVA was used to test for differentially expressed miRNAs. A cut off threshold was set to nominal $p < 0.01$.

Accession numbers

The accession numbers for the small RNA-seq and RNA-seq data reported in this article are NCBI SRA: SRP074885 and NCBI SRA: SRP070690, respectively.

Results

1. *KHSRP is downregulated during TGF-β-induced Epithelial-to-Mesenchymal Transition in mammary gland cells*

In order to investigate whether KHSRP is implicated in TGF-β-induced EMT, we adopted the murine immortalized mammary epithelial cell line NMuMg as a model. These cells acquire a mesenchymal spindle-like fibroblast phenotype and display the gene expression pattern typical of EMT in response to TGF-β (Avery-Cooper et al., 2014).

We treated NMuMg cells with 10ng/ml of TGF-β for different intervals of time (0, 1h, 8h, 24h, 48h, and 96h respectively) and we observed:

- a rapid increase of *Snai1*, *Zeb1*, and *Zeb2* mRNA expression levels;
- a late increase of *Cdh2* and *Fn1* mRNA expression levels;
- a rapid decrease of *Cdh1* mRNA expression levels;
- expression changes of EMT-related miRNAs, such as the decrease of miR-200-b (a member of miR-200 family) expression levels, and the increase of miR-155 expression levels (*Figures 13, left panel*).

Consistently with changes in mRNA levels, reduced levels of CDH1 protein as well as increased levels of CDH2 and FN1 proteins were detected after 48 hours of TGF-β treatment, as shown in *Figures 13* (*right panel*).

We verified that the TGF-β treatment is able to change the morphology of NMuMg cells from epithelial to mesenchymal after 48h from the beginning of treatment (*Figure 14*).

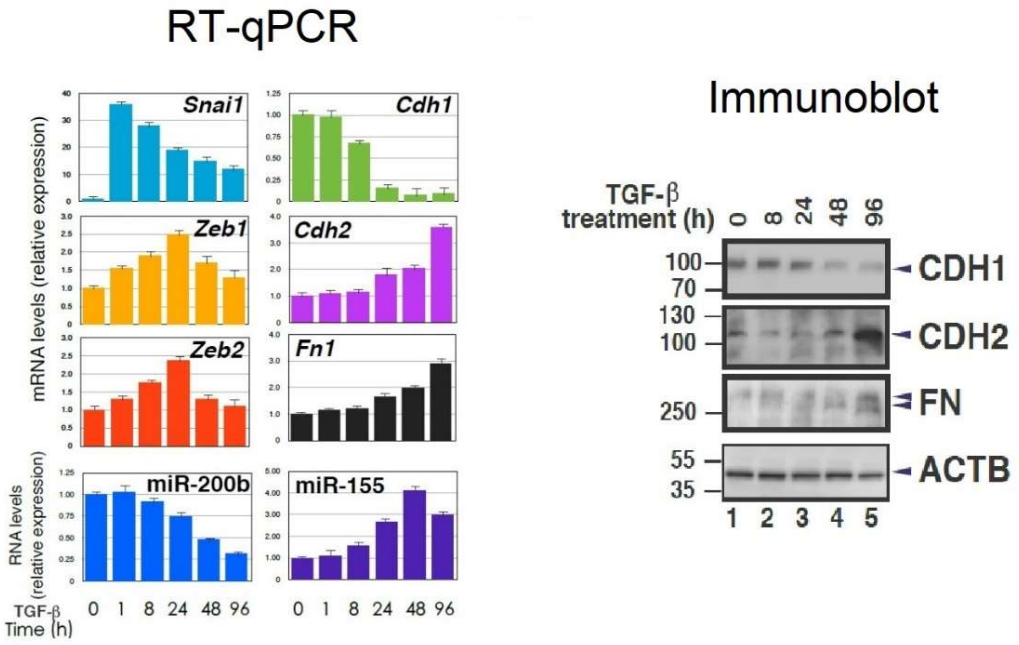

Figure 13; *Left panel.* RT-qPCR analysis of the indicated mRNAs and miRNAs in NMuMg cells treated with TGF-β for the indicated times. The values of RT-qPCR experiments shown are averages ± SEM of three independent experiments performed in triplicate.
Right panel. Immunoblot analysis of total cell extracts (20 µg) from NMuMg cells treated with TGF-β for the indicated times or untreated (time 0). The indicated antibodies were used.

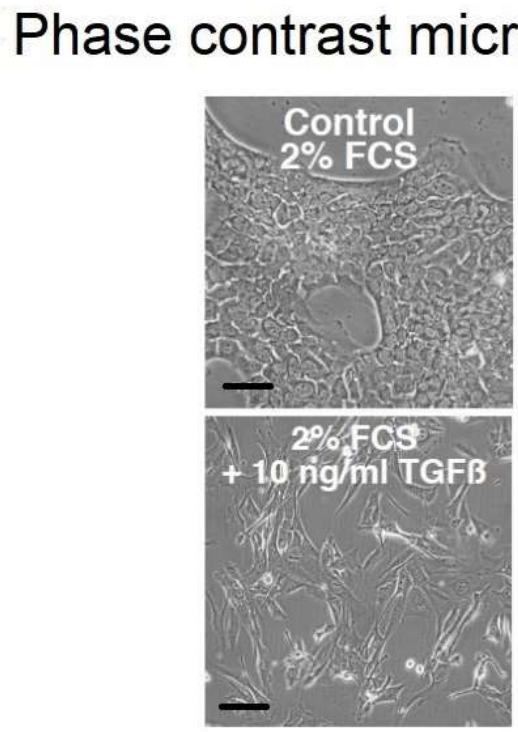

Figure 14; Phase contrast microscopy of NMuMg cells serum-starved and either untreated (*top panel*) or treated with 10ng/ml of TGF-β for 48h (*bottom panel*). Scale bars: 100 µm.

Importantly, RT-qPCR analysis and immunoblot analysis revealed that KHSRP expression (both mRNA and protein) was silenced in a time-dependent manner in response to TGF-β (*Figure 15*), while its levels were restored when TGF-β was removed from the culture medium of cells previously exposed for 7 days to TGF-β (*Figure 16*).

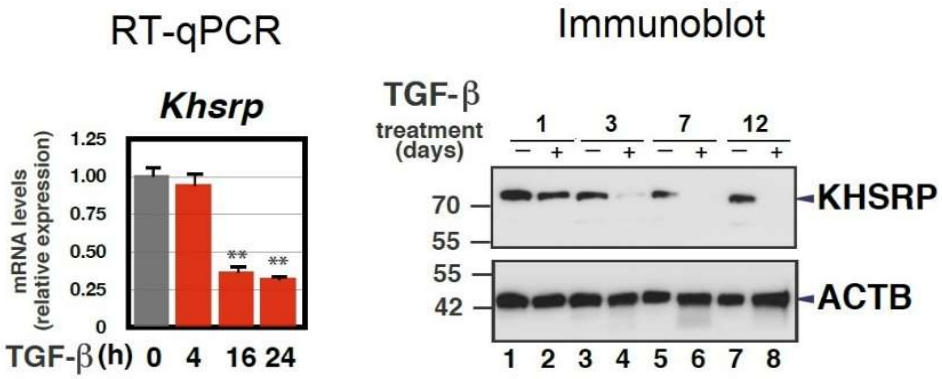

Figure 15; *Left panel*. RT-qPCR analysis of Khsrp in NMuMg either untreated (-) or treated (+) with TGF-β for the indicated times. The values of RT-qPCR experiments shown are averages ± SEM of three independent experiments performed in triplicate. Statistical significance: **p < 0.001 (Student's t-test).
Right panel. Immunoblot analysis of total cell extracts from NMuMg cells serum-starved and either treated with TGF-β (+) for the indicated times or untreated (-). The indicated antibodies were used.

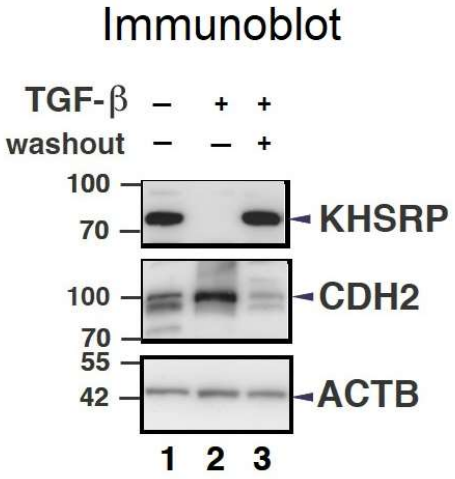

Figure 16; Immunoblot analysis of total cell extracts from NMuMg cells untreated (lane 1), treated with TGF-β for 7 days (lane 2), or treated with TGF-β for 7 days and then cultured in normal growth medium for 5 days (lane 3). The indicated antibodies were used. Representative gels are shown.

RT-qPCR analysis of nascent transcripts showed that TGF-β produces a limited change in *Khsrp* transcription (*Figure 17*) thus prompting us to investigate a post-transcriptional mechanism for TGF-β-dependent KHSRP silencing.

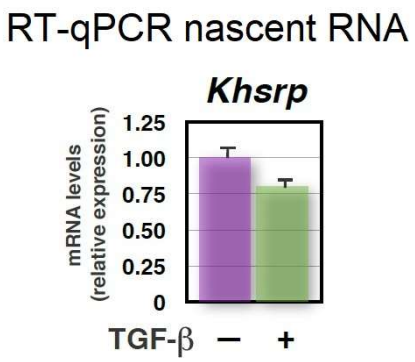

Figure 17; RT-qPCR analysis of nascent *Khsrp* transcript Click-iT (see the '*Experimental Procedures*') in NMuMg cells either untreated (-) or treated with TGF-β for 24h (+). The values of RT-qPCR experiments shown are averages ± SEM of three independent experiments performed in triplicate.

We focused on miRNAs as potential regulators of KHSRP expression in response to TGF-β. A genome-wide deep RNA sequencing (RNA-seq) analysis performed on the small RNA population (see below) revealed that two miRNAs, miR-27b-3p and miR-181a, are induced by TGF-β in NMuMg cells with timing compatible with KHSRP downregulation (*Figure 18*).

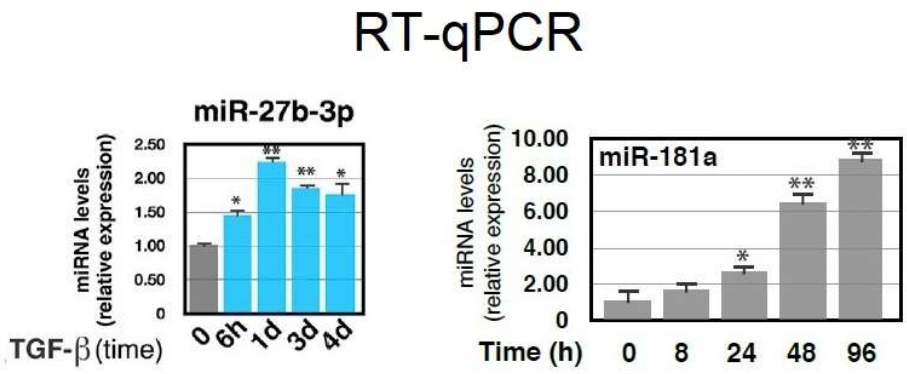

Figure 18; *Left panel.* RT-qPCR analysis of miR-27b-3p in NMuMg cells treated with TGF-β for the indicated times. *Right panel*. RT-qPCR analysis of miR-181a in serum-starved NMuMg cells TGF-β-treated for the indicated times. The values of RT-qPCR experiments shown are averages ± SEM of three independent experiments performed in triplicate. Statistical significance: *p < 0.01, **p < 0.001 (Student's t-test).

It was previously reported that both miR-27b-3p and miR-181a target KHSRP and modulate its expression (Zhou et al., 2012; Sundaram et al., 2013). Thus, we hypothesized that a similar regulatory pathway was operative also in NMuMg cells. In order to verify this hypothesis, we investigated if manipulations of the levels of miR-27b-3p and miR-181a were able to affect KHSRP expression levels. We overexpressed the

two miRNAs in NMuMg cells through transient transfections of either miR-27b-3p mimic or miR-181a mimic (*Figure 19*). Interestingly, miR-27b-3p overexpression caused KHSRP downregulation in NMuMg cells, while miR-181a did not produce any effect (*Figure 20*).

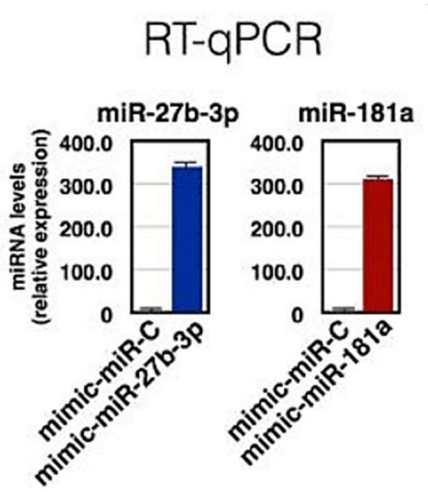

Figure 19; RT-qPCR analysis of miR-27b-3p and miR-181a in control (mimic-miR-C), mimic-miR-27b-3p, and mimic-miR-181a transfected NMuMg cells. The values of RT-qPCR experiments shown are averages ± SEM of three independent experiments performed in triplicate.

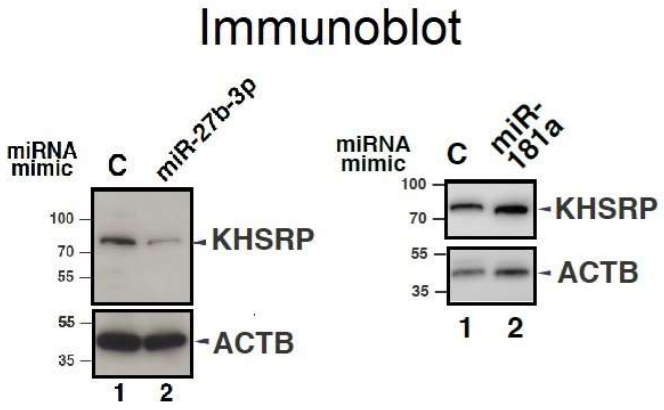

Figure 20; *Left panel*. Immunoblot analysis of total cell extracts (20 µg) from either control- (mimic-miR-C) or mimic-miR-27b-3p- transfected NMuMg cells.
Right panel. Immunoblot analysis of total cell extracts (20 µg) from either control- (mimic-miR-C) or mimic-miR-181a-transfected NMuMg cells.
The indicated antibodies were used. The position of molecular mass markers is indicated on the left of each immunoblot. Representative gels are shown.

Further, we transiently silenced miR-27b-3p expression and we demonstrated that miR-27b-3p silencing prevented TGF-β-induced KHSRP downregulation (*Figure 21*).

Altogether, these results indicate that KHSRP is silenced by miR-27b-3p in mammary gland cell lines that undergo EMT in response to TGF-β.

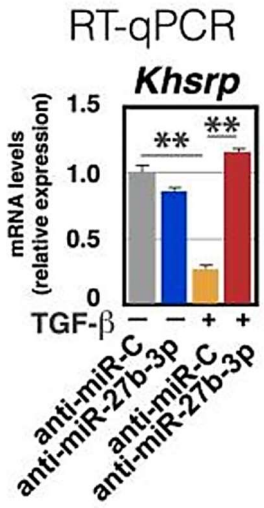

Figure 21; RT-qPCR analysis of *Khsrp* mRNA in either control (anti-miR-C) or anti-miR-27b-3p transfected NMuMg cells either untreated (-) or treated (+) with TGF-β for 24h. The values of RT-qPCR experiments shown are averages ± SEM of three independent experiments performed in triplicate. Statistical significance: **p < 0.001 (Student's t-test).

The observation that TGF-β causes KHSRP silencing was extended to other mammary epithelial cell lines known to undergo EMT in response to TGF-β treatment, such as human non-tumorigenic MCF 10A, human non-transformed mammary epithelial (HMLE) cells, and murine Py2T cells (*Figure 22*).

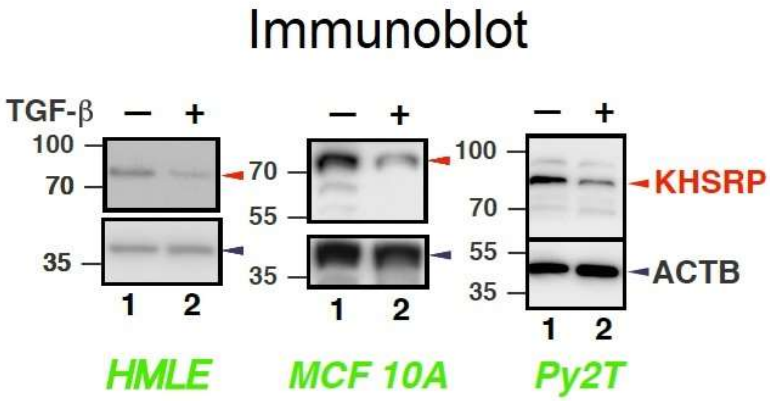

Figure 22; Immunoblot analysis of total cell extracts (20 µg) from HMLE, MCF 10 A, and Py2T cells, serum-starved and either treated with TGF-β (+) for 5 days or untreated (-). The position of molecular mass markers is indicated on the left of each immunoblot. Representative gels are shown.

Conversely, TGF-β did not reduce KHSRP expression in breast cancer cell lines that display a limited EMT response to TGF-β such as MDA-MB-231, 4T1, TS/A, HMLER, and MCF7 (*Figure 23* and data not shown). MDA-MB-231, MCF7 and HMLER are human mammary cells, while 4T1 and TS/A are murine mammary cells. All these cell lines are models of advanced stage of tumor transformation, and some of them have strong invasive properties.

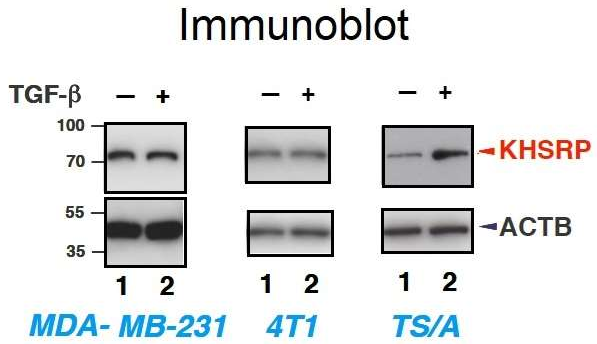

Figure 23; Immunoblot analysis of total cell extracts (20 µg) from MDA-MB-231, 4T1, and TS/A cells, serum-starved and either treated with TGF-β (+) for 3 days or untreated (-). The position of molecular mass markers is indicated on the left of each immunoblot. Representative gels are shown.

2. Forced KHSRP expression prevents TGF-β-induced EMT and reprograms the transcriptome of NMuMg cells

We decided to investigate whether KHSRP downregulation is required for TGF-β-induced EMT and, to this purpose, we manipulated KHSRP expression levels. We transiently overexpressed KHSRP cloned in an adenoviral vector (AdKHSRP) in order to maintain constant its levels during TGF-β treatment in NMuMg cells (*Figure 24*), and analyzed the expression of some factors known as hallmarks of EMT induction. As shown in *Figure 25*, KHSRP overexpression significantly impaired the TGF-β-dependent induction of *Snai1*, *Fn1* and *Cdh2* mRNAs as well as the expression of CDH2 protein when compared to control-infected (AdNull) cells.

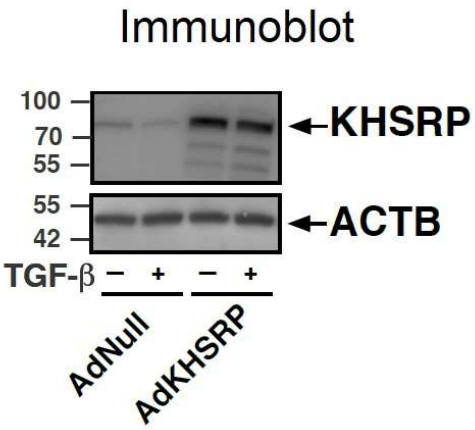

Figure 24; Immunoblot analysis of total cell extracts (20 µg) from NMuMg cells infected with either control (Ad-Null) or KHSRP-expressing (AdKHSRP) adenoviral vectors for 24h and subsequently serum-starved and either treated with TGF-β (+) for 24h or untreated (-). The indicated antibodies were used. The position of molecular mass markers is indicated on the left. Representative gels are shown.

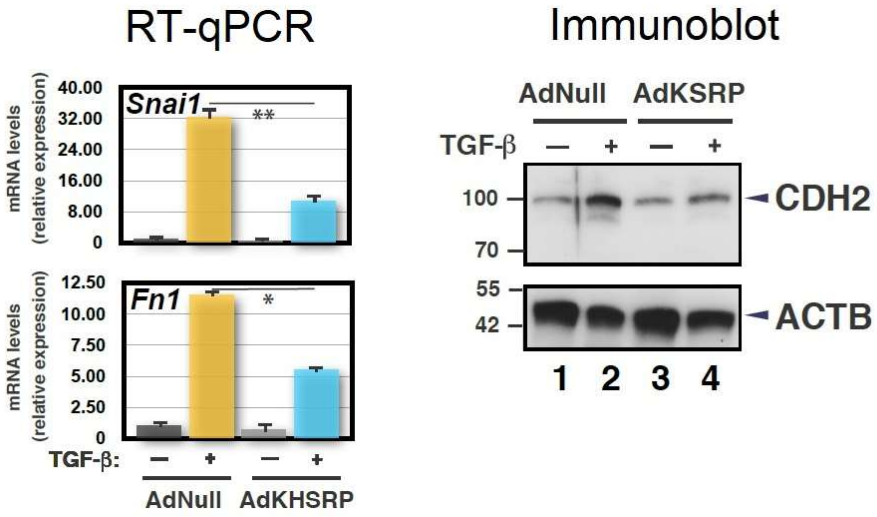

Figure 25; *Left panel*. RT-qPCR analysis of the indicated transcripts in NMuMg cells infected with either control (AdNull) or KHSRP-expressing (AdKHSRP) adenoviral vectors for 24h and subsequently serum-starved and either treated with TGF-β (+) for 24h or untreated (-).
Right panel. Immunoblot analysis of total cell extracts from cells treated as in *left panel*. The indicated antibodies were used. The position of molecular mass markers is indicated on the left. Representative gels are shown.

In order to investigate the changes induced in the whole transcriptome by sustained KHSRP expression, we performed RNA-seq analyses. The results of the bioinformatic analyses of RNA-seq data are accessible at NCBI SRA: SRP074885 and NCBI SRA: SRP070690. Gene Ontology (GO) enrichment analysis of RNA-seq data revealed that KHSRP-regulated transcripts were mainly involved in cell adhesion, cell motility/migration, and cytokine/receptor interaction (*Figure 26*).

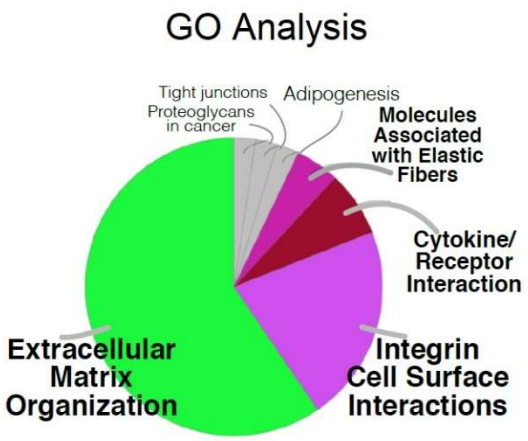

Figure 26; Gene Ontology (GO) analysis. RNA isolated from either AdNull- or AdKHSRP- expressing and TGF-β-treated NMuMg cells was subjected to RNA-seq analysis. Genes showing a log2-fold change >1.5 in the biological triplicates were used for GO analysis, and the enrichment of the KHSRP-regulated pathways are presented as pie graph.

The RT-qPCR-based validation of some of the RNA-seq data showed that KHSRP overexpression counteracts the TGF-β-dependent induction of transcripts relevant to collagen metabolism (e.g. *Col12a1* and *Col6a2*), cell adhesion (e.g. *Iglon5*), TGF-β signaling (e.g. *Fstl1*), extracellular matrix organization (e.g. *Adamtsl2*, *Gpc6* and *Wisp2*), cytokine-receptor interaction (e.g. *Ccl17*), and glycosaminoglycan metabolism (e.g. *Chst1*) (*Figure 27*). A detailed list of the expression levels of these transcripts in NMuMg in different contexts is presented in *Table 2* at the end of the '*Results'* section.

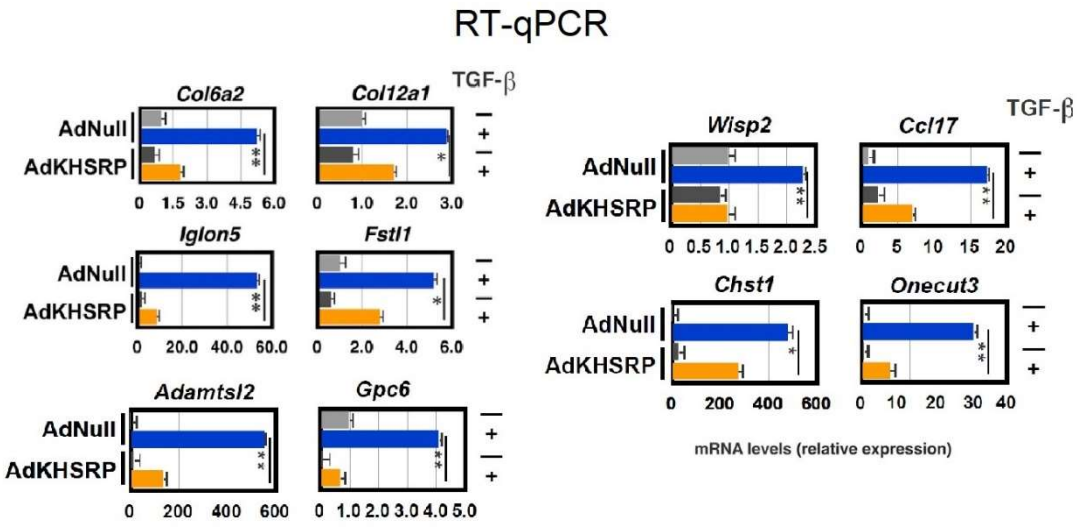

Figure 27; RT-qPCR analysis of the indicated transcripts in cells treated in NMuMg cells infected with either control (AdNull) or KHSRP-expressing (AdKHSRP) adenoviral vectors for 24h and subsequently serum-starved and either treated with TGF-β (+) for 24h or untreated (-).

Next, we verified if, as a consequence of KHSRP-induced changes in the expression of genes involved in cell adhesion and motility, KHSRP overexpression affected the migratory proprieties of NMuMg cells in comparison to control cells. We performed scratch wound assays in both cell lines and, in agreement with transcriptomic changes, we found that KHSRP overexpression in TGF-β-treated cells reduces the size of the wound closure when compared to negative control cells (*Figure 28*).

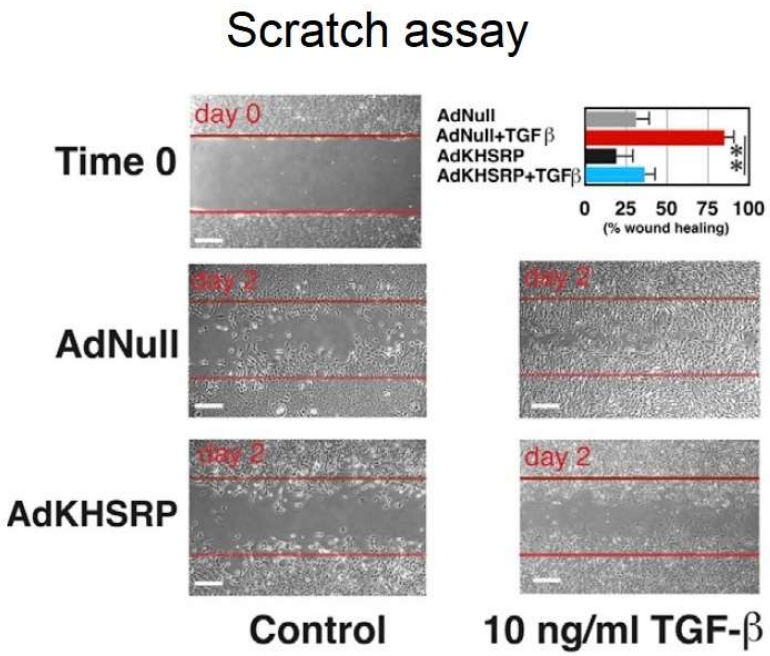

Figure 28; Scratch wound healing assay. NMuMg cells were cultured as described in '*Experimental Procedures'* section and scratch wounds were introduced into confluent monolayers. Cultures were photographed and the width of the wound was measured at 0h and 48h after the scratch was made. The percentage of the wound healed area for each culture condition was plotted (top right bar graph). Representative images are shown. Scale bars represent 100 mm.

Finally, miR-27b-3p downregulation, similar to KHSRP overexpression, prevented TGF-β-dependent induction of *Snai1*, *Fn1*, *Cdh2*, *Zeb1*, and *Zeb2* gene expression (*Figure 29* and *Table 2*).

Together, our results indicate that sustained KHSRP expression impairs the TGF-β-dependent induction of factors related to cell adhesion and motility and suggest that TGF-β-induced KHSRP silencing is required to enable NMuMg cells to acquire migratory properties.

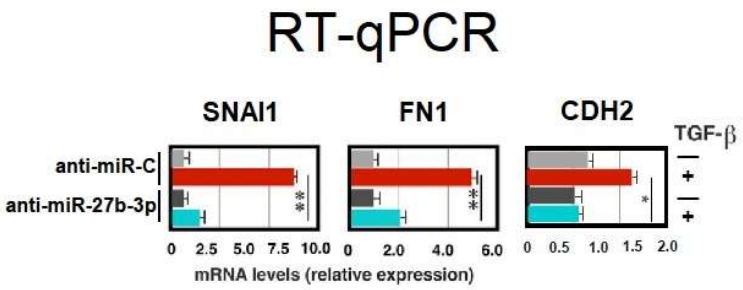

Figure 29; RT-qPCR analysis of the indicated transcripts in NMuMg cells transfected with either control anti-miRNA (anti-miR-C) or anti-miR-27b-3p and subsequently serum-starved and either treated with TGF-β (+) for 36h or untreated (-). The values of RT-qPCR experiments shown are averages (±SEM) of three independent experiments performed in triplicate. Statistical significance: *p < 0.005, **p < 0.001 (Student's t-test).

3. KHSRP knockdown mimics the phenotype of TGF-β-induced EMT

In order to unambiguously establish the role of KHSRP silencing as a key step in TGF-β-induced EMT, we stably knocked-down KHSRP (shKHSRP) in NMuMg cells (*Figure 30*).

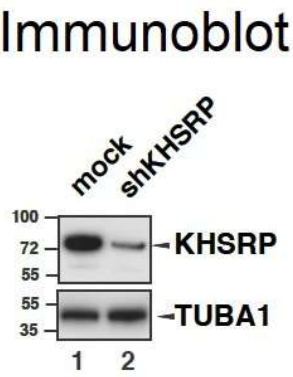

Figure 30; Immunoblot analysis of total cell extracts (20 µg) from either mock or shKHSRP NMuMg cells. The indicated antibodies were used. The position of molecular mass markers is indicated on the left of each immunoblot. Representative images are shown.

Analyzing the gene expression pattern of these cells, we found that shKHSRP mimics the effect of TGF-β increasing the expression of EMT-related factors, such as *Snail1*, *Fn1*, *Col6a2*, *Col12a1*, *Iglon5*, *Fstl1*, *Cd44*, and *Itga9* (*Figure 31* and *Table 2*).

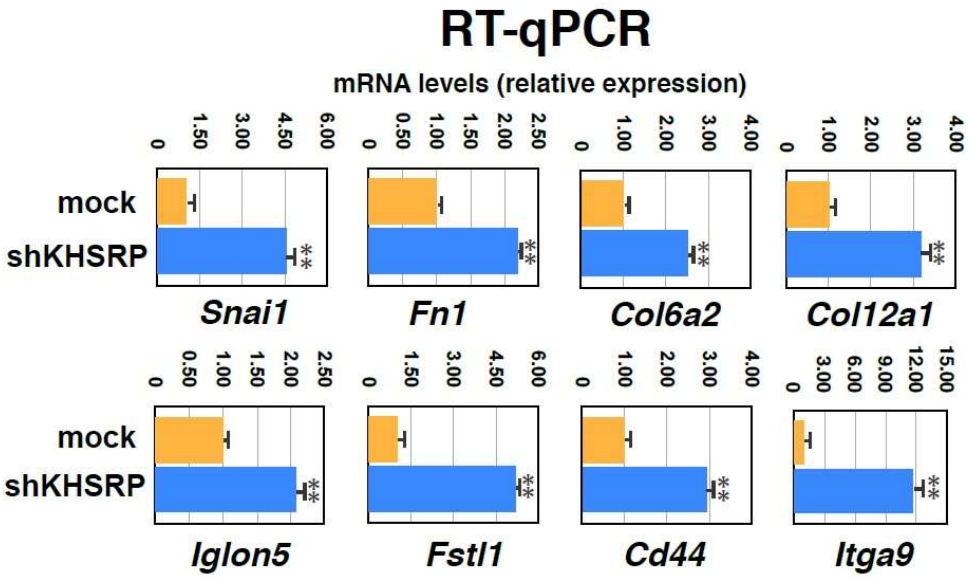

Figure 31; RT-qPCR analysis of the indicated transcripts in either mock or shKHSRP NMuMg cells that were serum-starved and then either treated with TGF-β for 24h (+) or untreated (-). The values of RT-qPCR experiments shown are averages ± SEM of three independent experiments performed in triplicate. Statistical significance: **p < 0.001 (Student's t-test).

In agreement with a role of miR-27b-3p in TGF-β-dependent KHRSP down-regulation, we found that the forced miR-27b-3p expression induces the expression of some of critical EMT factors similar to KHSRP knockdown (*Figure 32* and *Table 2*).

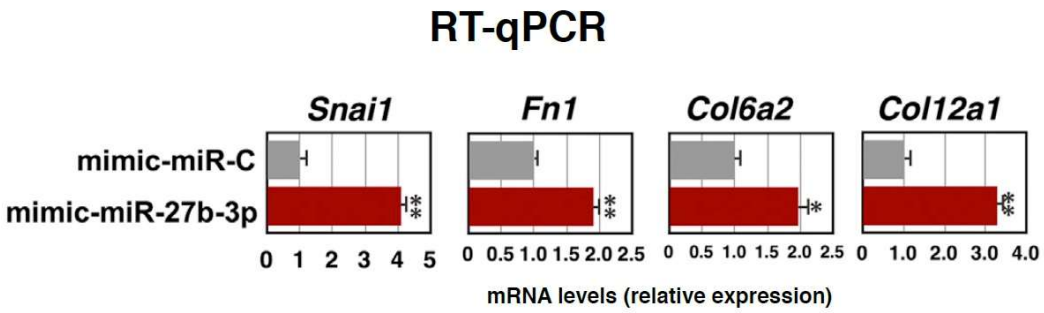

Figure 32; RT-qPCR analysis of the indicated transcripts in either control miRNA mimic (mimic-miR-C) or mimic-miR-27b-3p-transfected NMuMg cells. The values of RT-qPCR experiments shown are averages ± SEM of three independent experiments performed in triplicate. Statistical significance: *p < 0.01, **p < 0.001 (Student's t-test).

We also found that KHRSP silencing in NMuMg cells leads to changes on cell motility and morphology. Scratch wound assays showed that KHSRP knockdown accelerates the wound closure in both control and TGF-β-treated cells (*Figure 33*).

Moreover, transwell migration assays confirmed the evidence that KHSRP silencing enhances the migratory potential of NMuMg cells (*Figure 34*).

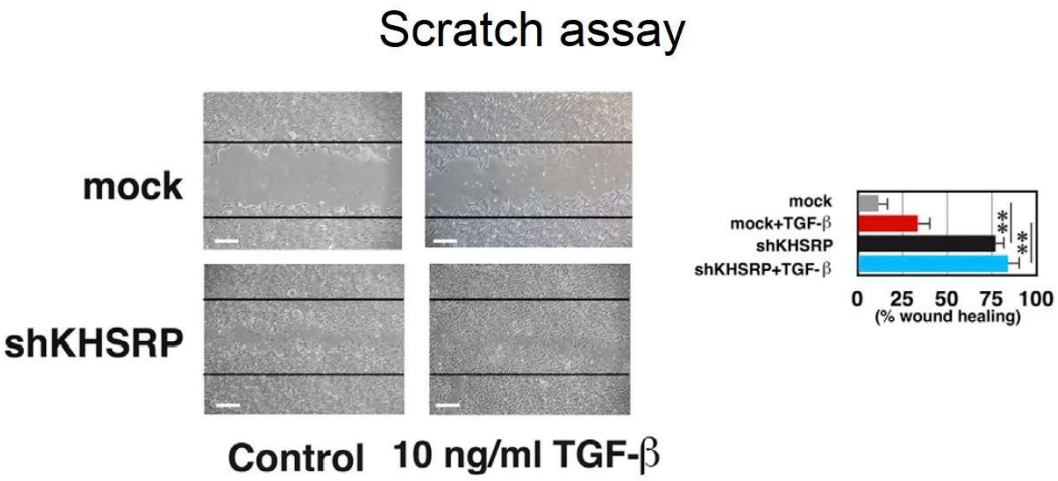

Figure 33; Scratch wound healing assay. Either mock or shKHSRP NMuMg cells were serum-starved and then either treated with TGF-β or untreated. Scratch wounds were introduced into confluent monolayers. Cultures were photographed and the width of the wound was measured at 48h after the scratch was made (*left panel*). The percentage of the wound healed area for each culture condition was plotted in a bar graph (*right panel*). Representative images are shown. Scale bars represent 100 mm.

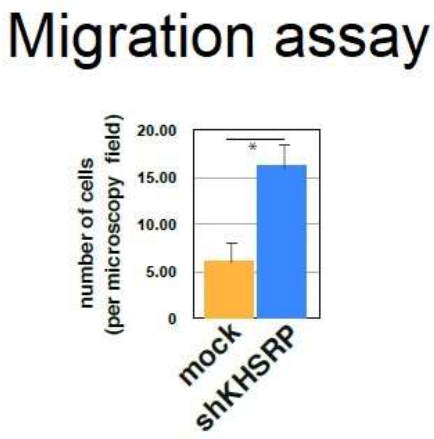

Figure 34; Either mock or shKHSRP NMuMg cells were seeded in the upper chamber of a 24-well transwell migration insert and migration was quantitated by DAPI staining after 48h using a fluorescent microscope. Images were analyzed using *ImageJ* software.

In agreement with the evidence that miR-27b-3p targets KHSRP (Yao et al., 2016) and induces gene expression changes similar to the effect of KHSRP silencing, we found that the transient miR-27b-3p overexpression in NMuMg cells caused the

appearance of increased migration areas in scratch wound assays similar to KHSRP knockdown (*Figure 35*).

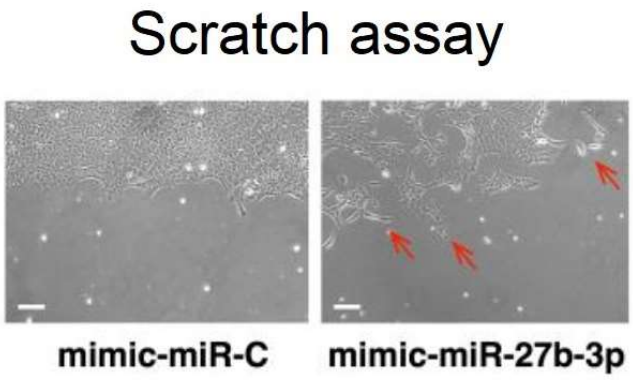

Figure 35; Scratch wound healing assay. NMuMg cells were transiently transfected with either control (mimic-miR-C) or mimic-miR-27b-3p and scratch wounds were introduced into confluent monolayers. Arrows point to cell migrating into the wound. Representative images are shown. Scale bars: 100 µm.

Furthermore, KHSRP downregulation mimicked the TGF-β-mediated remodeling of the cytoskeleton from cortical actin to stress fibers as detected by phalloidin staining (*Figure 36*).

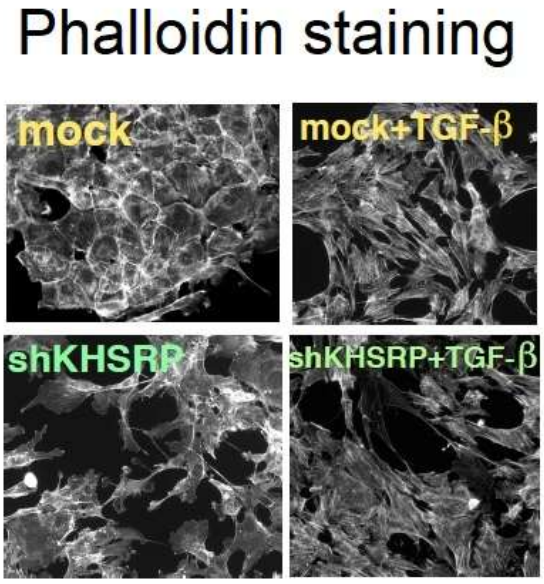

Figure 36; Either mock or shKHSRP NMuMg cells were serum-starved and then either treated with TGF-β or untreated for 48h. Cells were stained using Alexa Fluor 568 Phalloidin to visualize the actin cytoskeleton. Representative images are shown. Scale bars represent 50 mm.

In order to extend our observations to another non-transformed mammary gland cell line, we stably knocked-down KHSRP in Py2T cells (*Figure 37*). Stable KHSRP knockdown mimicked the changes induced by TGF-β also in this cellular context (*Figure 38* and data not shown). Consistently, similar to NMuMg cells, KHSRP overexpression impaired the wound healing in Py2T cells, while its downregulation enhanced the gap closure (*Figure 39* and data not shown).

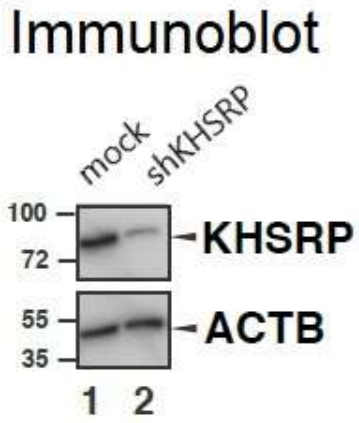

Figure 37; Immunoblot analysis of total cell extracts (20 µg) from either mock or shKHSRP Py2T. The indicated antibodies were used.

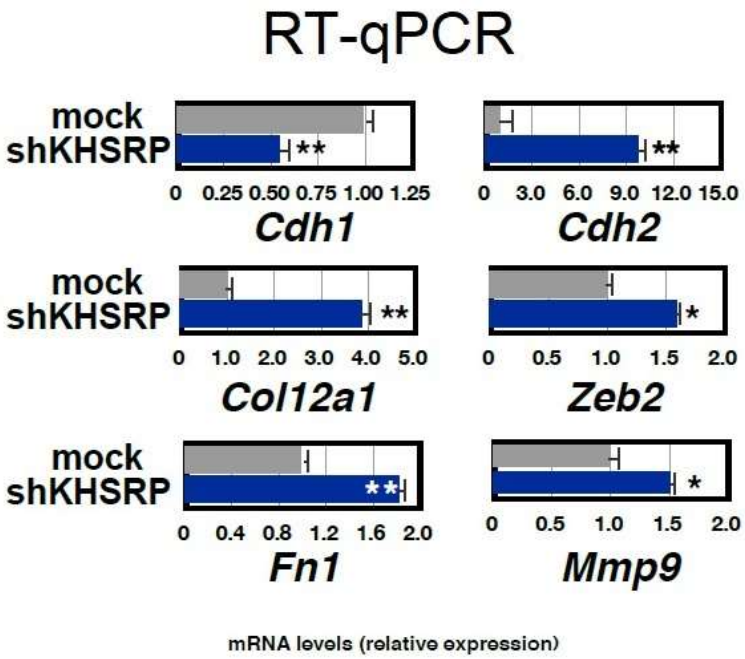

Figure 38; RT-qPCR analysis of the indicated transcripts in either mock or shKHSRP Py2T cells. The values of RT-qPCR experiments shown are averages ± SEM of three independent experiments performed in triplicate. Statistical significance: *p < 0.01, **p < 0.001 (Student's t-test).

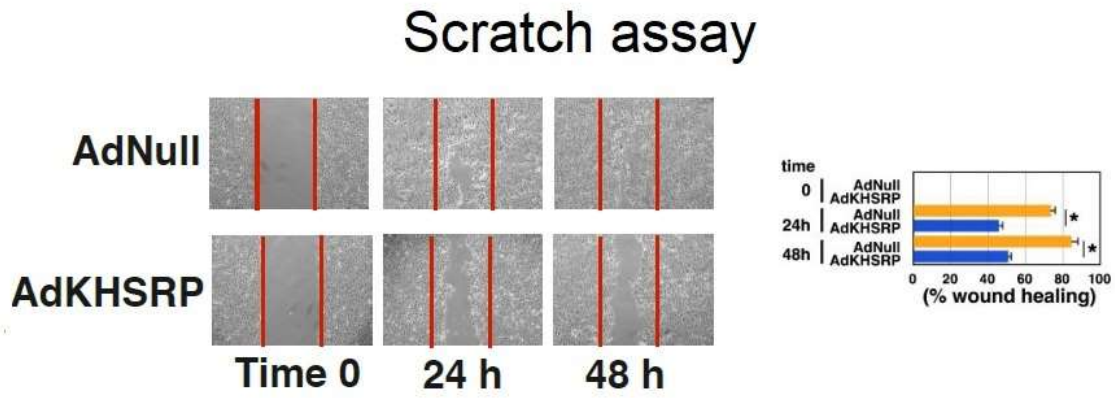

Figure 39; Scratch wound healing assay. Py2T cells were infected with either control (AdNull) or KHSRP-expressing (AdKHSRP) adenoviral vectors for 24 h and scratch wounds were introduced into confluent monolayers. Cultures were photographed 24 h and 48 h after scratch. Time 0 represents initial gap width at 0 h. The percentage of the wound healed area was plotted (*right panel*). Scale bars: 100 µm.

Since EMT that can be reverted, at least in part (Prieto-Garcìa et al, 2017), we explored the possibility that forced KHSRP expression in NMuMg cells that express low KHSRP level (either due to KHSRP silencing or to TGF-β-dependent KHSRP downregulation) is able to revert the phenotypical changes related to EMT (*Figure 40*).

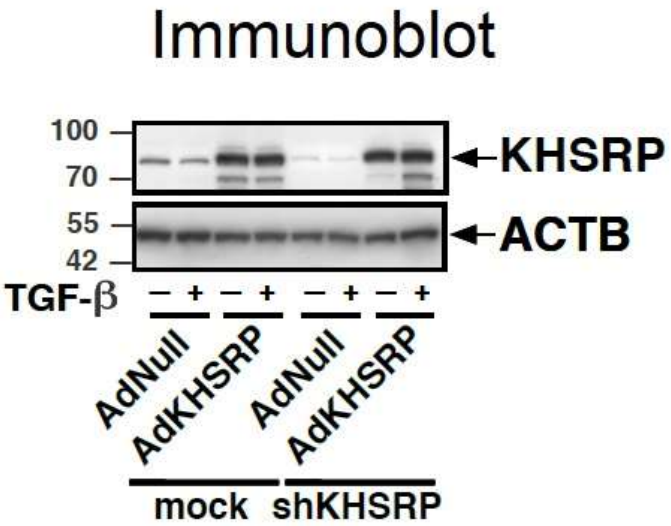

Figure 40; Immunoblot analysis of total cell extracts (20 µg) from either mock or shKHSRP NMuMg cells infected with either control (Ad-Null) or KHSRP-expressing (AdKHSRP) adenoviral vectors for 24h and subsequently serum-starved and either treated with TGF-β (+) for 24h or untreated (-). The indicated antibodies were used.

We found that the transient KHSRP re-expression could revert the EMT-like phenotype of shKHSRP NMuMg cells to the epithelial phenotype (*Figure 41*).

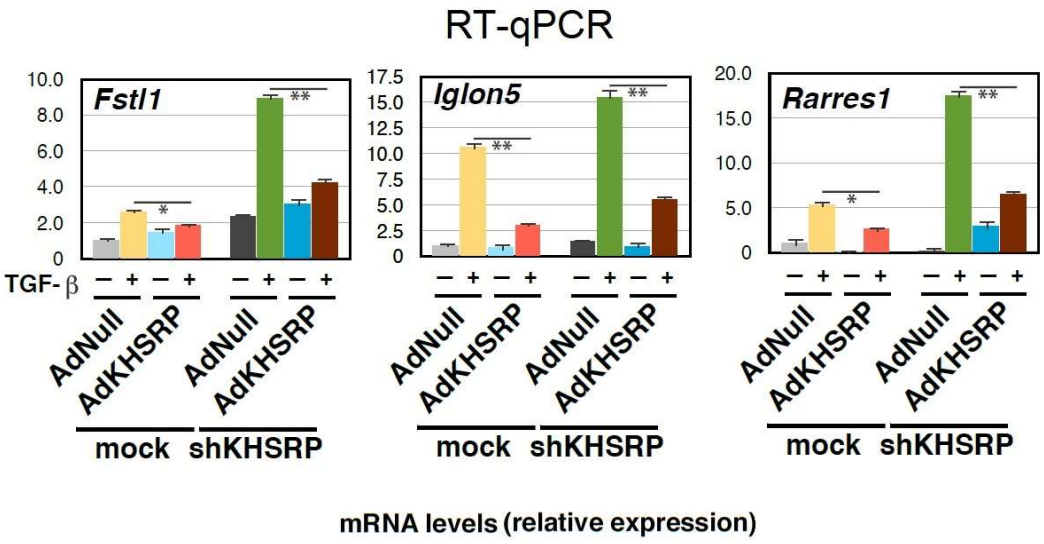

Figure 41; RT-qPCR analysis of the indicated transcripts in either mock or shKHSRP NMuMg cells infected with either control (AdNull) or KHSRP-expressing (AdKHSRP) adenoviral vectors for 24h and subsequently serum-starved and either treated with TGF-β (+) for 24h or untreated (-). The values of RT-qPCR experiments shown are averages (±SEM) of three independent experiments performed in triplicate. Statistical significance: *p < 0.01, **p < 0.001 (Student's t-test).

Most importantly, we showed that cells that achieved an established mesenchymal phenotype through a prolonged treatment with TGF-β reacquire an epithelial phenotype upon KHSRP re-expression and despite the continuous presence of TGF-β (*Figure 42*).

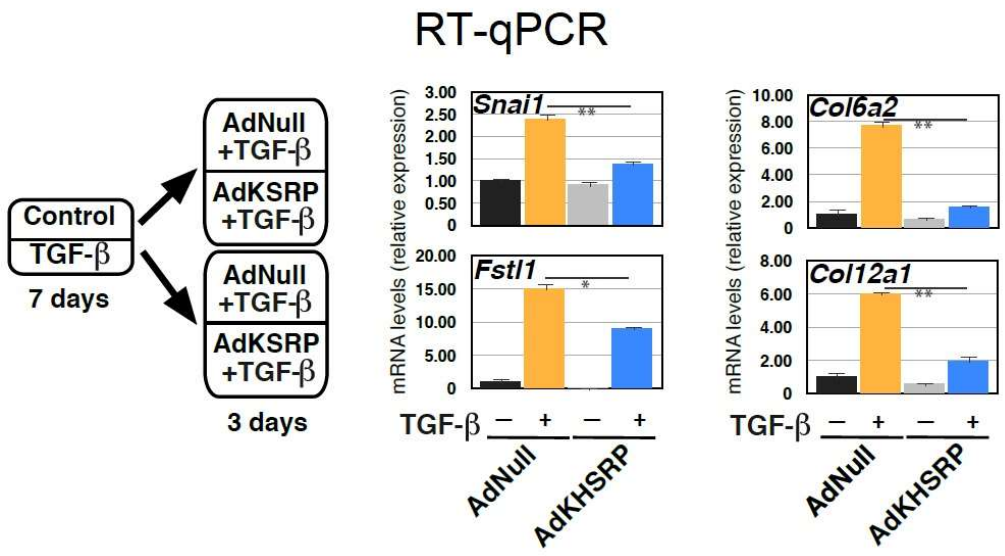

Figure 42; *Left panel.* Schematic of the NMuMg cell treatment. *Right panel.* RT-qPCR analysis of the indicated transcripts in cells treated as summarized in the left panel. The values of RT-qPCR experiments shown are averages ± SEM of three independent experiments performed in triplicate. Statistical significance: *p < 0.01, **p < 0.001 (Student's t-test).

As a whole, these data indicate that KHSRP knockdown in untreated cells induces phenotypic changes that mimic TGF-β-induced EMT thus supporting our hypothesis that KHSRP silencing is a required event for EMT occurring in response to TGF-β.

4. KHSRP-dependent maturation of miR-192-5p prevents the expression of some EMT factors

KHSRP is a ubiquitous protein whose cellular localization varies in distinct cell types (Gherzi et al., 2014). Here, we found that KHSRP is almost exclusively located in the nucleus of mammary gland cells (*Figure 43* and data not shown).

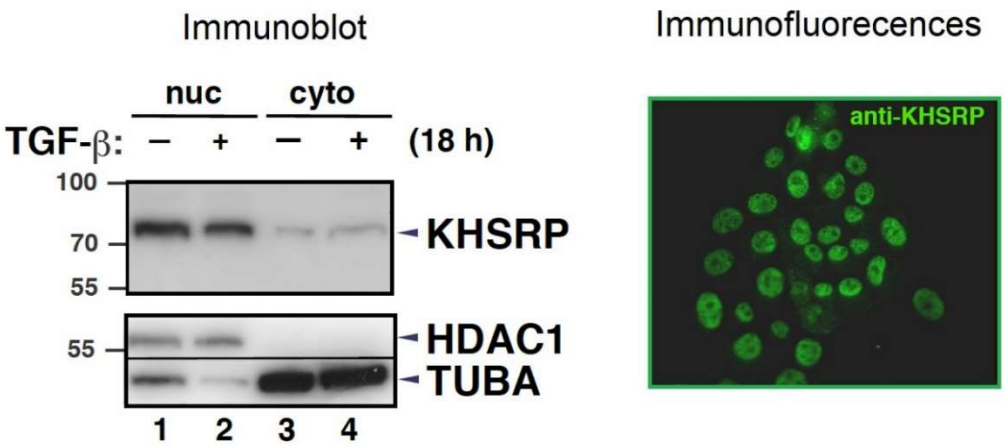

Figure 43; *Left panel.* Immunoblot analysis of either nuclear (nuc) or cytoplasmic (cyto) extracts (20 µg) from NMuMg cells serum-starved and either treated with TGF-β (+) for the indicated time or untreated (-) for 18h. The indicated antibodies were used. The position of molecular mass markers is indicated on the left. Representative gels are shown.
Right panel. Immunofluorescence microscopy analysis of KHSRP localization in NMuMg cells. Scale bars: 50 µm.

In keeping with this finding, KHSRP does not affect the cytoplasmatic decay rates of inherent unstable mRNAs whose steady state levels are regulating by either its overexpression or down-regulation (data not shown).

Either KHSRP silencing in cultured cell line and KHSRP gene knock-down in mice have demonstrated that KHSRP favors miRNA maturation from precursors (reviewed in Briata et al., 2016). To explore the role of KHSRP in TGF-β-controlled miRNA maturation on a transcriptomic scale, we performed an RNA-seq analyses of small RNAs in shKHSRP NMuMg cells as well as in mock-transfected cells as control.

Bioinformatic analysis of small RNA-seq data revealed that KHSRP knockdown significantly reduces the expression of a limited number of miRNAs (33 with p value < 10^{-3} using ANOVA test). Our RT-qPCR-based validation revealed that KHSRP knockdown reduces the expression of miR-192-5p and miR-194-5p without affecting the levels of the corresponding primary transcripts (*Figure 44* and data not shown) thus suggesting that KHSRP is required for the maturation of these miRNAs. Importantly, the levels of miR-192-5p and miR-194-5p were downregulated in the course of TGF-β-induced EMT (*Figure 45*).

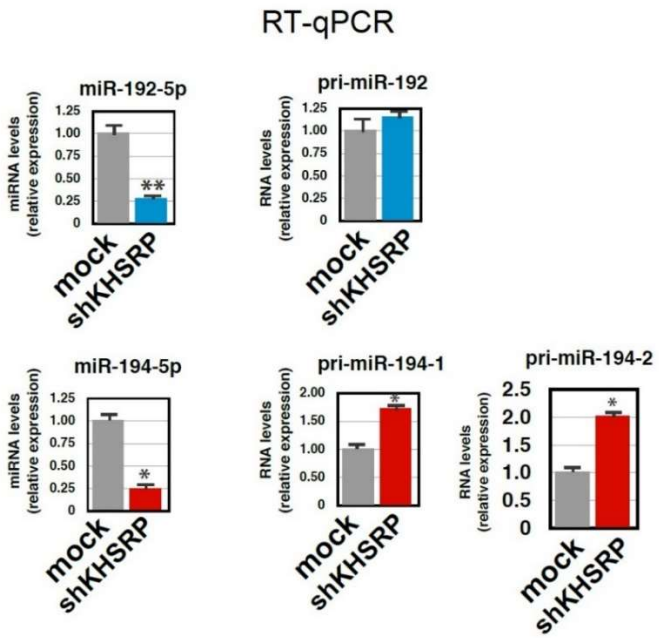

Figure 44; RT-qPCR analysis of the indicated miRNAs or their primary transcripts in either mock or shKHSRP NMuMg cells. The values of RT-qPCR experiments shown are averages ± SEM of three independent experiments performed in triplicate. Statistical significance: *p < 0.01, **p < 0.001 (Student's t-test).

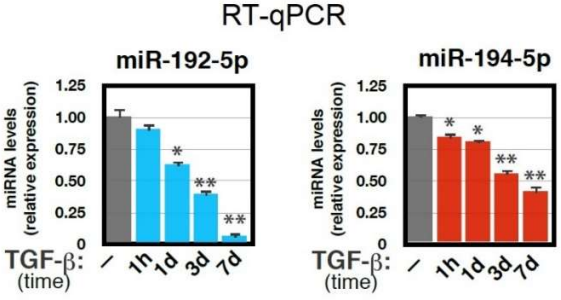

Figure 45; RT-qPCR analysis of the indicated miRNAs in serum-starved NMuMg cells either untreated (/) or treated with TGF-β for the indicated times. The values of RT-qPCR experiments shown are averages ± SEM of three independent experiments performed in triplicate. Statistical significance: *p < 0.01, **p < 0.001 (Student's t-test).

These observations, in addition to the evidence that the expression of miR-192-5p and miR-194-5p inversely correlates with the metastatic potential of different cancer cells (Kim et al., 2011; Geng et al., 2014; Dong et al., 2011; Le et al., 2012), prompted us to investigate whether miR-192-5p and miR-194-5p silencing recapitulates gene expression changes induced by KHSRP silencing. Expression of anti-miR-192-5p in NMuMg cells upregulated *Zeb1*, *Zeb2*, as well as *Snai1*, *Iglon5*, and *Mmp9* expression, while it did not affect *Fstl1* mRNA levels and even caused downregulation of *Fn1*, *Col6a2*, and *Col12a1* (*Figure 46* and *Table 2*). Conversely, expression of anti-miR-194-5p did not affect the expression of EMT factors whose levels are regulated by KHSRP knockdown with the exception of a moderate increase in *Mmp9* expression (*Figure 47* and *Table 2*). The simultaneous silencing of the two miRNAs produced gene expression changes overlapping those caused by miR-192-5p silencing alone (data not shown).

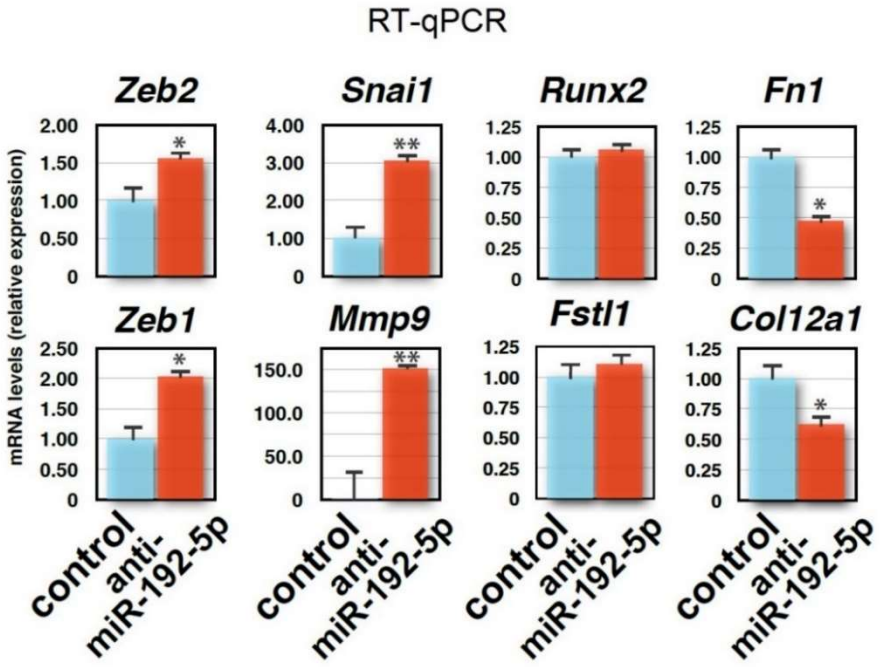

Figure 46; RT-qPCR analysis of the indicated transcripts in NMuMg cells transfected with either miRNA inhibitor negative control or with miRCURY LNA miR-192-5p inhibitor. The values of RT-qPCR experiments shown are averages ± SEM of three independent experiments performed in triplicate. Statistical significance: *p < 0.01, **p < 0.001 (Student's t-test).

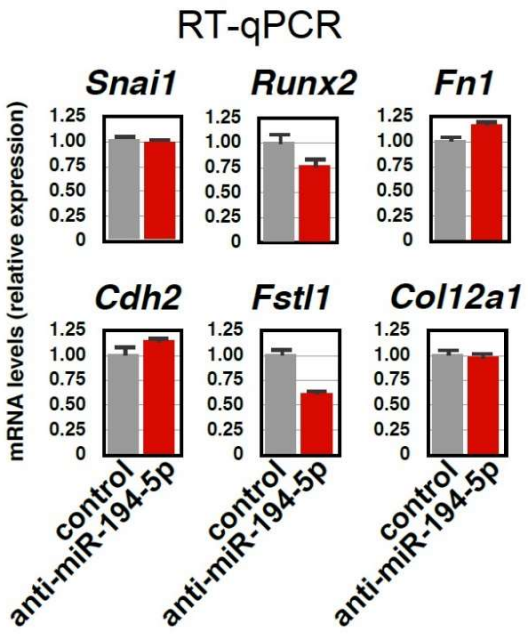

Figure 47; RT-qPCR analysis of the indicated transcripts in NMuMg cells transfected with either miRNA Inhibitor negative control or with miRCURY LNA miR-194-5p Inhibitor (anti-miR-194-5p). The values of RT-qPCR experiments shown are averages (±SEM) of three independent experiments performed in triplicate.

The above data indicate that neither miR-192-5p or miR-194-5p silencing are able to reproduce the whole spectrum of gene expression changes induced by KHSRP downregulation. This fact prompted us to hypothesize that KHSRP silencing during TGF-β-induced EMT impacts on an additional layer of post-transcriptional gene regulation.

5. KHSRP controls alternative splicing of a cohort of pre-mRNAs involved in cell adhesion and migration

Considering that KHSRP mainly localizes in the nuclei of NMuMg cells and that a role of KHSRP in alternative splicing has already been suggested (Min et al., 1997; Russo et al., 2011), we decided to investigate KHSRP potential role in regulatory pre-mRNA alternative splicing in NMuMg cells. To this purpose, we applied a sensitive bioinformatic approach to analyze our RNA-seq results in order to detect genes that are subject to a Differential Exon usage (DEXSeq) (Anders et al., 2012). We identified 763 alternative splicing events (log2 fold changes (FC) >|1.2|, BH (Bonferroni-corrected, two-sided

hypergeometric test) adjusted p value (adj.pval) < 0.01) involving 518 unique Ensembl transcripts that were controlled by KHSRP overexpression. Among the regulated single cassette exons, 412 exons were less included while 351 exons were more included upon KHSRP overexpression. This ratio is similar to those recently reported for other RBPs in a genome-wide analysis of alternative splicing in human cells (Huelga et al., 2012). Furthermore, our findings are in line with the recent evidence suggesting that the modulation of alternative mRNA splicing plays a causative role in EMT (Cieply & Carstens, 2015). Interestingly, GO enrichment analysis revealed that mRNAs whose splicing is affected by KHSRP overexpression are mainly involved in biological processes such as cytoskeleton organization, cell junction assembly, and regulation of small GTPase-mediated signal transduction (*Figure 48*).

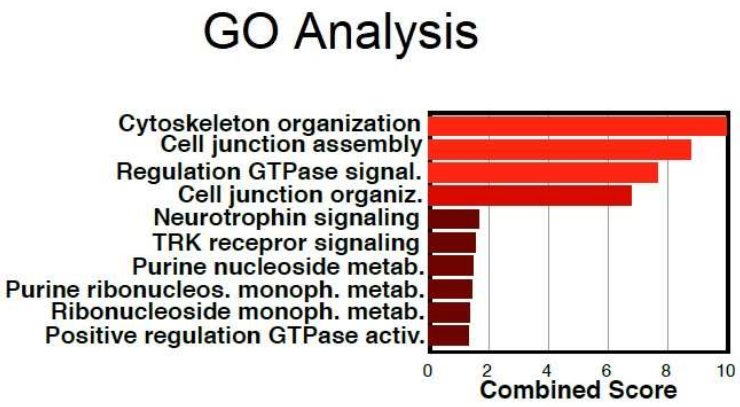

Figure 48; Gene Ontology (GO) analysis was performed on genes subject to differential exon usage (log2 fold changes (FC) > |1.2|, BH adj.pval < 0.01) and the enrichment of the KHSRP-regulated pathways are presented as bar graph.

Among these transcripts, we validated by RT-qPCR some of the KHSRP controlled cassettes utilizing exon-specific primers and focused exclusively on exons that have been proven to generate alternative protein isoforms (according to the Ensembl annotation GRCm38.74; http://www.ensembl.org). Representative examples of transcripts whose alternative splicing is controlled in a KHSRP-dependent way and have subsequently been validated by RT-qPCR analysis are presented in *Figure 49*. Among them *Enah* gene, whose alternative splicing has been previously implicated in EMT (Warzecha et al., 2012), is controlled in a KHSRP-dependent, and we found that KHSRP overexpression significantly increased the ratio between the epithelial-type *Enah6L* isoform and the mesenchymal-type *Enah6* isoform (*Enah6L*/*Enah6*), while KHSRP

knockdown significantly impaired the *Enah6L/Enah6* ratio mimicking TGF-β effect (*Figure 50).*

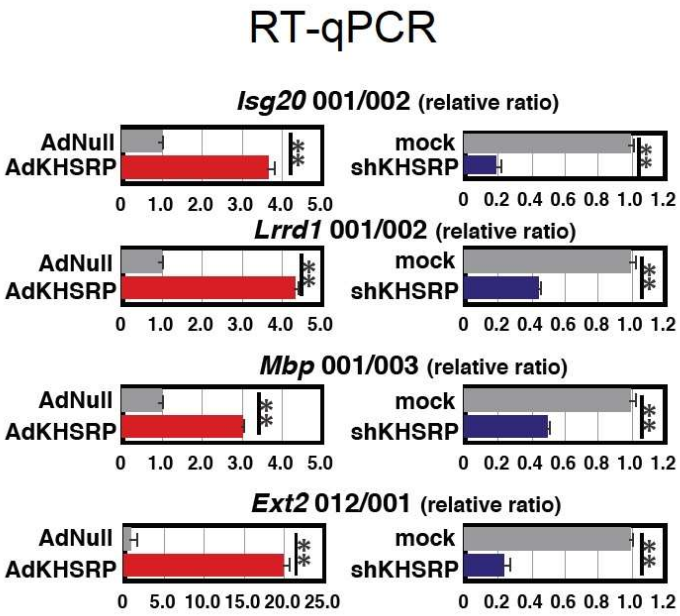

Figure 49; RT-qPCR analysis performed using exon-specific primers. The results are presented as ratio between the expression levels of two alternatively spliced forms of the indicated transcripts (nomenclature of mRNA forms derived from alternative splicing is presented according the Ensembl nomenclature). RNA was extracted from NMuMg cells infected with either control (AdNull) or KHSRP-expressing adenoviral vectors (AdKHSRP) for 24h (*left*) and from either mock or shKHSRP NMuMg cells (*right*).

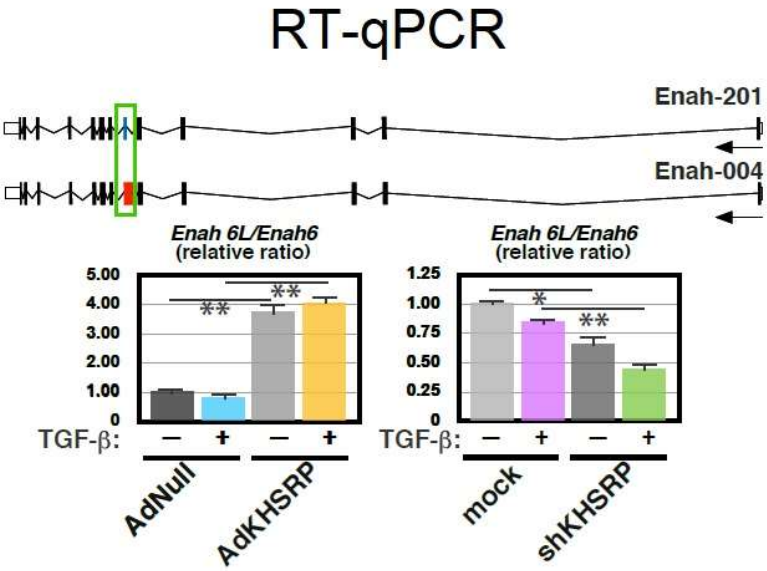

Figure 50; *Top panel*. Schematic of the exon-intron structure (not in scale) of *Enah* mRNA splice variants *201* and *004* (ENSMUSG00000022995). The green open box marks the alternatively spliced *exons 6* and *exon 6L* (in red), respectively.

Bottom panel. RT-qPCR analysis performed using exon-specific primers. The results are presented as ratio between the expression levels of *Enah exon 6L*-including and *exon 6*-including mRNA isoforms. NMuMg cells were infected with either control (AdNull) or KHSRP-expressing adenoviral vectors (AdKHSRP) for 24h and subsequently serum-starved and either treated with TGF-β (+) for 24h or untreated (-) (*left*). Either mock or shKHSRP NMuMg cells were serum-starved and then either treated with TGF-β or untreated for 24h (*right*).

Interestingly, Ribonucleoprotein immunoprecipitation (RIP) analysis followed by RNA deep-sequencing performed in NMuMg cells (Briata & Gherzi, unpublished data) revealed that KHSRP interacts with a number of pre-mRNAs including those encoding CD44 and FGFR2 (Warzecha et al., 2009; Brown et al., 2011) (*Figure 51*; data not shown).

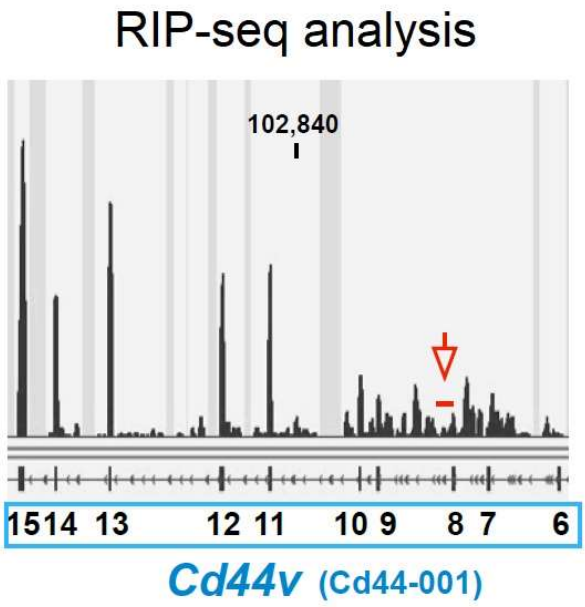

Figure 51; Screenshot from Integrative Genomic Viewer output. RIP-seq analysis revealing that KHSRP interacts with *Cd44* pre-mRNA in NMuMg cells. Arrow points to the region (*intron 8-9*) used as a probe in EMSA experiments.

It has been previously demonstrated that TGF-β treatment induces a shift from the epithelial forms of *Cd44* and *Fgfr2* (*Cd44v* and *Fgfr2 IIIb*, respectively) to the mesenchymal-specific forms (*Cd44s* and *Fgfr2 IIIc*, respectively) that are known to play a causative role in EMT (Warzecha et al., 2009; Brown et al., 2011; Cieply & Carstens, 2015). Although the log2 fold expression changes in the levels of the alternatively spliced *Cd44* and *Fgfr2* cassettes in our differential exon usage analysis of RNA-seq experiments did not reach the stringent cutoff value that we initially established, their expression changes

were statistically relevant (p.adj< 0.01). We found that KHSRP overexpression significantly reduced the ratio between the mesenchymal-type *Cd44*s and the epithelial-type *Cd44v* isoform (*Cd44s*/*Cd44v*), meanwhile KHSRP knockdown significantly enhanced the *Cd44s*/*Cd44v* ratio mimicking TGF-β effect (*Figure 52*). Similarly, KHSRP overexpression favored the inclusion of the *Fgfr2* epithelial-specific exon (*Fgfr2 IIIb*), whereas KHSRP silencing favored the inclusion of the mesenchymal cassette (*Fgfr2 IIIc*) in *Fgfr2* mRNA (*Figure 53*). In addition, we show that KHSRP silencing induced a similar splicing pattern also in Py2T cells (*Figure 54*).

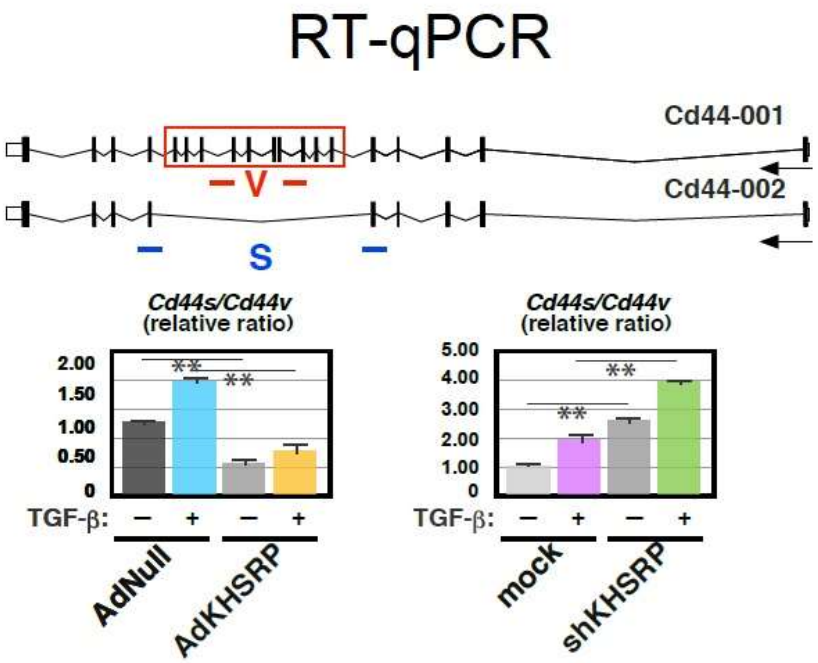

Figure 52; *Top panel.* Schematic of the exon-intron structure (not in scale) of *Cd44* mRNA splice variants 001 and 002 (ENSMUSG00000005087). The red open box marks the alternatively spliced variable exons. The bars mark the position of primers used to detect, by RT-qPCR, the expression levels of variable (*v*) and standard (*s*) exons. *Bottom panel.* RT-qPCR analysis performed using the indicated primers. The results are presented as ratio between the expression levels of *Cd44s* and *Cd44v* mRNA isoforms. NMuMg cells were cultured as described in *Figure 50*. Arrows in the schematics indicate the transcription direction.

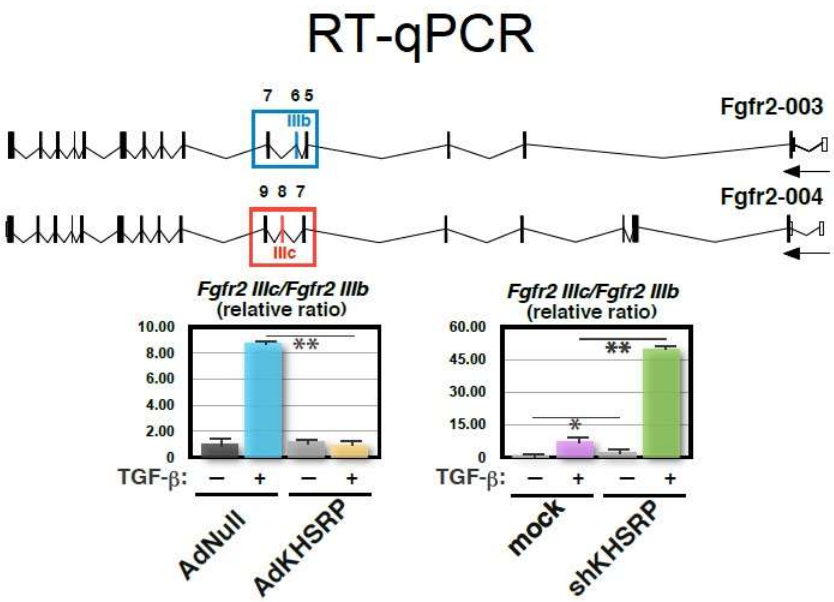

Figure 53; *Top panel.* Schematic of the exon-intron structure (not in scale) of *Fgfr2* mRNA splice variants *003* and *004* (ENSMUSG00000030849). The light blue and red open boxes mark the region including exon *IIIb* (*exon 6* in *Fgfr2-003*) and exon *IIIc* (*exon 8* in *Fgfr2-004*), respectively.
Bottom panel. RT-qPCR analysis performed using exon specific primers. The results are presented as ratio between the expression levels of exon IIIc- and exon IIIb- including mRNA isoforms. NMuMg cells were cultured as described in *Figure 50*. Arrows in the schematics indicate the transcription direction.

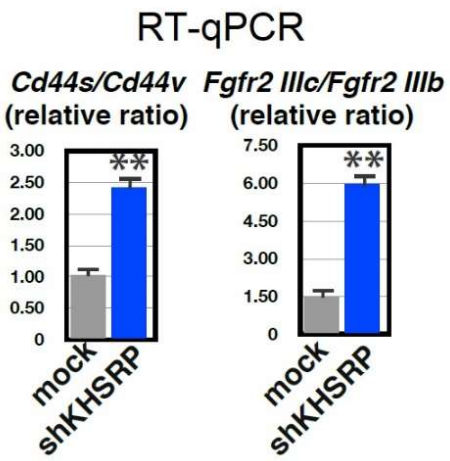

Figure 54; RT-qPCR analysis performed using exon-specific primers in either mock or shKHSRP Py2T cells. The results are presented as ratio between *Cd44s* and *Cd44v* (*left*) and between *Fgfr2 IIIc* and *Fgfr2 IIIb* (*right*). The values of RT-qPCR experiments shown are averages ± SEM of three independent experiments performed in triplicate. Statistical significance: **p < 0.001 (Student's t-test).

Furthermore, when we re-express KHSRP in NMuMg cells that achieved an established mesenchymal phenotype through a prolonged treatment with TGF-β (see *Figure 40* and *Figure 42* shown before), we found that KHSRP expression is able to revert the TGF-β-induced mesenchymal pattern of *Cd44* splicing (*Figure 55*).

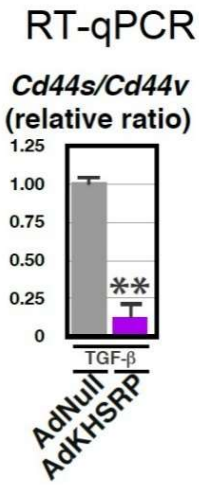

Figure 55; RT-qPCR analysis performed using *Cd44* exon-specific primers in NMuMg cells serum-starved and treated with TGF-β for 7 days and subsequently infected with either AdNull or AdKHSRP and cultured for 3 days in the presence of TGF-β. The results are presented as ratio between *Cd44s* and *Cd44v* forms. The values of RT-qPCR experiments shown are averages ± SEM of three independent experiments performed in triplicate. Statistical significance: **p < 0.001 (Student's t-test).

We finally checked if the modulation of miR-27b-3p expression could affect *Cd44* splicing, and we found that miR-27b-3p overexpression in untreated NMuMg cells mimicked both TGF-β effect and KHSRP silencing by favoring mesenchymal-type splicing pattern of *Cd44* pre-mRNA. Conversely, miR-27b-3p silencing prevented in part the TGF-β-mediated exclusion of variable *Cd44* exons (*Figure 56*).

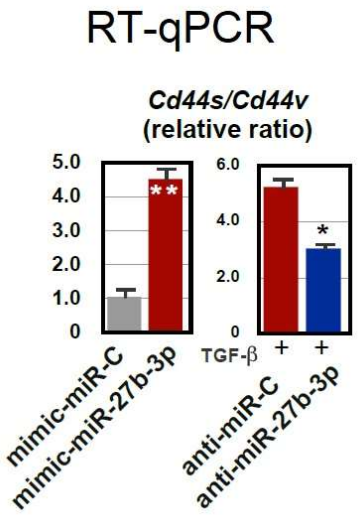

Figure 56; RT-qPCR analysis performed using *Cd44* exon-specific primers in NMuMg cells transiently transfected with either control miRNA mimic (mimic-miR-C) or mimic-miR-27b-3p (*left panel*) as well as in NMuMg cells transiently transfected with either control anti-miRNA (anti-miRC) or anti-miR-27b-3p and treated with TGF-β for 48h (*right panel*). The values of RT-qPCR experiments shown are averages ± SEM of three independent experiments performed in triplicate. Statistical significance: *p < 0.01, **p < 0.001 (Student's t-test).

In order to identify the *Enah*, *Cd44*, and *Fgfr2* pre-mRNA regions that are bound by KHSRP, we probed anti-KHSRP RIP experiments using intron-specific primers for each transcript. These experiments revealed a prominent KHSRP interaction with *Enah intron* 5-6, *Cd44 intron* 8-9, and *Fgfr2 intron* 5-6 (*Figure 57* and data not shown).

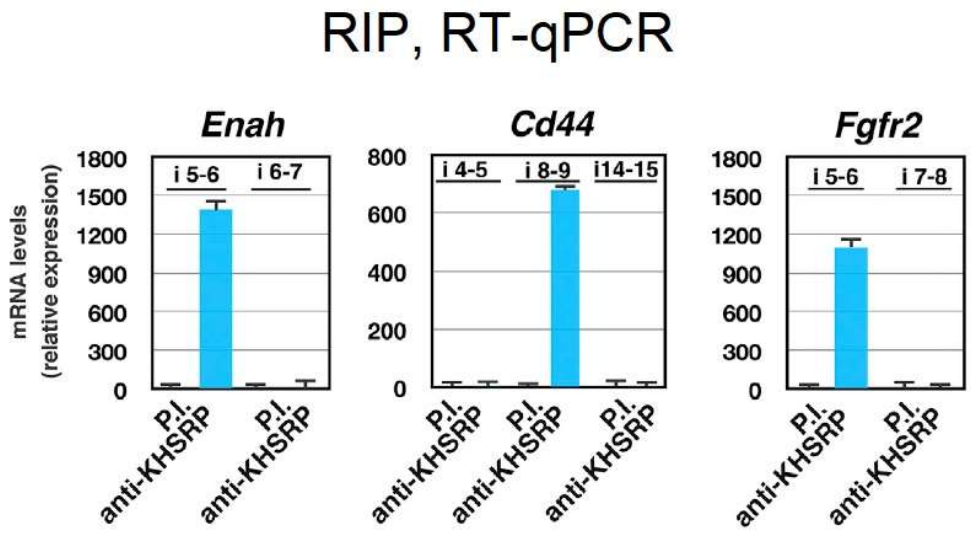

Figure 57; Total extracts from NMuMg cells were immunoprecipitated as indicated. RNA was purified from immunocomplexes and analyzed by RT-qPCR to detect the indicated pre-mRNAs. The values of RT-qPCR experiments shown are averages ± SEM of three independent experiments performed in triplicate.

In agreement with these findings, the *Cd44* region spanning *i8-9* includes a consensus binding motif for KHSRP identified on the basis of HITS-CLIP experiments that have been previously performed in the laboratory (Bucci & Bordo, unpublished data). In addition, we proved the direct interaction of recombinant KHSRP with this region by Electrophoretic mobility shift assay (EMSA) (*Figure 58*).

Further, in order to support a direct regulation of *Cd44* alternative splicing by KHSRP, we transiently expressed a minigene splicing reporter construct including *Cd44* exon *v8* (*Cd44v8*) and its flanking introns in HEK293 cells. *Figure 59* shows that KHSRP interacts with the minigene in RIP experiments, and that KHSRP knockdown favors exon *Cd44v8* skipping as evaluated by RT-qPCR using specific primer sets that amplify exon *Cd44v8*-included and *Cd44v8*-skipped products.

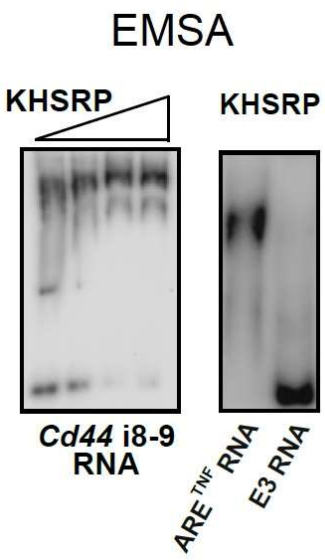

Figure 58; EMSA performed to detect the interaction between highly purified recombinant KHSRP (50–300 nM) with 32P-labeled RNA corresponding to the 5' region of *Cd44* pre-mRNA *intron 8-9* (*left panel*) as well as the interaction between KHSRP (50 nM) with either *ARE*^{TNF} or the inherently stable *E3* control RNA as indicated (*right panel*). Representative autoradiograms are displayed.

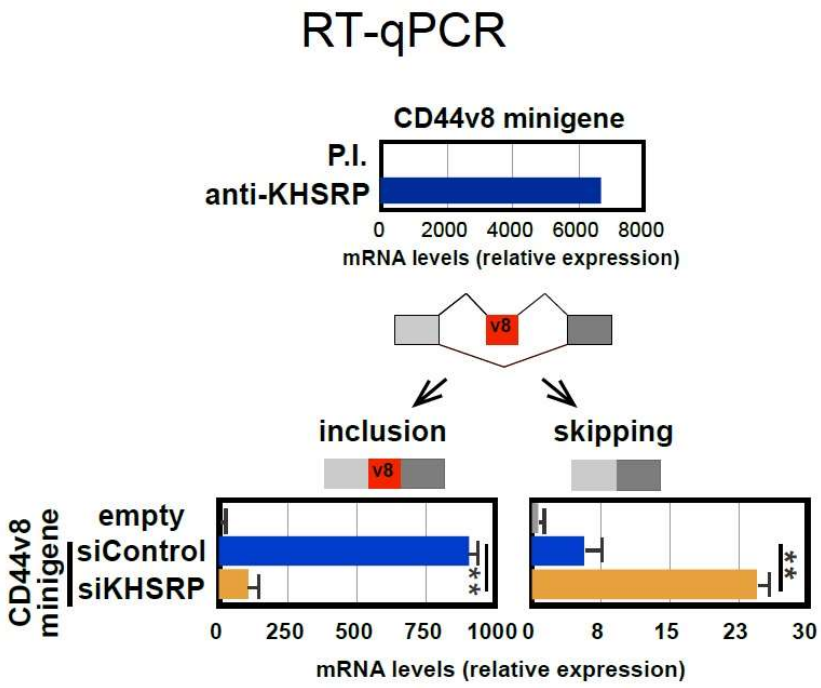

Figure 59; *Top panel*. Total extracts from HEK 293 cells transfected with the *Cd44v8* minigene (see *Experimental Procedures* section) were immunoprecipitated as indicated. RNA was purified from immunocomplexes and analyzed by RT-qPCR to detect the RNA transcribed from the minigene.
Mid panel. Schematic of the *Cd44v8* minigene construct. The *v8* exon and its flanking introns are inserted between two constitutive exons.
Bottom panel. RT-qPCR analysis performed on RNA extracted from HEK293 cells co-transfected with the *v8* minigene and either control siRNA (siControl) or KHSRP-specific siRNA (siKHSRP).
The values of RT-qPCR experiments shown are averages (±SEM) of three independent experiments performed in triplicate. Statistical significance: *p <0.01, **p < 0.001 (Student's t-test).

Altogether, our results indicate that KHSRP influences the alternative splicing of a group of pre-mRNAs encoding factors involved in cell-cell and cell-matrix interactions as well as in cell migration.

6. KHSRP and hnRNPA1 cooperate to maintain the epithelial-type pre-mRNA splicing pattern of Enah, Cd44, and Fgfr2

In the last few years, ribonucleoprotein complexes that involve multiple regulatory RBPs able to modulate alternative splicing have been studied in detail (Aparicio et al., 2013; Fu & Ares 2014; Cieply & Carstens, 2015). We wanted to explore whether KHSRP associates with other RBPs that are able to control alternative splicing events in EMT. It is well known that ESRP1 and ESRP2, here collectively indicated as ESRPs, are critical coordinators of an epithelial cell-type-specific splicing program in different cellular contexts (Warzecha et al., 2009; Bebee et al., 2015). We found that KHSRP co-immunoprecipitates with ESRPs in 4T1 mammary gland cells, and that this association is RNA-independent because RNase A treatment does non abrogate this association (*Figure 60*). Furthermore, KHSRP and ESRPs share similar pre-mRNA targets in 4T1 cells, such as *Enah*, *Cd44* and *Fgfr2b* pre-mRNAs (*Figure 61* and data not shown).

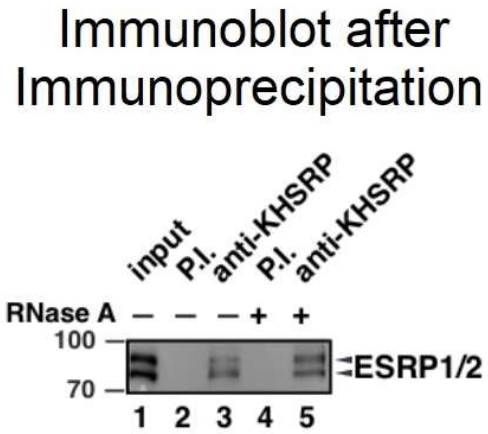

Figure 60; Co-immunoprecipitation of ESRPs and KHSRP in total extracts from 4T1 mammary gland cells. Cell lysates either control-treated or treated with RNAse A (10 µg/ml for 30 minutes at 37°C) were immunoprecipitated as indicated and analyzed by immunoblotting using anti-ESRP1/ESRP2 monoclonal antibody. The position of molecular mass markers is indicated on the left of each immunoblot. Representative images are shown.

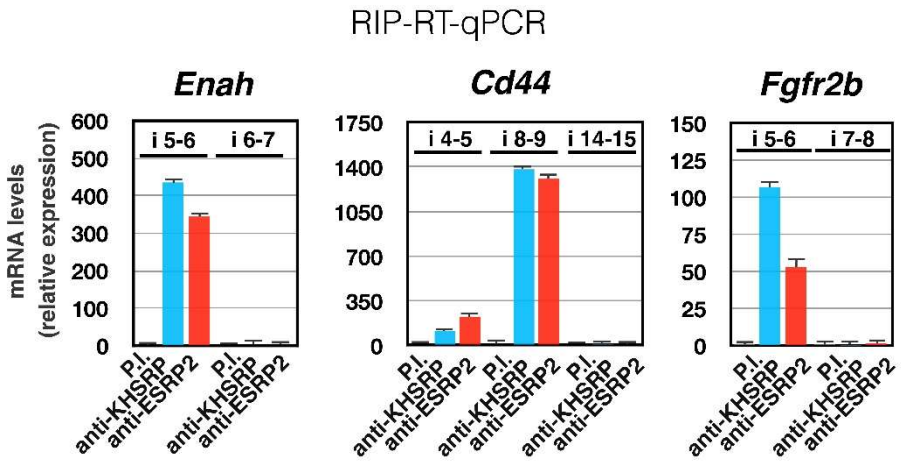

Figure 61; Total extracts from 4T1 cells were immunoprecipitated as indicated. RNA was purified from immunocomplexes and analyzed by RT-qPCR to detect the indicated pre-mRNAs. The values of RT-qPCR experiments shown are averages (±SEM) of three independent experiments performed in triplicate.

However, we found that ESRP1 is not expressed in NMuMg cells, while ESRP2 protein is expressed at low levels (data not shown). Furthermore, we did not detect any interaction between KHSRP and ESRP2 in NMuMg cells (*Figure 62*). Therefore, we explored the possibility that KHSRP may associate with a different ribonucleoprotein complex able to control alternative splicing events in EMT in NMuMg cells.

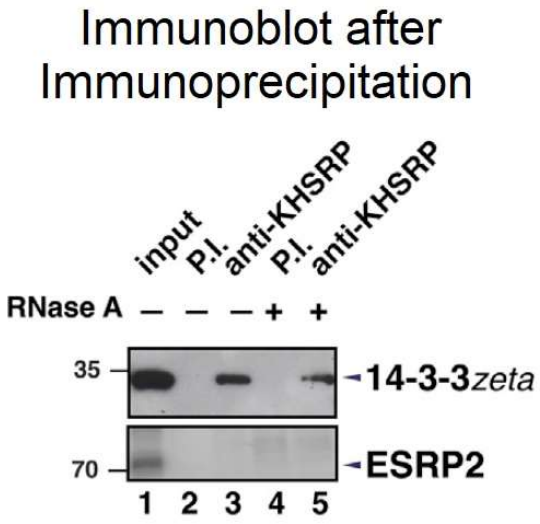

Figure 62; Co-immunoprecipitation of ESRP2 and KHSRP in total extracts from NMuMg cells. Cell lysates either control-treated or treated with RNase A (10 mg/ml for 30 minutes at 37°C) were immunoprecipitated as indicated and analyzed by immunoblotting using the indicated antibodies. The position of molecular mass markers is indicated on the left of each immunoblot. Representative images are shown.

We found that some RBPs that have been implicated in splicing regulation during EMT (such as DDX5, DDX17, hnRNPM, and RBFOX2) are either not expressed or do not interact with KHSRP in NMuMg cells (data not shown; see the '*Discussion*' section). Conversely, the multifunctional hnRNPA1, a well-known molecular partner of KHSRP that has been demonstrated to be implicated in cell-type-specific pre-mRNA splicing events, is expressed in NMuMg cells (Ruggiero et al., 2007; Michlewski & Càceres, 2010; Bonomi et al., 2013; Douablin et al., 2015). Interestingly, whereas the expression of KHSRP and other alternative splicing regulators is progressively silenced during EMT in NMuMg cells, the levels of hnRNPA1 remain constant during cell exposure to TGF-β (*Figure 63*; data not shown).

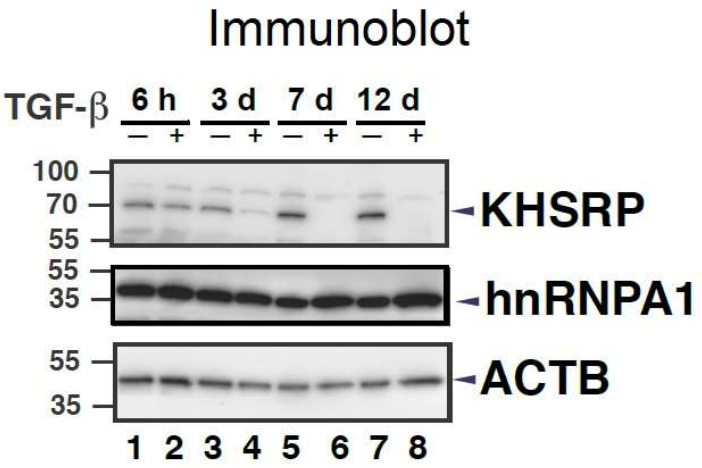

Figure 63; Immunoblot analysis of total cell extracts from NMuMg cells serum-starved and either treated with TGF-β (+) for the indicated times or untreated (-). The indicated antibodies were used. The position of molecular mass markers is indicated on the left of each immunoblot. Representative gels are shown.

Co-immunoprecipitation experiments confirmed that KHSRP associates with hnRNPA1 in NMuMg cells and that this interaction is abrogated by RNase A treatment (*Figure 64*). This observation prompted us to explore whether KHSRP and hnRNPA1 interact with the same pre-mRNA regions of *Enah*, *Cd44*, and *Fgfr2*. To this purpose, we performed RIP experiments, and we found that KHSRP and hnRNPA1 interact with the same regions of these pre-mRNAs (*Figure 65*).

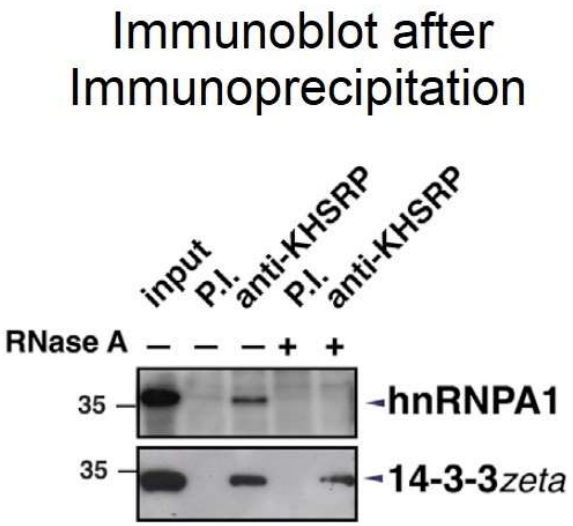

Figure 64; Co-immunoprecipitation of hnRNPA1 and KHSRP in total extracts from NMuMg cells. Cell lysates either control-treated or treated with RNase A (10 mg/ml for 30 minutes at 37°C) were immunoprecipitated as indicated and analyzed by immunoblotting using the indicated antibodies. The position of molecular mass markers is indicated on the left of each immunoblot. Representative gels are shown.

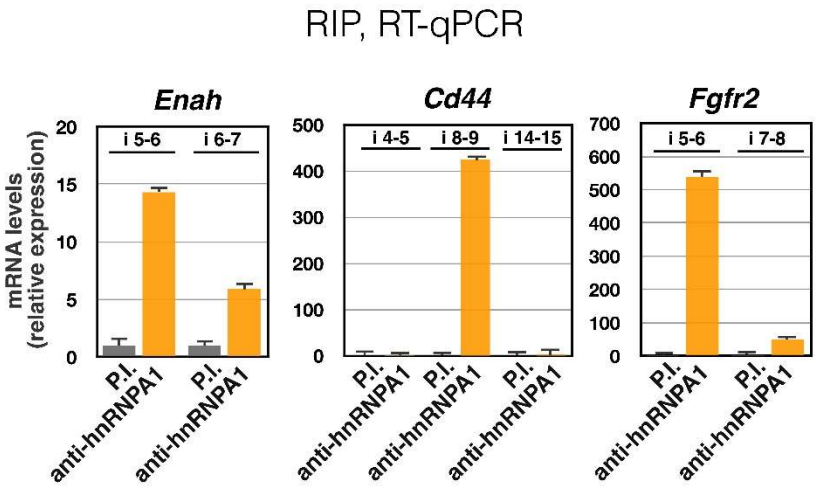

Figure 65; Total extracts from NMuMg cells were immunoprecipitated as indicated. RNA was purified from immunocomplexes and analyzed by RT-qPCR to detect the indicated pre-mRNAs. The values of RT-qPCR experiments shown are averages (±SEM) of three independent experiments performed in triplicate.

Further, EMSA experiments revealed that recombinant hnRNPA1 directly interacts with *Cd44 intron* 8-9 (*Figure 66*, and see also *Figure 58*).

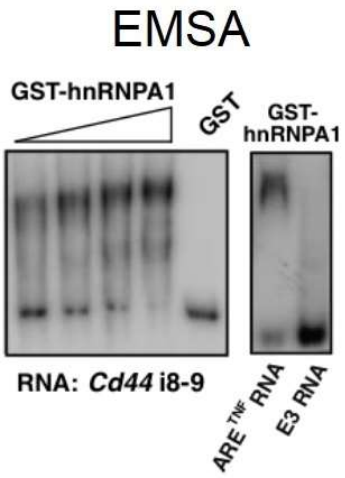

Figure 66; Electrophoretic mobility shift assays (EMSA) performed to detect the interaction between either recombinant GST-hnRNPA1 (50–300 nM) or GST (300 nM) with 32P-labeled RNA corresponding to the 5' region of *Cd44* pre-mRNA *intron 8-9* (*left panel*) as well as the interaction between GST-hnRNPA1 (300 nM) with either *ARE* ^{TNF} or the inherently stable *E3* control RNA as indicated (*right panel*). Representative autoradiograms are displayed.

In order to investigate a possible role of hnRNPA1 in the molecular events that are regulated by KHSRP in NMuMg cells, we transiently silenced hnRNPA1 in untreated NMuMg cells (*Figure 67*) and found that its knockdown enhances the expression of a subset of EMT factors, such as *Fstl1*, *Mmp9*, and *Iglon5*, whereas it does not affect miR-192-5p and miR-194-5p expression (*Figure 68* and *Table 2*).

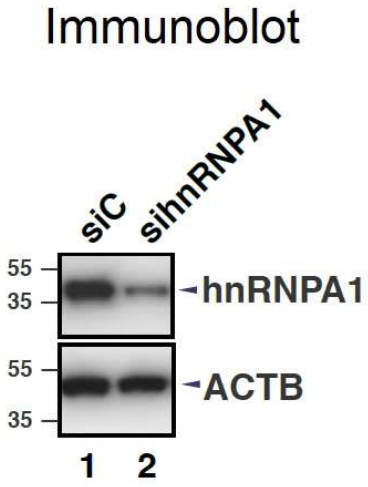

Figure 67; Immunoblot analysis of total cell extracts (20 µg) from NMuMg cells transiently transfected with either control siRNA (siC) or hnRNPA1-specific siRNAs (sihnRNPA1). The indicated antibodies were used. The position of molecular mass markers is indicated on the left of each immunoblot. Representative images are shown.

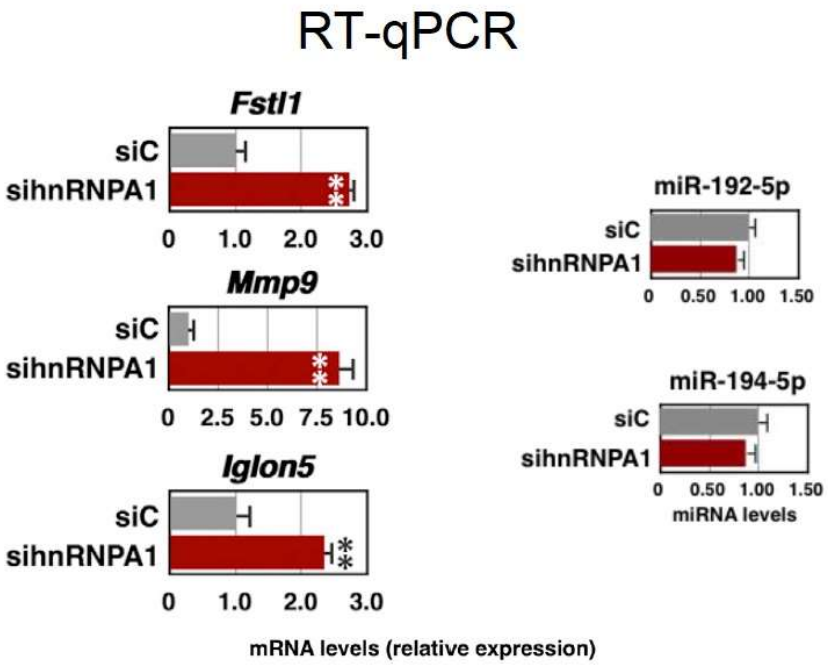

Figure 68; RT-qPCR analysis of the indicated transcripts in either control siRNA (siC) or sihnRNPA1-transfected NMuMg cells. The values of RT-qPCR experiments shown are averages (±SEM) of three independent experiments performed in triplicate. Statistical significance: **p <0.001 (Student's t-test).

Further, we demonstrated that hnRNPA1 knockdown, similar to KHSRP silencing, promoted the mesenchymal-type exon usage of *Enah*, *Cd44,* and *Fgfr2* pre-mRNA (*Figure 69)*. The interaction of hnRNPA1 with these pre-mRNAs is largely impaired by TGF-β treatment although the protein continues to be expressed (*Figure 70* and data not shown).

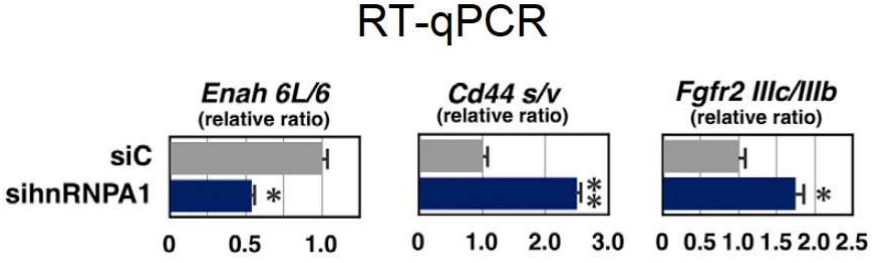

Figure 69; RT-qPCR analysis performed using primers specific for the two isoforms of *Enah*, *Cd44*, and *Fgfr2* mRNAs, respectively. The results are presented as ratio between the expression levels of the indicated mRNA isoforms. NMuMg cells were transfected with either siC or sihnRNPA1 and collected 48h after transfection. The values of RT-qPCR experiments shown are averages ± SEM of three independent experiments performed in triplicate. Statistical significance: *p < 0.01, **p < 0.001 (Student's t-test).

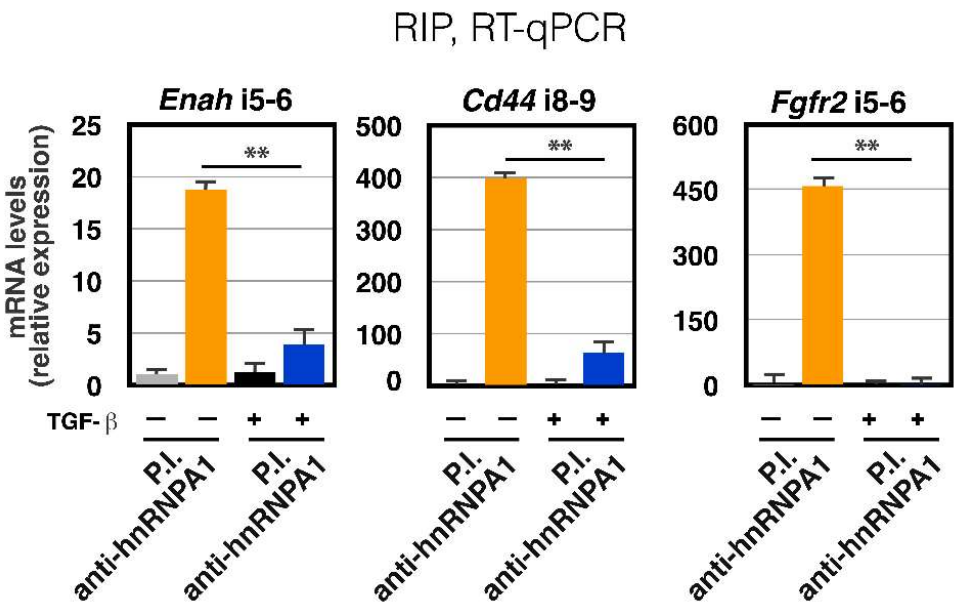

Figure 70; Total extracts from NMuMg cells serum starved and either treated with TGF-β (+) for 24h or untreated (-) were immunoprecipitated as indicated. RNA was purified from immunocomplexes and analyzed by RT-qPCR to detect the indicated pre-mRNAs. The values of RT-qPCR experiments shown are averages (±SEM) of three independent experiments performed in triplicate. Statistical significance: **p <0.001 (Student's t-test).

Based on these findings, we investigated whether KHSRP and hnRNPA1 mutually influence their binding activity to *Enah*, *Cd44*, and *Fgfr2* pre-mRNAs. Although we previously demonstrated that either recombinant protein is able to bind a common target RNA *in vitro*, RIP analyses indicate that the ability of hnRNPA1 to interact with *Enah*, *Cd44*, and *Fgfr2* pre-mRNAs is significantly impaired by KHSRP knockdown, whereas the interaction of KHSRP with the same pre-mRNAs is strongly reduced in hnRNPA1-knockdown NMuMg cells (*Figure 71b*). Finally, we showed that KHSRP re-expression in shKHSRP NMuMg cells was able to restore the ability of hnRNPA1 to interact with *Enah*, *Cd44*, and *Fgfr2* pre-mRNAs (*Figure 72* and data not shown).

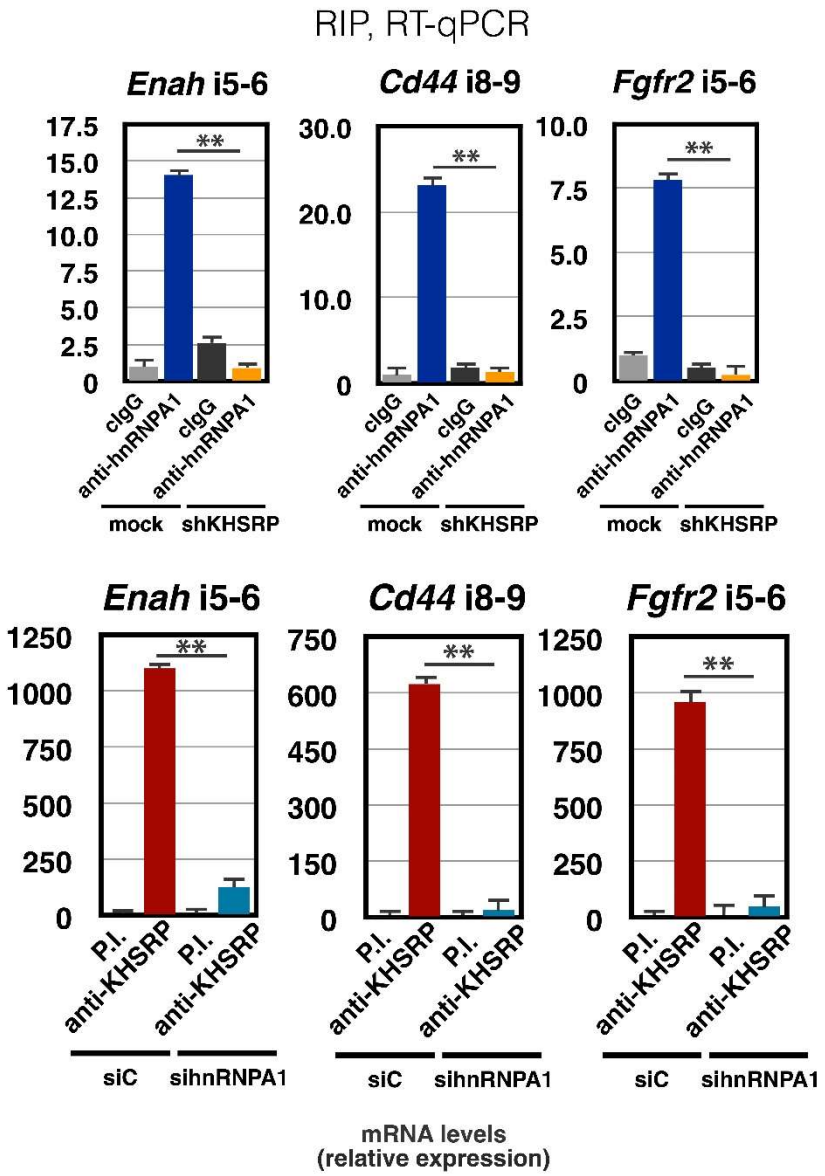

Figure 71; *Upper panel.* Total extracts from either mock or shKHSRP NMuMg cells were immunoprecipitated as indicated. RNA was purified from immunocomplexes and analyzed by RT-qPCR to detect the indicated transcripts. *Bottom panel.* Total extracts from NMuMg cells transfected with either siC or sihnRNPA1 were immunoprecipitated as indicated. RNA was purified from immunocomplexes and analyzed by RT-qPCR to detect the indicated transcripts.
The values of RT-qPCR experiments shown are averages (±SEM) of three independent experiments performed in triplicate. Statistical significance: **p <0.001 (Student's t-test).

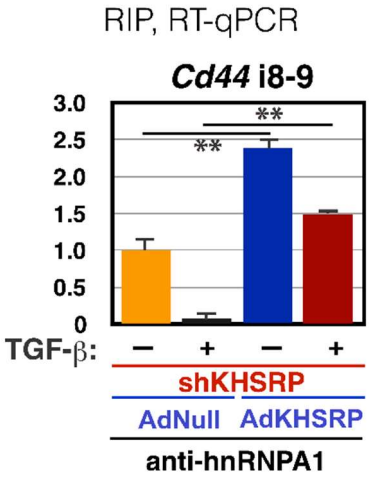

Figure 72; Total extracts from shKHSRP NMuMg cells, infected with either control (AdNull) or KHSRP-expressing (AdKHSRP) adenoviral vectors for 24h and subsequently serum-starved and either treated with TGF-β (+) for 24h or untreated (-), were immunoprecipitated as indicated. RNA was purified from immunocomplexes and analyzed by RT-qPCR to detect the indicated transcript. The values of RT-qPCR experiments shown are averages ± SEM of three independent experiments performed in triplicate. Statistical significance: **p < 0.001 (Student's t-test).

As a whole, our results suggest that KHSRP and hnRNPA1 are mutually necessary for binding to *Enah*, *Cd44*, and *Fgfr2* pre-mRNAs and for maintaining the epithelial-type exon usage of these transcripts in NMuMg cells.

7. Resveratrol prevents TGF-β-induced EMT in mammary gland cells

As a part of a screening that has been carried out in the laboratory where I conducted my thesis, aimed at the identification of compounds that can prevent TGF-β-induced gene expression changes in NMuMg cells, we investigated the effects of resveratrol (RESV), a natural polyphenolic compound. To this purpose, we pretreated NMuMg cells for 2h with RESV (concentrations ranging from 5 to 150 μM), and then we exposed cells to 10 ng/ml TGF-β for 2 days (see also '*Experimental procedures*' section). The expression levels of a representative group of factors crucial to EMT were analyzed by RT-qPCR, and we found that RESV (used at a concentration of 75 μM) significantly impaired both basal and TGF-β-induced expression of mesenchymal factors (such as *Fn1*, *Fstl1*, *Col6a2*, *Cdh2*, *Zeb1*, and *Col12a1*). Further, RESV enhanced miR-200c expression, while reduced miR-155 levels (*Figure 73*).

The observation that RESV prevents the TGF-β-induced expression of mesenchymal factors was extended to murine Py2T cells (*Figure 74* and data not shown).

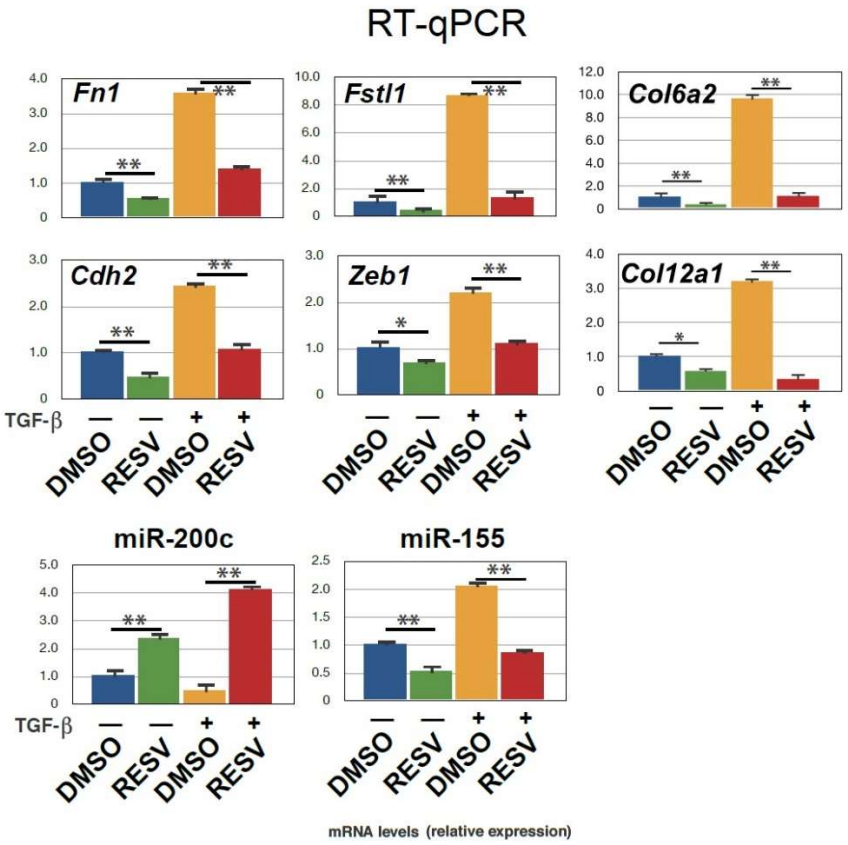

Figure 73; RT-qPCR analysis of the indicated transcripts (mRNAs and miRNAs) in NMuMg cells serum starved (2% FBS, 16h), pre-treated for 2 h with either RESV (75 µM) or DMSO, and then either treated with TGF-β (10 ng/ml) for 48h or left untreated. The values of RT-qPCR experiments shown are averages ±SEM of three independent experiments performed in triplicate. Statistical significance: *p<0.01, **p<0.001 (Student's t-test).

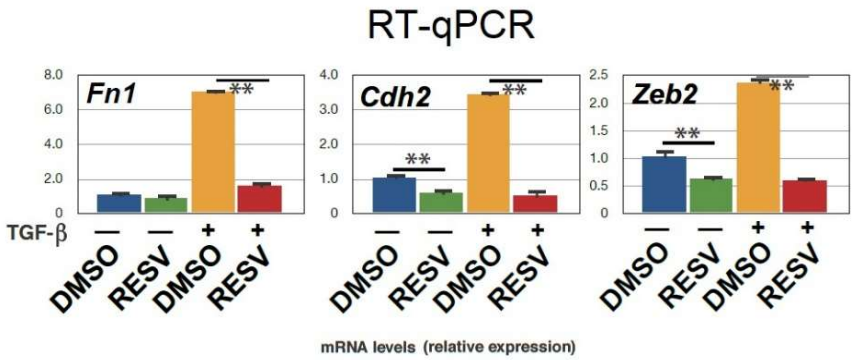

Figure 74; RT-qPCR analysis of the indicated transcripts in Py2T cells serum-starved (1% FBS, 16h), pre-treated for 2h with either RESV (75 µM) or DMSO and then either treated with TGF-β (10 ng/ml) for 48h or left untreated. The values of RT-qPCR experiments shown are averages ±SEM of three independent experiments performed in triplicate. Statistical significance: *p<0.01, **p<0.001 (Student's t-test).

A major role of TGF-β in mammary gland cells is to enhance their inherent migratory proprieties. In order to investigate whether RESV was able to affect the migratory proprieties of NMuMg cells, we performed scratch assays. We observed that RESV treatment reduces the gap closure in a time-dependent manner when compared to negative control (DMSO)-treated cells (*Figure 75*).

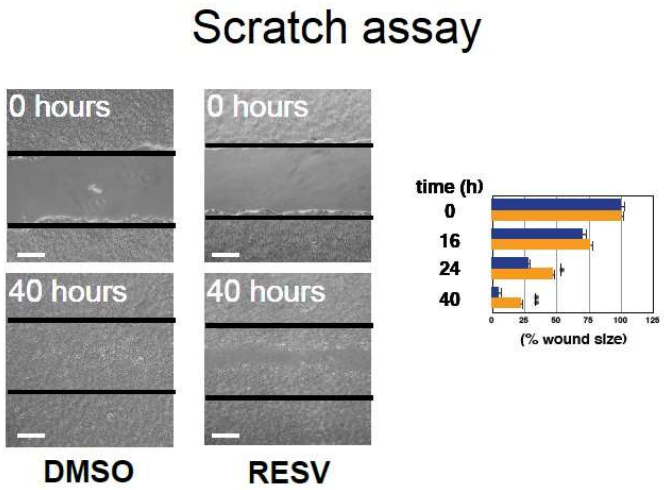

Figure 75; Scratch wound healing assay. NMuMg cells were pre-treated for 2h with either RESV (75 µM) or DMSO and then scratch wounds were introduced into confluent monolayers. Cultures were photographed and the width of the wound was measured at different intervals of time from 0 to 40h after the scratch was made. Representative images are taken at 0 and 40h. Scale bars: 100 µm. The percentage of the wound healed area for each culture condition was plotted (*right panel*).

In addition, RESV treatment was able to revert the expression of EMT makers also in NMuMg cells that had achieved a complete mesenchymal phenotype in response to a three days TGF-β treatment (*Figure 76).*

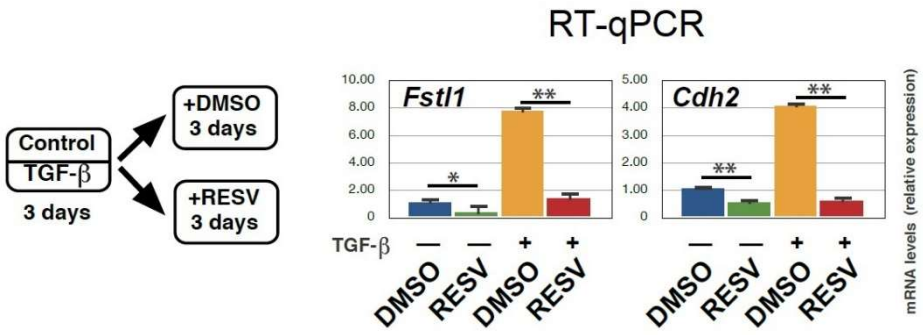

Figure 76; *Left panel.* Schematic of the NMuMg cell treatment.
Right panel. RT-qPCR analysis of the indicated transcripts in cells treated as summarized in the left panel. The values of RT-qPCR experiments shown are averages ±SEM of three independent experiments performed in triplicate. Statistical significance: *p<0.01, **p<0.001 (Student's t-test).

Altogether these observations indicate that RESV is able to strongly counteract the TGF-β-induced EMT phenotype in mammary gland cells.

8. Resveratrol promotes the epithelial-type alternative splicing of Cd44, Enah, and Fgfr2 pre-mRNAs in mammary gland cells

One of the major consequences of TGF-β treatment in NMuMg cells is the modulation of the alternative splicing of a cohort of pre-mRNAs implicated in EMT (including *Cd44*, *Enah*, and *Fgfr2*). Thus, we investigated whether RESV affects the alternative splicing of these pre-mRNAs in NMuMg cells. We found that RESV affects the alternative splicing of *Cd44*, *Enah*, and *Fgfr2* pre-mRNAs favoring the inclusion of epithelial-type of each of transcript (*Cd44s*, *Enah6L*, and *Fgfr2 IIIb* respectively) thus significantly reducing both *Cd44s/Cd44v* and *Fgfr2 IIIc/IIIb* ratio, and increasing *Enah6L/Enah6* ratio (*Figure 77*). We observed a similar splicing pattern of *Cd44* and *Enah* transcript also in PY2T cells (*Figure 78*).

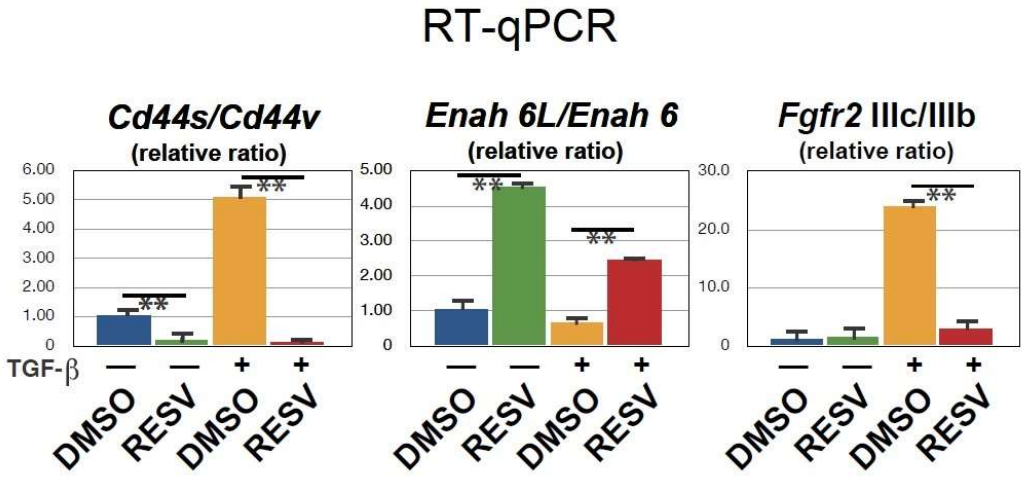

Figure 77; NMuMg cells were serum-starved (2% FBS, 16h), pretreated for 2h with either RESV (75 μM) or DMSO, and then either treated with TGF-β (10 ng/ml) for 48h or left untreated. RT-qPCR analysis was performed using exon-specific primers of the indicated transcripts. The results are presented as the ratio between the expression levels of each isoform as indicated. The values of RT-qPCR experiments shown are averages ±SEM of three independent experiments performed in triplicate. Statistical significance: **p<0.001 (Student's t-test).

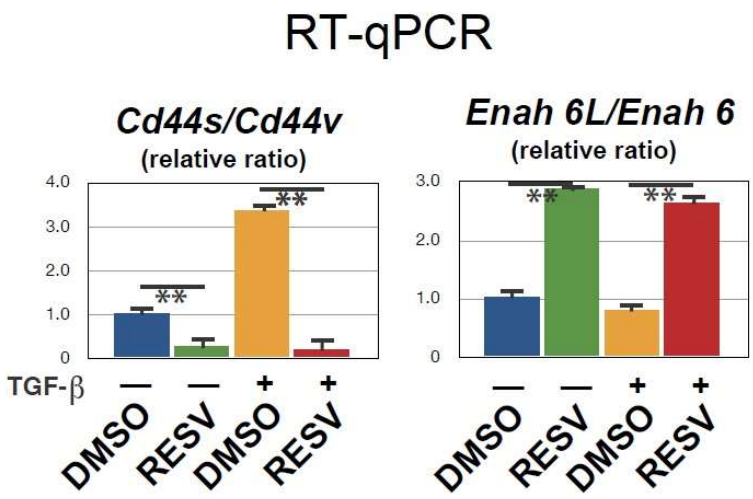

Figure 78; PY2T cells were serum-starved (2% FBS, 16h), pretreated for 2h with either RESV (75 µM) or DMSO, and then either treated with TGF-β (10 ng/ml) for 48h or left untreated. RT-qPCR analysis was performed using exon-specific primers of the indicated transcripts. The results are presented as the ratio between the expression levels of each isoform as indicated. The values of RT-qPCR experiments shown are averages ±SEM of three independent experiments performed in triplicate. Statistical significance: **p<0.001 (Student's t-test).

NMuMg cells express seven *Cd44* mRNA isoforms as a consequence of alternative usage of the ten variable exons (*Figure 79*). TGF-β treatment induces the exclusion of *exon 6* of *Cd44* and RESV pre-treatment of NMuMg cells prevents TGF-β-dependent *exon 6* skipping (*Figure 80*).

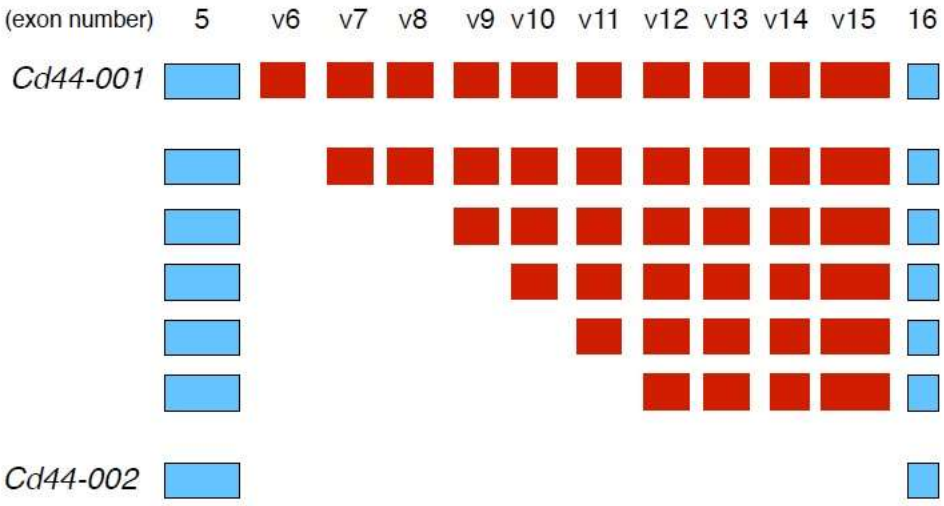

Figure 79; Schematic representation of variable *Cd44* exons in NMuMg cells.

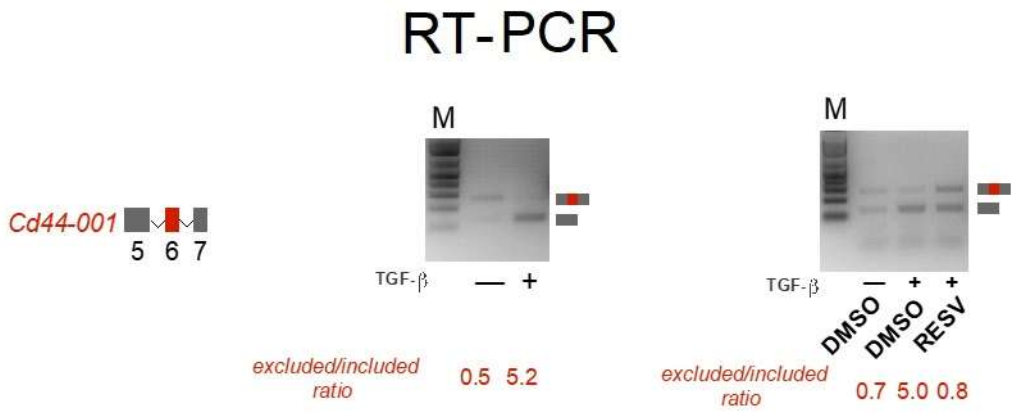

Figure 80; *Left panel.* A schematic of *Cd44-001* exons 5 to 7.
Middle panel. RT-PCR analysis of total RNA samples from NMuMg cells that were serum-starved (2% FBS, 16h) and either treated with 10 ng/ml TGF-β for 48h or left untreated.
Right panel. RT-PCR analysis of total RNA samples from NMuMg cells that were serum-starved (2% FBS, 16h), pre-treated for 2h with either RESV (75 µM) or DMSO, and then either treated with TGF-β (10 ng/ml) for 48h or left untreated.
Representative gels are presented. The ratio between the intensity of bands corresponding to *exon 6*- excluding and *exon6*- including amplicons (quantitated in three independent experiments) is presented at the bottom of each gel.

Further, we observed that RESV treatment of NMuMg cells that achieved an overt mesenchymal phenotype (through a three-day treatment with TGF-β) reverted the mesenchymal-type splicing pattern of *Cd44*, *Enah*, and *Fgfr2* pre-mRNAs despite the continuous presence of TGF-β (*Figure 81*).

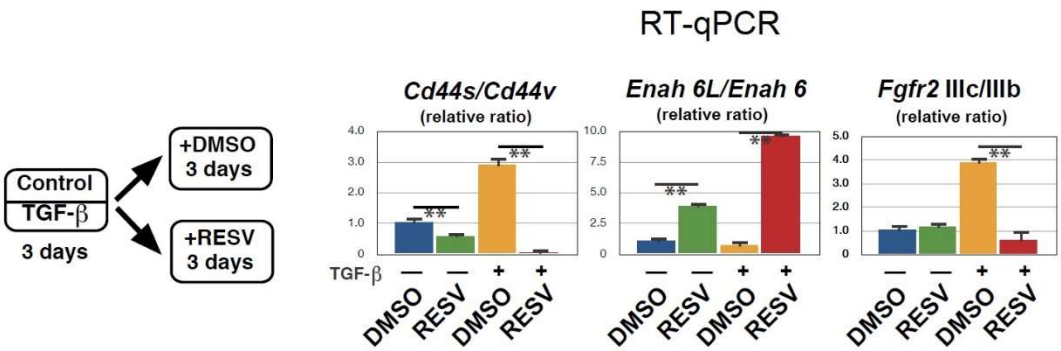

Figure 81; *Left panel.* Schematic of the NMuMg cell treatment.
Right panel. RT-qPCR analysis of the expression of the alternative splicing forms of either *Cd44*, *Enah*, or *Fgfr2* in cells treated as summarized in the left panel. The results are presented as the ratio between the expression levels of each isoform as indicated.
The values of RT-qPCR experiments shown are averages ± SEM of three independent experiments performed in triplicate. Statistical significance: **p < 0.001 (Student's t-test).

It has been reported that RESV limits breast cancer cells proliferation and invasiveness (Dandawate et al., 2016). For these reasons, we investigated whether RESV is able to increase the expression of epithelial-type versus mesenchymal-type factors in transformed mammary gland cells, both murine and human. We found that a 24 hours RESV treatment significantly enhanced the expression of epithelial-type cadherin *Cdh1*, while reduced the levels of mesenchymal and invasiveness- related factors such as *Fn1*, *Fstl1*, and *Mmp9* in 4T1, TS/A, and MDA-MB-231 cells (*Figure 82* and data not shown). In line with these results, scratch wound assays revealed that the gap closure was significantly reduced by RESV treatment in 4T1 and TS/A cells when compared to control (DMSO-treated) cells suggesting that RESV reduces the migratory propriety of these cells (*Figure 83* and data not shown).

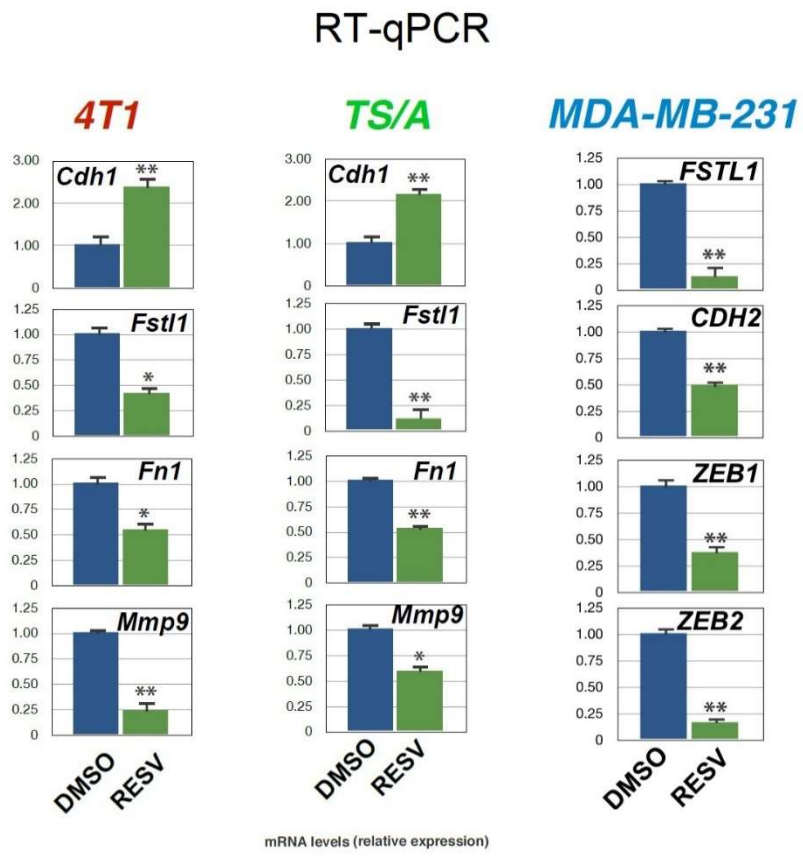

Figure 82; RT-qPCR analysis of the indicated transcripts in 4T1, TS/A, and MDA-MB-231 cell lines. Cells were serum-starved and then treated with either RESV (75 µM) or DMSO for 24 h, respectively. The values of RT-qPCR experiments shown are averages ± SEM of three independent experiments performed in triplicate. Statistical significance: *p < 0.01, **p < 0.001 (Student's t-test).

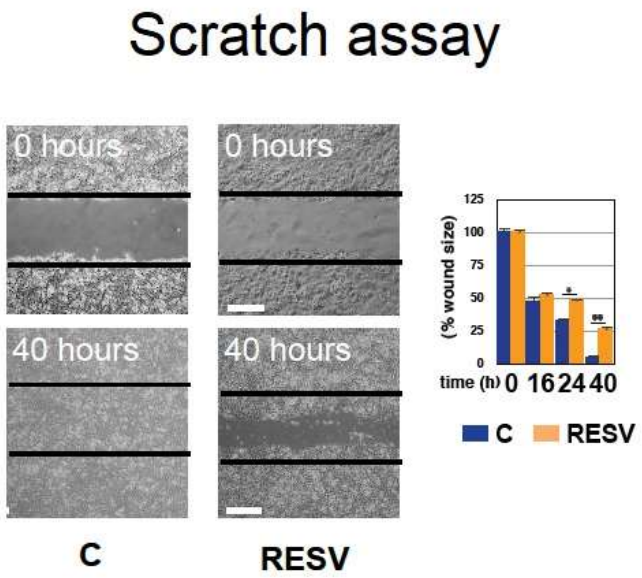

Figure 83; Scratch wound healing assays. 4T1 cells were pre-treated for 2h with either RESV (75 µM) or DMSO and then scratch wounds were introduced into confluent monolayers. Cultures were photographed and the width of the wound was measured at different intervals of time from 0 to 40 h after the scratch was made. Representative images at 0 and 40h are shown (*Left panel*). Scale bars: 100 µm. The percentage of the wound healed area for each culture condition was plotted (*Right panel*).

Recent experimental evidence connected the molecular program of alternative splicing regulation with the occurrence of metastasis in patients (Xu et al., 2014; Matsuda et al., 2012; Oudin et al., 2016). For these reasons, we decided to investigate whether the ability of RESV to affect the alternative exon usage of *Cd44* and *Enah* in transformed mammary gland cell lines. Cultures were treated with RESV for 24h and the expression of epithelial- and mesenchymal- type splicing variants of *Cd44* and *Enah* pre-mRNAs was quantitated by RT-qPCR analysis. We found that RESV favored the inclusion of the respective epithelial-type splicing variants of *Cd44* and *Enah* also in 4T1, TS/A, and MDA-MB-231 cells (*Figure 84*).

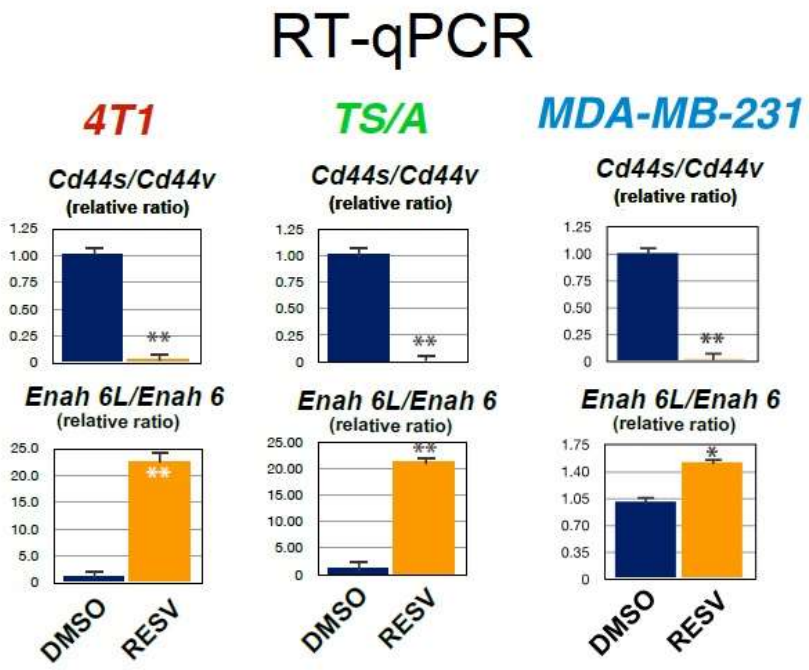

Figure 84; RT-qPCR analysis of the alternative isoforms of *Cd44* and *Enah* in 4 T1, TS/A, and MDA-MB-231 cells. Cells were serum-starved and then treated with either RESV (75 µM) or DMSO for 24h, respectively. The results are presented as the ratio between the expression levels of each isoform as indicated. The values of RT-qPCR experiments shown are averages ± SEM of three independent experiments performed in triplicate. Statistical significance: *p < 0.01, **p < 0.001 (Student's t-test).

Altogether our data indicate that RESV affects the alternative exon usage of pre-mRNAs that encode factors crucial to adhesion and migration in both immortalized and transformed mammary gland cells.

9. Resveratrol upregulates KHSRP and hnRNPA1 expression to favor the epithelial-type alternative splicing of Cd44 pre-mRNA in mammary gland cells

Data presented in the first part of the '*Results*' section indicate that TGF-β-dependent KHSRP down-regulation is required to favor the mesenchymal-type splicing pattern of *Cd44*, *Enah*, *Fgfr2*, and other pre-mRNAs during EMT. Consequently, we hypothesized that RESV may affect the alternative splicing of select pre-mRNAs by influencing KHSRP expression. Indeed, RESV treatment increases the expression of KHSRP in untreated NMuMg cells and restored, in part, its levels in TGF-β-treated cells (*Figure 85*).

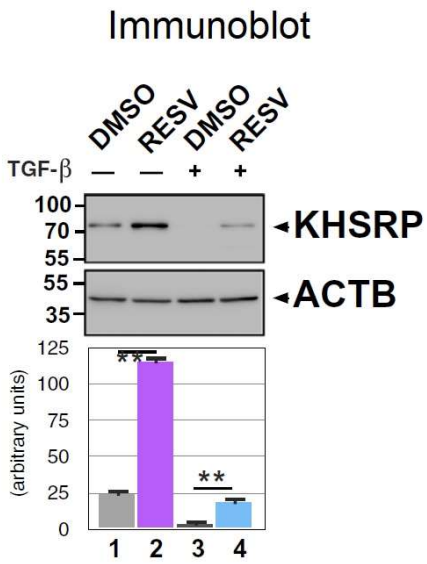

Figure 85; Immunoblot analysis of total cell extracts from NMuMg cells serum-starved and pre-treated for 2h with either RESV (75 µM) or DMSO and then either treated with TGF-β for 48h or left untreated. The indicated antibodies were used. Bands corresponding to anti-KHSRP and anti-ACTB immunoreactivity were quantitated in three independents immunoblots (using ImageJ 1.49 software) and the ratio between their intensities is presented in Arbitrary Units.

In agreement with our observation that miR-27b-3p causes KHSRP down-regulation, we found that RESV prevented TGF-β-induced miR-27b-3p up-regulation thus suggesting that RESV affects KHSRP expression at post-transcriptional level (*Figure 86*). Further support to our hypothesis that RESV influences alternative splicing by regulating KHSRP levels was provided by the evidence that RESV treatment controls the alternative isoform usage of a group of pre-mRNAs that are splicing targets of KHSRP (*Figure 87* and see above).

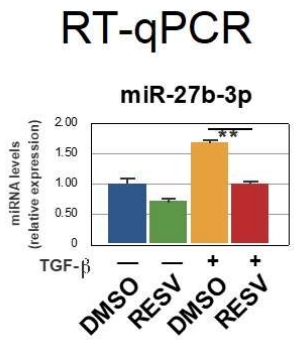

Figure 86; RT-qPCR analysis of miR-27b-3p in NMuMg cells serum-starved (2% FBS, 16h), pre-treated for 2h with either RESV (75 µM) or DMSO and then either treated with TGF-β (10 ng/ml) for 48h or left untreated. The values of RT-qPCR experiments shown are averages ± SEM of three independent experiments performed in triplicate. Statistical significance: **p < 0.001 (Student's t-test).

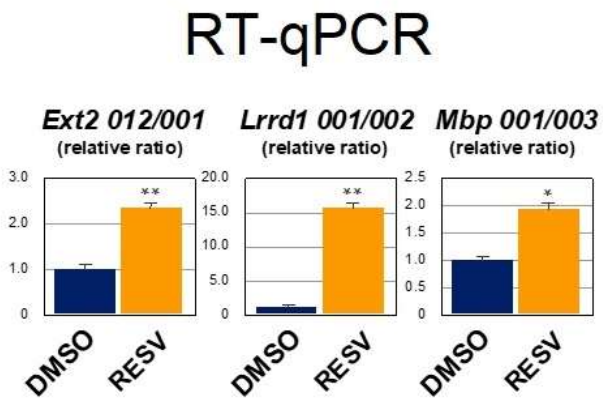

Figure 87; RT-qPCR analysis performed in NMuMg cells serum-starved (2% FBS, 16h), and treated with either RESV (75 µM) or DMSO for 24h using exon-specific primers. The results are presented as ratio between the expression levels of two alternatively spliced forms of the indicated transcripts (nomenclature of mRNA forms derived from alternative splicing is presented according to Ensembl).

In order to verify our hypothesis, we analyzed the response to RESV in KHSRP-silenced mammary gland cells compared to mock-silenced cells. KHSRP silencing significantly limited, but failed to abrogate, the RESV-dependent reduction of the *Cd44s/Cd44v* ratio in NMuMg cells (*Figure 88*). Similar effect of KHSRP silencing was obtained in 4T1 cells (*Figure 89*).

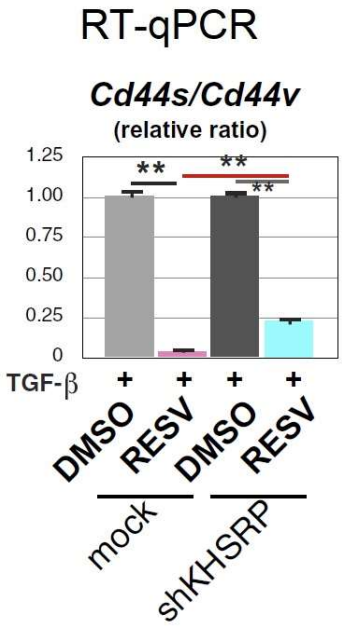

Figure 88; Either mock or shKHSRP NMuMg cells were serum-starved and pre-treated for 2h with either RESV (75 µM) or DMSO and then treated with TGF-β (+) for 4h. The expression levels of *Cd44v* and *Cd44s* were measured by RT-qPCR and presented as ratio between the expression levels of *Cd44s* and *Cd44v* forms.

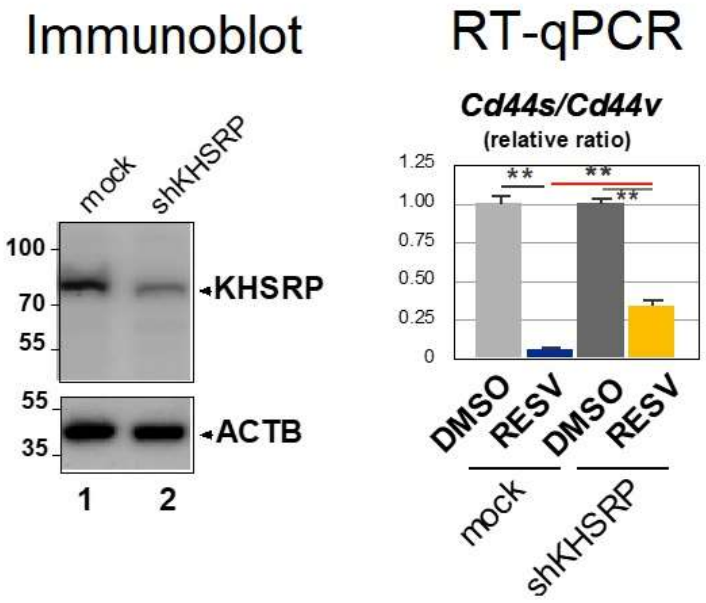

Figure 89; *Left panel.* Immunoblot analysis of total cell extracts from either mock or shKHSRP 4T1 cells as marked. The indicated antibodies were used.
Right panel. Either mock or shKHSRP 4T1 cells were treated for 24h with either RESV (75 µM) or DMSO. The expression levels of *Cd44v* and *Cd44s* were measured by RT-qPCR and presented as ratio between *Cd44s* and *Cd44v* forms.

Even though the ability of RESV to up-regulate the expression of the small residual amount of KHSRP still present in shKHSRP cells (*Figure 90* and data not shown) could explain, at least in part, the incomplete effect of KHSRP silencing, our results prompted us to investigate additional mechanisms for the effect of RESV on *Cd44* alternative splicing modulation.

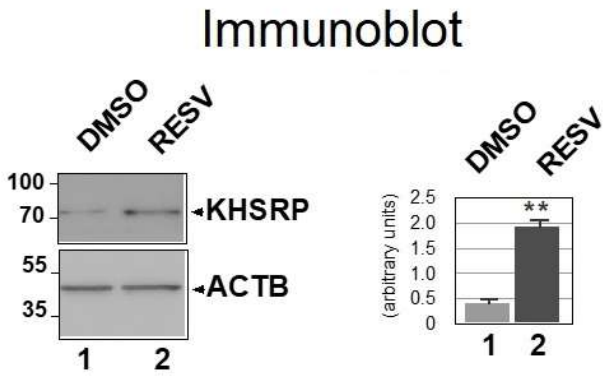

Figure 90; Immunoblot analysis of total cell extracts from shKHSRP NMuMg treated with either RESV (75 µM) or DMSO for 48h. The indicated antibodies were used. Bands corresponding to anti-KHSRP and anti-ACTB immune-reactivity were quantitated in three independents immunoblot (using *ImageJ 1.49* software) and the ratio between their intensities is presented in Arbitrary Units.

Considering that KHSRP is able to interact with hnRNPA1 to form a ribonucleoprotein complex that regulates alternative exon usage in NMuMg cells (see above), we explored the possibility that RESV may affect the expression of hnRNPA1. Indeed, we found that RESV enhances hnRNPA1, similar to KHSRP expression, in both NMuMg and 4T1 cells (*Figure 91*).

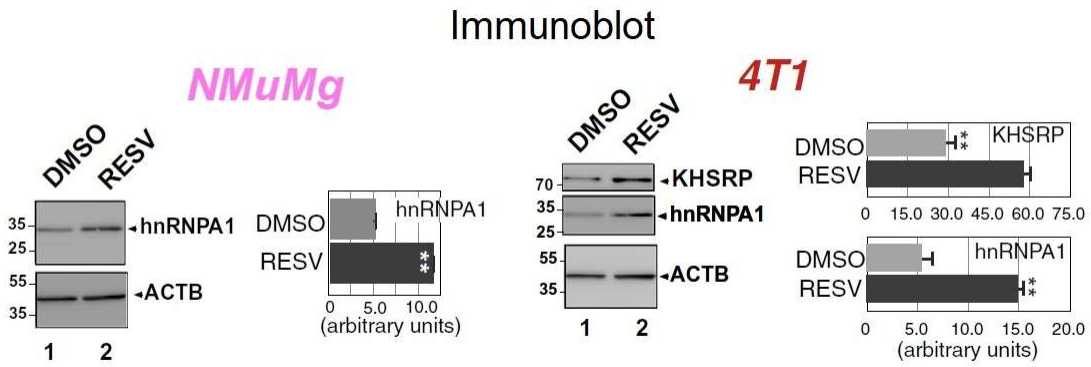

Figure 91; *Left panel.* Immunoblot analysis of total cell extracts from NMuMg cells serum-starved (2% FBS, 16h), pre-treated for 2h with either RESV (75 µM) or DMSO and then treated with TGF-β for 48h.
Right panel. Immunoblot analysis of total cell extracts from 4 T1 cells treated for 24 h with either RESV (75 µM) or DMSO. The indicated antibodies were used. Bands were quantitated in three independents immunoblot (using ImageJ 1.49 software) and the ratio between the intensity of either KHSRP or hnRNPA1 immunoreactivity and ACTB immunoreactivity is presented in Arbitrary Units.

To further support our hypothesis, we stably silenced hnRNPA1 in 4T1 cells and we analyzed the effects of RESV on *Cd44* pre-mRNA alternative splicing. We found that hnRNPA1 silencing significantly limited the RESV-dependent reduction of the *Cd44s/Cd44v* ratio although failed to completely prevent the RESV-induced epithelial-type *Cd44* alternative splicing (*Figure 92*).

Thus, considering that the individual silencing of either KHSRP or hnRNPA1 failed to completely abrogate RESV effect on *Cd44* alternative splicing, we decided to simultaneously silence both KHSRP and hnRNPA1 in 4T1 cells and to quantitate the *Cd44* pre-mRNA alternative splicing isoforms. The double stable silencing of KHSRP and hnRNPA1 almost completely prevented the induction of the epithelial-type *Cd44* exon usage by RESV (*Figure 93*).

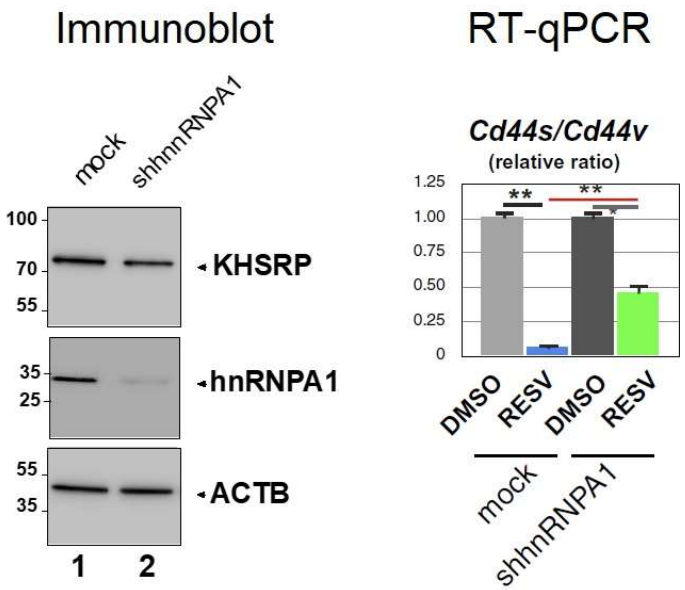

Figure 92; *Left panel.* Immunoblot analysis of total cell extracts from either mock or shhnRNPA1 4T1 cells. The indicated antibodies were used. The position of molecular mass markers is indicated on the left of each immunoblot.
Right panel. Either mock or shhnRNPA1 4 T1 cells were treated for 24h with either RESV (75 µM) or DMSO. The expression levels of *Cd44v* and *Cd44s* were measured by RT-qPCR and presented as ratio between *Cd44s* and *Cd44v* forms. The values of RT-qPCR experiments shown are averages (±SEM) of three independent experiments performed in triplicate. Statistical significance: **p < 0.001 (Student's t-test).

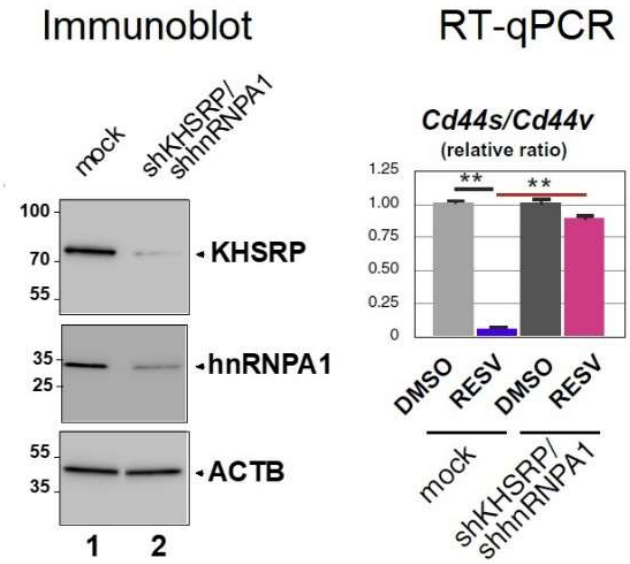

Figure 93; *Left panel.* Immunoblot analysis of total cell extracts from either mock or shKHSRP/shhnRNPA1 4T1 cells. The indicated antibodies were used. The position of molecular mass markers is indicated on the left of each immunoblot.
Right panel. Either mock or shKHSRP/shhnRNPA1 4T1 cells were treated for 24h with either RESV (75 µM) or DMSO. The expression levels of Cd44v and Cd44s were measured by RT-qPCR and presented as ratio between Cd44s and Cd44v forms. The values of RT-qPCR experiments shown are averages (±SEM) of three independent experiments performed in triplicate. Statistical significance: **p < 0.001 (Student's t-test).

In order to strengthen our findings, we transiently expressed the minigene splicing reporter construct including *Cd44v8* and its flanking introns in HEK-293 cells in which RESV is able to modulate the alternative splicing of endogenous *Cd44* pre-mRNA (*Figure 94*). We found that RESV significantly decreased the skipped/included exon *Cd44v8* ratio as evaluated by RT-qPCR using specific primer sets that amplify exon *Cd44v8*-included and *Cd44v8*-skipped products (*Figure 95*).

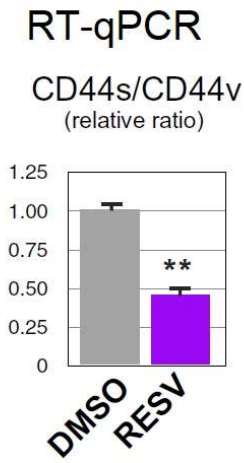

Figure 94; HEK-293 cells were treated with either DMSO or RESV (75 µM) (as indicated) for 24h. The expression levels of *Cd44v* and *Cd44s* were measured by RT-qPCR and presented as ratio between the expression levels of the two forms as indicated. The values of RT-qPCR experiments shown are averages (±SEM) of three independent experiments performed in triplicate. Statistical significance: **p < 0.001 (Student's t-test).

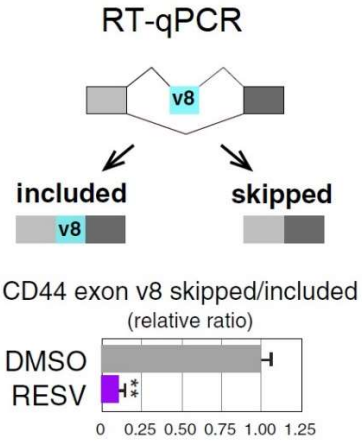

Figure 95; *Upper panel*. Schematic of the *Cd44v8* minigene construct. The *Cd44v8* exon and its flanking introns are inserted between two constitutive exons.
Lower panel. RT-qPCR analysis performed on RNA extracted from HEK-293 cells co-transfected with the *Cd44v8* minigene and treated with either DMSO or RESV (75 µM) (as indicated) for 24h. The values of RT-qPCR experiments shown are averages (±SEM) of three independent experiments performed in triplicate. Statistical significance: **p < 0.001 (Student's t-test).

Agarose gel electrophoresis of end-point RT-qPCR reactions shows a reduction of the exon *Cd44v8*-skipped product and a strong increase of the exon *Cd44v8*-included PCR product (*Figure 96*). Finally, silencing of both KHSRP and hnRNPA1 almost completely hindered the effect of RESV on the splicing pattern of *Cd44v8* minigene in HEK-293 cells (*Figure 97*).

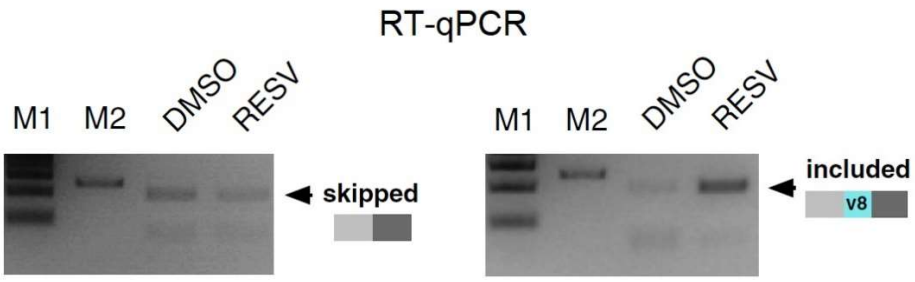

Figure 96; Agarose gel electrophoresis of end-point RT-qPCR reactions as described in *Figure 94*. M1 and M2 correspond to two distinct molecular weight markers. A representative gel is shown.

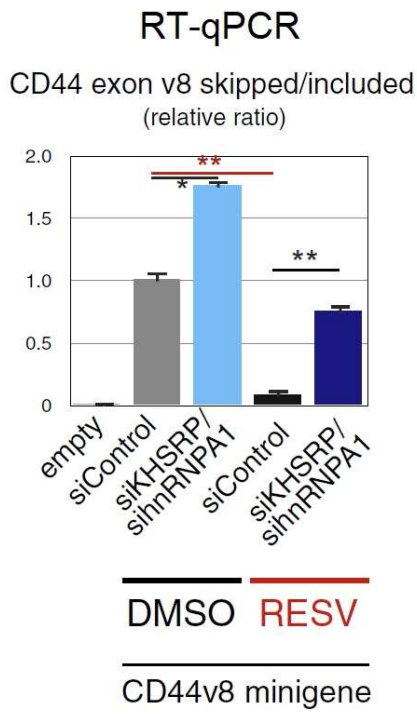

Figure 97; RT-qPCR analysis performed on RNA extracted from HEK-293 cells co-transfected with the *Cd44v8* minigene and either control siRNA (siControl) or KHSRP-specific siRNA (siKHSRP) together with hnRNPA1-specific siRNA (sihnRNPA1). 24h after transfection cells were treated with either DMSO or RESV (75 µM) (as indicated) for 24h. The values of RT-qPCR experiments shown are averages (±SEM) of three independent experiments performed in triplicate. Statistical significance: *p < 0.01, **p < 0.001 (Student's t-test).

As a whole our data indicate that RESV affects *Cd44* alternative splicing by upregulating the expression of KHSRP and hnRNPA1 and that the combined silencing of these two RBPs prevents its action.

Experimental condition	Snai1	Fn1	Col6a2	Col12a1	Fstl1	Iglon5	Mmp9	Zeb1	Zeb2
AdNull	1	1	1	1	1	1	1	1	1
AdNull+TGFβ	**31.85**	**11.72**	**5.19**	**2.84**	**5.24**	**52.30**	**9280.6**	**2.38**	**6.59**
AdKHSRP	0.79	0.73	0.70	0.83	0.62	1.09	0.70	0.40	0.60
AdKHSRP+TGFβ	**11.14**	**5.46**	**1.76**	**1.61**	**2.41**	**7.64**	**3327.0**	**1.14**	**4.02**
mock	1	1	1	1	1	1	1	1	1
mock+TGFβ	**16.60**	**2.75**	**3.28**	**4.16**	**8.52**	**3.90**	**2936.7**	**2.64**	**4.26**
shKHSRP	**4.61**	**2.19**	**2.42**	**3.12**	**8.57**	**2.09**	**2418.7**	**2.13**	**2.13**
shKHSRP+TGFβ	**38.70**	**4.08**	**5.98**	**7.82**	**20.82**	**5.85**	**10085.5**	**3.29**	**4.66**
mimic-miR-C	1	1	1	1	na	na	na	1	1
mimic-miR-27b	**4.11**	**1.92**	**1.97**	**3.29**	na	na	na	**2.71**	**2.53**
anti-miR-C C	1	1	na	na	na	na	na	1	1
anti-miR-C+TGFβ	**8.51**	**5.54**	na	na	na	na	na	**1.47**	**3.09**
anti-miR-27b C	0.81	0.97	na	na	na	na	na	0.79	0.92
anti-miR-27b+TGFβ	**2.30**	**2.04**	na	na	na	na	na	**0.59**	**0.67**
anti-miR-C	1	1	1	1	1	1	1	1	1
anti-miR-192-5p	**3.12**	**0.44**	**0.55**	0.62	1.10	**3.01**	**152.64**	**2.06**	**1.55**
anti-miR-194-5p	0.99	1.16	0.92	0.97	0.61	0.91	**8.46**	1.13	1.31
si-C	1	1	1	1	1	1	1	1	1
si-hnRNPA1	1.32	1.08	0.96	0.89	**2.73**	**2.35**	**8.63**	0.91	0.68

Table 2; Synopsis of the expression changes, quantitated by RT-qPCR analysis, of EMT markers under distinct experimental conditions. The values of RT-qPCR experiments shown are averages of at least three independent experiments performed in triplicate. Values indicated in bold are statistically different, p-value at least < 0.01, Student's t-test. 'Na' is for not assayed.

Discussion

The major finding of the experimental work described in this thesis is that TGF-β-dependent early induction of miR-27b-3p silences the multifunctional single-strand nucleic acid binding protein KHSRP in non-transformed mammary gland cells. This silencing produces a vast rearrangement of the transcriptome and contributes to EMT. KHSRP silencing impairs maturation of miR-192-5p, with the consequent upregulation of a subset of EMT factors, and favors alternative exon usage of genes involved in cell adhesion and migration (*Figure 98*).

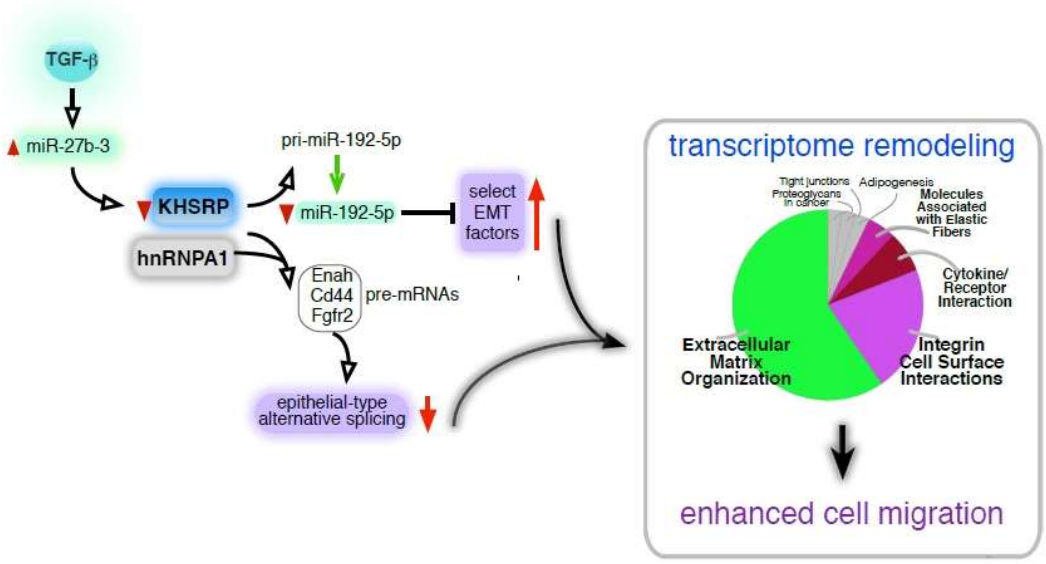

Figure 98; Schematic pathway of results reported here.

Previous studies conducted in the laboratory and current experiments suggest that ligands belonging to the TGF-β family need to overcome KHSRP function in order to orient cell differentiation decisions. This is achieved either through SMAD-mediated inhibition of KHSRP activity that leads to a maturation blockade of pro-myogenic miRNAs (Pasero et al, 2012) or through abrogation of KHSRP expression, as in the case of this study.

In my thesis, I report that miR-27b-3p is a component of the TGF-β signaling pathway that contributes to the EMT process through KHSRP silencing. A miRNA-mediated downregulation of KHSRP expression by TGF-β has also been reported by Sundaram and colleagues showing that miR-181a-dependent KHSRP silencing leads to a switch between maturation from precursors of the primate-specific miR-198 and expression of FSTL1, a glycoprotein produced mainly by cells of mesenchymal origin, during wound healing (Sundaram et al, 2013). The fact that in our model KHSRP silencing is achieved through a distinct miRNA and results in a different cascade of events put forward the idea that TGF-β family members operate in a variety of ways to silence KHSRP expression/function and emphasize the importance of the "TGF-β/KHSRP antagonism" as a hub during TGF-β-family-member-driven cell differentiation.

One of the more extensively investigated functions of KHSRP is to promote miRNA maturation from precursors (Briata et al., 2016). Although TGF-β-dependent KHSRP silencing controls the expression of miRNAs previously implicated in EMT (Zhang et al, 2014; data not shown), we decided to analyze in detail the miR-192-5p function because its maturation from primary transcripts is directly controlled by KHSRP. However, the evidence that miR-192-5p silencing fails to reproduce the whole spectrum of gene expression changes caused by KHSRP silencing prompted us to explore the impact of KHSRP on an additional layer of regulation.

Despite the fact that biochemical experiments uncovered KHSRP involvement in alternative splicing 20 years ago (Min et al, 1997), the data that I present in my thesis show the role of KHSRP-modulated exon usage in a cell trans-differentiation model. Regulation of gene expression by alternative splicing was the first post-transcriptional mechanism linked to EMT (Savagner et al, 1994) and, indeed, it can impact on all the events described as "hallmarks of cancer". RBPs able to control alternative splicing have emerged as critical regulators of EMT in the last few years. Huelga and colleagues demonstrated on a genomic scale that RBPs coordinately regulate hundreds of pre-mRNA alternative splicing events forming dynamically regulated complexes (Huelga et al, 2012). ESRPs have been reported as epithelial-specific splicing regulators implicated in EMT-associated alternative exon usage (Warzecha et al., 2009; Bebee et al., 2015). Here, we report on the interaction between KHSRP and ESRPs in cells that co-express the three proteins. However, ESRP1 is not expressed while ESRP2 protein levels are low in

NMuMg cells (data not shown). Similarly, Lin28, a factor recently reported as a modulator of alternative splicing in breast cancer cells (Yang et al, 2015), is not expressed in NMuMg cells (data not shown). RNA helicases DDX5 and DDX17 have been implicated at different transcriptional and post-transcriptional levels in EMT and their expression is silenced by TGF-β treatment (Dardenne et al, 2014). However, their knockdown failed to affect the expression of EMT factors and to influence the KHSRP-dependent alternative splicing events in NMuMg cells (Briata & Gherzi, unpublished observation). Xu and colleagues have recently demonstrated that hnRNPM, competing with ESRP1, favors the mesenchymal-type alternative splicing of *Cd44* and other pre-mRNAs and promotes breast cancer metastasis by activating EMT (Xu et al, 2014). Also in this case, the fact that ESRP1 is absent and hnRNPM expression is silenced in a time-dependent manner in response to TGF-β in NMuMg cells (data not shown) makes it unlikely that this regulatory network is operative in our model. RBFOX2 is another important alternative splicing regulator in different tissues (Shapiro et al, 2011; Braeutigam et al, 2014; Damianov et al, 2016). However, a comparison of RBFOX2 target transcripts described elsewhere (Braeutigam et al, 2014) with the results of our analysis failed to reveal any overlap.

hnRNPA1 is a ubiquitous and predominantly nuclear RBP implicated in a number of cellular processes, including pre-mRNA splicing regulation (Matter et al, 2000; He & Smith, 2009; Bonomi et al, 2013; Douablin et al, 2015), and we and others have previously observed that KHSRP and hnRNPA1 associate in different cell types (Ruggiero et al, 2007; Michlewski & Càceres, 2010). Michlewski and Càceres demonstrated that the two proteins show similar binding preferences to RNA sequences (Michlewski & Càceres, 2010), and our *in vitro* binding data indicate that KHSRP and hnRNPA1 directly bind to a region located in the *intron 8-9* of *Cd44* pre-mRNA. Interestingly, this sequence includes two 'GGG' triplets, a preferred binding site for both KHSRP (Trabucchi et al, 2009), and hnRNPA1 (Michlewski & Càceres, 2010). On the basis of our RIP analyses, it is tempting to speculate that KHSRP and hnRNPA1 form a complex with *Enah*, *Cd44*, and *Fgfr2* pre-mRNAs, respectively, and that each protein is required to allow the other to interact with these target transcripts. TGF-β-induced KHSRP downregulation causes a destabilization of the RNA/protein complex and hnRNPA1, although still present, is unable to interact with *Enah*, *Cd44*, and *Fgfr2* pre-mRNAs.

Two recent reports suggested a major role for EMT in chemoresistance, and the analysis of our RNA-seq data showed that KHSRP regulates the expression of a relevant number of transcripts involved in drug transport and metabolism (Fischer et al, 2015; Zheng et al, 2015) (*Table 3*). This allows us to hypothesize that, in addition to affecting cell adhesion and migration, KHSRP could influence the expression of factors relevant to other crucial EMT-driven events.

equilibrative nucleoside transporters (Zheng et al., 2015)	**AdNull (TGF-b/ Untreated)**	**AdKHSRP (TGF-b/ Untreated)**	**log2FC AdNull/ AdKHSRP**	**p value AdNull (TGF-b/Untreated)**	**p value AdKHSRP (TGF-b/Untreated)**	**adj.pval AdNull/ AdKHSRP**
Slc29a1	0.496	-0.556	-1.052	0.01587	0.01535	0.00204
Slc29a4	1.889	0.871	-1.018	0	0.01404	0.01616
Slc29a2	0.329	-0.425	-0.753	0.18007	0.13148	0.05329
Slc29a3	0.132	0.071	-0.061	0.21356	0.54506	0.6918
concentrating nucleoside transporters Zheng et al., 2015)						
Slc28a2	-0.609	0.616	1.225	0.29068	0.25853	0.13292
Slc28a1	-0.34	0.462	0.801	0.5826	0.4861	0.38097
Slc28a3	-0.102	-1.008	-0.905	0.90362	0.22782	0.44506
chemoresistance-related (Fischer et al. 2015)						
Il6	4.775	3.047	-1.727	0	0.00022	0.04372
Postn	1.258	1.5	0.242	0.09578	0.08116	0.8199
Enpp2	-1.461	-1.745	-0.284	0.00079	2.00E-05	0.48625
Pdgfra	0.989	2.911	1.923	0.01841	5.00E-05	0.00654
Pdgfrl	0.253	-2.01	-2.263	0.52173	0.00515	0.00759
Pdgfrb	6.318	4.282	-2.036	0	0	0.01004
Krt5	-0.114	-2.754	-2.64	0.84954	0.00038	0.00725
Tle2	-0.988	-0.983	0.005	0.00033	0.00055	0.98663
phase II metab. enzymes (Fischer et al. 2015)						
Aox1	1.471	-0.311	-1.782	0	0.00566	0
Ces2g	-5.108	-3.19	1.917	0	0	0
Ces2e	-3.687	-2.14	1.547	0	0	0.00347
Ces2f	-2.996	-0.647	2.349	0.00074	0.22634	0.01528
Chst1	4.491	0.529	-3.962	0	0.22204	9.00E-05
Gsta3	-6.328	-4.955	1.373	0	0	0.00054
Gsto1	-1.149	-0.783	0.367	0	0	0.00023
Maoa	-1.198	-0.526	0.672	2.00E-05	0.00766	0.01431
Ugt1a6a	-4	-2.736	1.264	0	0	2.00E-04
Ugt1a7c	-4.364	-2.764	1.599	0	0	0.00019
phase I drug-metabolizing enzymes (Fischer et al. 2015)						
Aldh18a1	0.802	-0.066	-0.868	0	0.5219	7.00E-05
Aldh5a1	-1.776	-1.058	0.719	0	7.00E-05	0.00838
Aldh1a1	-5.204	-3.777	1.427	0	0	0.00993
Cyp4b1	-3.728	-2.375	1.352	0	0	1.00E-05
Cyp26b1	3.853	0.473	-3.38	0	0.10198	2.00E-05
Cyp3a13	-4.735	-2.651	2.083	0	0	2.00E-05
Cyp2ab1	3.071	-0.556	-3.628	0.00011	0.11383	0.00011
Cyp2c44	-3.357	-0.372	2.985	0	0.29559	0.00014
Cyp4a12b	-7.786	-4.964	2.822	0	0	0.00027
Cyp2d34	-3.754	-0.997	2.757	0	0.0416	0.00056
Cyp2j9	-4.893	-2.11	2.784	0	0.00162	0.00106
Cyp2c65	-8.396	-5.795	2.601	0	0	0.00114
Cyp3a16	-6.02	-2.865	3.154	0	0.00047	0.00149
Cyp2c69	-5.565	-2.989	2.576	0	0.00014	0.00246
Cyp2d9	-4.033	-1.756	2.277	0	0.0039	0.00326
Cyp2j5	-6.835	-4.459	2.377	0	0	0.00426
Ptgs2	4.76	3.151	-1.609	0	0	8.00E-05
Ptgs1	-1.471	-0.502	0.969	0	0.00098	0.00012

Table 3; Regulation by KHSRP of the expression levels of transcripts involved in drug transport and metabolism described in Fischer et al., 2015 and in Zheng et al., 2015.

NMuMg cells used in our studies are representative of an early stage of mammary transformation and respond to TGF-β-inducing KHSRP silencing and, as a consequence, a variety of EMT-like phenotypic changes. In more advanced stages of transformation, cells become independent of TGF-β signaling and TGF-β treatment fails to silence KHSRP expression. This is in agreement with the evidence that human tumors acquire loss-of-function mutations in genes encoding TGF-β receptors or SMAD proteins (Pardali & Moustakas, 2007). We speculate that KHSRP silencing is required in early stages of transformation in order to enable TGF-β to initiate cell trans-differentiation process. Our contribution to the understanding of how TGF-β-modulated KHSRP expression affects distinct layers of post-transcriptional gene control provides insights in the biology of epithelial cells that are poised to undergo a transition toward a mesenchymal phenotype.

In addition to greater chemoresistance, cells that have undergone EMT increase stem-like traits *in vitro* (Mani et al., 2008; Morel et al., 2008) and *in vivo* (Guo et al., 2012). This observation raised the hope that targeting EMT could eradicate the rare self-renewing and multipotent 'cancer stem cells' (CSCs) that persist following conventional chemotherapy. Several candidate EMT-reversing agents are already available clinically and it has been proposed to use these "EMT-reversing" inhibitors in combination with other drugs to generate synthetic lethality. Along these lines, small chemical inhibitors of various signaling pathway are currently being used in clinical trials for their anti-EMT activities. Our strategy was to investigate the potential of a natural compound, the resveratrol (RESV), previously proved to affect KHSRP function to revert EMT-associated gene expression changes.

We show that RESV limits EMT in mammary gland cells by affecting the alternative splicing pattern of pre-mRNAs related to cell adhesion and motility including *Cd44*, *Fgfr2*, and *Enah*. Our data indicate that RESV causes a shift from the mesenchymal-specific forms of the encoded factors to the respective epithelial forms in both immortalized and transformed mammary gland cells by modulating the expression of KHSRP and hnRNPA1 (*Figure 99*).

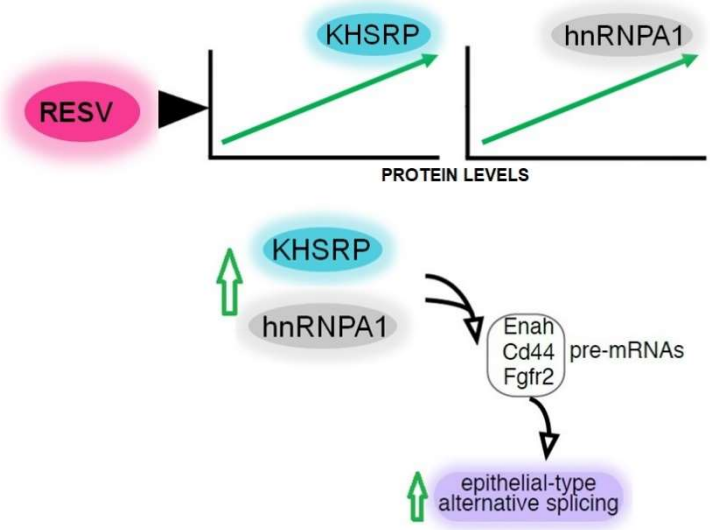

Figure 99; Schematic pathway of results reported here.

Markus and colleagues previously reported that RESV can affect the alternative splicing of transfected minigenes suggesting that this might be due to enhanced expression of a group RBPs (Markus et al, 2011). Our data demonstrate that RESV modulates the alternative splicing of endogenous pre-mRNAs that exert a crucial role in EMT and that RESV-dependent upregulation of KHSRP and hnRNPA1 is critical to enhance the epithelial-type exon usage of *Cd44* pre-mRNA in mammary gland cells.

Using a target-fishing approach with RESV as a bait and peripheral blood mononuclear cells as target source, Pautz and coworkers have proved that RESV directly interacts with KHSRP and modulates its mRNA decay promoting activity thus resulting in down-regulation of pro-inflammatory cytokine expression in colon cancer cells (Bollmann et al, 2014). In their report, authors show that RESV reduces the MAPK14-dependent threonine phosphorylation that has inhibitory effects on KHSRP mRNA decay-promoting function (Bollmann et al, 2014; Briata et al, 2005). It is well known that KHSRP can operate on multiple layers of post-transcriptional control in response to distinct stimuli depending on the cellular context (Briata et al, 2013; Briata et al, 2016). In the laboratory where I conducted my thesis as well as in other laboratories, it has been demonstrated that various cellular effectors influence KHSRP function through phosphorylation and/or cellular localization (Briata et al, 2013; Briata et al, 2016). However, in this thesis we demonstrate that KHSRP down-regulation is able to reshape the transcriptome preventing, in part, TGF-β-induced EMT in mammary gland cells.

Moreover, RESV seems to exert its effect regulating KHSRP levels even though our experiments cannot exclude a RESV-induced modulation of KHSRP function. It is interesting to note that here we observed that several breast cancer cell lines, including 4T1, display a limited EMT response to TGF-β and that TGF-β fails to reduce KHSRP levels. Our current data indicate that RESV up-regulates KHSRP expression also in 4T1 cells and that KHSRP silencing strongly influence alternative splicing in these cells. This reinforces the idea that RESV controls KHSRP function through modulation of its expression levels, at least in mammary gland cells.

Recent evidence demonstrated that several RBPs coordinately regulate hundreds of pre-mRNA alternative splicing events forming dynamically regulated ribonucleoprotein complexes (Huelga et al, 2012; Fu & Ares, 2014). Thus, although in our cellular models RESV activity on *Cd44* pre-mRNA splicing is abrogated by the combined silencing of KHSRP and hnRNPA1, it is very likely that RESV may target distinct ribonucleoprotein complexes to modulate pre-mRNA alternative splicing in other cellular contexts.

The importance of alternative splicing in various diseases (Cieply & Carstens, 2015) makes the identification of non-toxic compounds that inhibit certain splicing events of notable interest. Indeed, RESV ability to modulate the function and expression of different RBPs including KHSRP and hnRNPA1 might account for a part of the wide range of beneficial effects shown by the compound. However, RESV ability to affect different targets at different levels raises a specificity issue and makes compelling the necessity to investigate the whole spectrum of RESV potentialities at the molecular level.

Altogether, data presented in my thesis underscore the ability of KHSRP to exert a coordinate regulation of distinct post-transcriptional events in gene expression control during EMT. KHSRP controls pre-mRNA alternative splicing, unstable miRNA decay, and maturation of miRNAs from their precursors, depending on its cellular localization and on its cellular partners. Our findings point to KHSRP as a potential target for bioactive compounds that can be exploited to manipulate gene expression in cells undergoing tumor progression.

References

A

Acs G, Lawton TJ, Rebbeck TR, LiVolsi VA, and Zhang PJ. *Differential expression of E-cadherin in lobular and ductal neoplasms of the breast and its biologic and diagnostic implications.* Am J Clin Pathol. (2001); 115:85–98. doi: 10.1309/FDHX-L92R-BATQ-2GE0.

Anders S & Huber W. *Differential expression analysis for sequence count data.* Genome Biology (2010) 11(10): R106.

Anders S, Reyes A, and Huber W. *Detecting differential usage of exons from RNA-seq data.* Genome Research. 2012;22(10):2008-2017. doi:10.1101/gr.133744.111.

Anders S, Pyl PT, and Huber W. *HTSeq–a Python framework to work with high-throughput sequencing data.* Bioinformatics (2015); 31,166-169.

Andriani F, Bertolini G, Facchinetti F, Baldoli E, Moro M, Casalini P, et al. *Conversion to stem-cell state in response to microenvironmental cues is regulated by balance between epithelial and mesenchymal features in lung cancer cells.* Mol Oncol. (2016). doi: 10.1016/j.molonc.2015.10.

002.

Aparicio LA, Abella V, Valladares M, and Figueroa A. *Posttranscriptional regulation by RNA-binding proteins during epithelial-to-mesenchymal transition.* Cell Mol Life Sci. (2013) 70, 4463-4477.

Avery-Cooper G, Doerr M, Gilbert RW, Youssef M, Richard A, Huether P, and Viloria-Petit AM. (2014). *Par6 is an essential mediator of apoptotic response to transforming growth factor beta in NMuMG immortalized mammary cells.* Cancer Cell Int. 14, 19.

B

Batista PJ & Chang HY. *Long noncoding RNAs: cellular address codes in development and disease.* Cell (2013); 152, 1298–1307.

Baur JA & Sinclair DA. *Therapeutic potential of resveratrol: the in vivo evidence.* Nat Rev Drug Discov (2006); 5:493–506.

Bebee TW, Park JW, Sheridan KI, et al. *The splicing regulators Esrp1 and Esrp2 direct an epithelial splicing program essential for mammalian development*. eLife. 2015; 4:e08954. doi:10.7554/eLife.08954.

Bicknell AA & Ricci EP. *When mRNA translation meets decay*. Biochem Soc Trans (2017), Apr 15;45(2):339-351. doi: 10.1042/BST20160243.

Bierie B & Moses HL. *Tumour microenvironment: TGFβ: the molecular Jekyll and Hyde of cancer*. Nat Rev Cancer (2006); 6: 506–20.

Bindea G, Mlecnik B, Hackl H, Charoentong P, Tosolini M, Kirilovsky A, Fridman WH, Pagès F, Trajanoski Z, Galon J. *ClueGO: a Cytoscape plug-in to decipher functionally grouped gene ontology and pathway annotation networks*. Bioinformatics (2009); Apr 15; 25(8):1091-3.

Black DL & Grabowski PJ. *Alternative pre-mRNA splicing and neuronal function*. Prog Mol Subcell Biol. 2003;31:187-216.

Blahna MT & Hata A. *Smad-mediated regulation of microRNA biosynthesis*. FEBS Lett. (2012); 586, 1906-1912.

Block KI, Gyllenhaal C, Lowe L, et al. *A Broad-Spectrum Integrative Design for Cancer Prevention and Therapy*. Seminars in cancer biology (2015), 35(Suppl): S276-S304. doi:10.1016/j.semcancer.2015.09.007.

Bollmann F, Art J, Henke J, Schrick K, Besche V, Bros M, Li H, Siuda D, Handler N, Bauer F, Erker T, Behnke F, Mönch B, Härdle L, Hoffmann M, Chen CY, Förstermann U, Dirsch VM, Werz O, Kleinert H, and Pautz A. *Resveratrol post-transcriptionally regulates pro-inflammatory gene expression via regulation of KHSRP RNA binding activity*. Nucleic Acids Res 42, 12555-12569 (2014). doi: 10.1093/nar/gku1033.

Bolos V, Peinado H, Perez-Moreno MA, Fraga MF, Esteller M, and Cano A. *The transcription factor slug represses E-cadherin expression and induces epithelial to mesenchymal transitions: a comparison with Snail and E47 repressors*. J Cell Sci. 2003; 116:499–511.

Bonomi S, di Matteo A, Buratti E, Cabianca DS, Baralle FE, Ghigna C, and Biamonti G. *HnRNP A1 controls a splicing regulatory circuit promoting mesenchymal-to-epithelial transition.* Nucleic Acids Res. 41, 8665-8679 (2013).

Braddock DT, Louis JM, Baber JL, Levens D, and Clore GM. *Structure and dynamics of KH domains from FBP bound to single-stranded DNA*. Nature 415,1051–1056 (2002).

Braeutigam C, Rago L, Rolke A, Waldmeier L, Christofori G, and Winter J. *The RNA-binding protein Rbfox2: an essential regulator of EMT-driven alternative splicing and a mediator of cellular invasion*. Oncogene. 2014 Feb 27;33(9):1082-92. doi: 10.1038/onc.2013.50.

Briata P, Bordo D, Puppo M, Gorlero F, Rossi M, Perrone-Bizzozero N, and Gherzi R. *Diverse roles of the nucleic acid-binding protein KHSRP in cell differentiation and disease*. WIREs RNA (2016). doi: 10.1002/wrna.1327.

Briata P, Chen CY, Ramos A, and Gherzi R. *Functional and molecular insights into KHSRP function in mRNA decay*. Biochim. Biophys. Acta1829, 689-694 (2013). doi: 10.1016/j.bbagrm.2012.11.003.

Briata P, Forcales SV, Ponassi M, Corte G, Chen CY, Karin M, Puri PL, and Gherzi R. *p38-dependent phosphorylation of the mRNA decay-promoting factor KHSRP controls the stability of select myogenic transcripts*. Mol. Cell 20, 891-903 (2005).

Briata P, Lin WJ, Giovarelli M, Pasero M, Chou CF, Trabucchi M, Rosenfeld MG, Chen CY, and Gherzi R. *PI3K/AKT signaling determines a dynamic switch between distinct KSRP functions favoring skeletal myogenesis*. Cell Death Differ (2012) Mar; 19(3):478-87. doi: 10.1038/cdd.2011.117.

Britton RG, Kovoor C, and Brown K. *Direct molecular targets of resveratrol: identifying key interactions to unlock complex mechanisms*. Ann N Y Acad Sci. 2015 Aug; 1348(1):124-33. doi: 10.1111/nyas.12796.

Brivanlou A & Darnell J. *Signal Transduction and the Control of Gene Expression*. Science 01 Feb 2002: Vol. 295, Issue 5556, pp. 813-818. doi: 10.1126/science.1066355

Brown RL, Reinke LM, Damerow MS, Perez D, Chodosh LA, Yang J, and Cheng C. *CD44 splice isoform switching in human and mouse epithelium is essential for epithelial-mesenchymal transition and breast cancer progression*. J. Clin. Invest. 121, 1064-1074 (2011). doi: 10.1172/JCI44540.

Bullock MD, Sayan AE, Packham GK, and Mirnezami AH. *MicroRNAs: Critical regulators of epithelial to mesenchymal (EMT) and mesenchymal to epithelial transition (MET) in cancer progression*. Biol. Cell 2012, 104, 3–12.

C

Calin GA & Croce CM. *MicroRNA signatures in human cancers*. Nat Rev Cancer. 2006 Nov; 6(11):857-66.

Canel M, Serrels A, Frame MC, and Brunton VG. *E-cadherin-integrin crosstalk in cancer invasion and metastasis*. J Cell Sci. (2013). doi:10.1242/jcs.100115.

Canto C & Auwerx J. *Targeting sirtuin 1 to improve metabolism: all you need is NAD (+)?* Pharmacol. Rev. 64, 166–187 (2012).

Chaudhury A, Chander P, and Howe PH. *Heterogeneous nuclear ribonucleoproteins (hnRNPs) in cellular processes: Focus on hnRNP E1's multifunctional regulatory roles*. RNA (2010); 16(8):1449-1462. doi:10.1261/rna.2254110.

Chen CY, Gherzi R, Ong SE, Chan EL, Raijmakers R, Pruijn GJ, Stoecklin G, Moroni C, Mann M, and Karin M. *AU binding proteins recruit the exosome to degrade ARE-containing mRNAs*. Cell. (2001); 107:451–464.

Chen EY, Tan CM, Kou Y, Duan Q, Wang Z, Meirelles GV, Clark NR, and Ma'ayan A. *Enrichr: interactive and collaborative HTML5 gene list enrichment analysis tool.* BMC Bioinformatics. 2013 Apr 15;14:128.

Chen J, Zhou Y, Mueller-Steiner S, Chen LF, Kwon H, Yi S, Mucke L, and Gan L. *SIRT1 protects against microglia-dependent amyloid-beta toxicity through inhibiting NF-kappaB signaling*. J Biol Chem 2005; 280:40364–40374.

Chen CY, Gherzi R, Andersen JS, Gaietta G, Jürchott K, Royer HD, Mann M, and Karin M. *Nucleolin and YB-1 are required for JNK-mediated interleukin-2 mRNA stabilization during T-cell activation*. Genes Dev. (2000); 14, 1236-1248.

Chen Y & Varani G. *Engineering RNA-binding proteins for biology*. The FEBS Journal, 280 (16), 3734–3754. (2013) http://doi.org/10.1111/febs.12375.

Chong J, Poutaraud A, and Hugueney P. *Metabolism and roles of stilbenes in plants*. Plant Science, Volume 177, 3, 2009, 143-155. doi: 10.1016/j.plantsci.2009.05.012.

Cieply B & Carstens RP. *Functional roles of alternative splicing factors in human disease*. Wiley Interdiscip. Rev. RNA. 6, 311-326 (2015). doi: 10.1002/wrna.1276.

D

Damianov A, Ying Y, Lin C-H, et al. *Rbfox proteins regulate splicing as part of a large multiprotein complex LASR*. Cell 2016; 165(3):606-619. doi:10.1016/j.cell.2016.03.040.

Dandawate PR, Subramaniam D, Jensen RA, and Anant S. *Targeting cancer stem cells and signaling pathways by phytochemicals: Novel approach for breast cancer therapy*. Semin. Cancer Biol. (2016). doi: 10.1016/j.semcancer.2016.09.001.

Dardenne E, Polay Espinoza M, Fattet L, Germann S, Lambert MP, Neil H, Zonta E, Mortada H, Gratadou L, Deygas M, Chakrama FZ, Samaan S, Desmet FO, Tranchevent LC, Dutertre M, Rimokh R, Bourgeois CF, and Auboeuf D. *RNA helicases DDX5 and DDX17 dynamically orchestrate transcription, miRNA, and splicing programs in cell differentiation*. Cell Rep (2014); 7, 1900-1913.

Das S, Sarkar D, and Das B. *The interplay between transcription and mRNA degradation in Saccharomyces cerevisiae*. Microbial Cell. (2017); 4(7):212-228. doi:10.15698/mic2017.07.580.

Davis-Smyth T, Duncan RC, Zheng T, Michelotti G, and Levens D. *The far upstream element-binding proteins comprise an ancient family of single-strand DNA-binding transactivators*. J. Biol. Chem. (1996); 271, 31679-31687.

De Craene B & Berx G. *Regulatory networks defining EMT during cancer initiation and progression*. Nat. Rev. Cancer 13, 97-110 (2013) .

Dewick PM. *Medicinal natural products: A biosynthetic approach, 2nd Edition*. New York, NY: John Wiley & Sons, Ltd, 2002; 1–507.

Ding XM. *MicroRNAs: Regulators of cancer metastasis and epithelial-mesenchymal transition (EMT)*. Chin. J. Cancer 2014, 33, 140–147.

Dinger ME, Pang KC, Mercer TR, and Mattick JS. *Differentiating Protein-Coding and Noncoding RNA: Challenges and Ambiguities*. PLoS Computational Biology 2008; 4(11): e1000176. doi:10.1371/journal.pcbi.1000176.

Dobin A, Davis, C.A, Schlesinger, F, Drenkow, J, Zaleski, C, Jha, S, Batut, P, Chaisson, M, and Gingeras, T.R. *STAR: ultrafast universal RNA-seq aligner*. Bioinformatics 29,15-21 (2013).

Dong P, Kaneuchi, M, Watari, H, Hamada, J, Sudo, S, Ju, J, and Sakuragi, N. *MicroRNA-194 inhibits epithelial to mesenchymal transition of endometrial cancer cells by targeting oncogene.* BMI-1. Mol. Cancer 10, 99 (2011).

Douablin A, Deguillien, M, Breig, O, and Baklouti, F. *HnRNP A1 tethers KHSRP to an exon splicing silencer that inhibits an erythroid-specific splicing event in PU.1-induced erythroleukemia.* Am. J. Cancer Res. 5,1410-1422 (2015).

Duncan R, Bazar L, Michelotti G, Tomonaga T, Krutzsch H, Avigan M and Levens D. *A sequence-specific, single-stranded binding protein activates the far upstream element of c-myc and defines a new DNA-binding motif.* Genes Dev 8, 465–480 (1994).

E

Ehata S, Hanyu A, Hayashi M et al. *Transforming growth factor-β promotes survival of mammary carcinoma cells through induction of antiapoptotic transcription factor DEC1.* Cancer Res 2007; 67: 9694–703.

Elenbaas B, Spirio L, Koerner F, Fleming MD, Zimonjic DB, Donaher JL, Popescu NC, Hahn WC, and Weinberg, RA. *Human breast cancer cells generated by oncogenic transformation of primary mammary epithelial cells.* Genes Dev. 15, 50–65 (2001).

Esteller M. *Non-coding RNAs in human disease.* Nat. Rev. Genet. 12, 861–874 (2011).

F

Ferraz da Costa DC, Fialho E, and Silva JL. *Cancer Chemoprevention by Resveratrol: The p53 Tumor Suppressor Protein as a Promising Molecular Target.* Molecules (2017) Jun 18;22(6). pii: E1014. doi: 10.3390/molecules22061014.

Fischer KR, Durrans A, Lee S, Sheng J, Li F, Wong ST, Choi H, El Rayes T, Ryu S, Troeger J, Schwabe RF, Vahdat LT, Altorki NK, Mittal V, and Gao D. *Epithelial-to-mesenchymal transition is not required for lung metastasis but contributes to chemoresistance.* Nature 527, 472-476 (2015).

Flynn RA & Chang HY. *Long noncoding RNAs in cell-fate programming and reprogramming.* Cell Stem Cell. 2014 Jun 5;14(6):752-61. doi: 10.1016/j.stem.2014.05.014.

Fredericks AM, Cygan KJ, Brown BA, and Fairbrother WG. *RNA-Binding Proteins: Splicing Factors and Disease.* Gerber AP, ed. Biomolecules. 2015; 5(2):893-909. doi:10.3390/biom5020893.

G

García-Mayoral MF, Diaz-Moreno I, Hollingworth D, and Ramos A. *The sequence selectivity of KHSRP explains its flexibility in the recognition of the RNA targets.* Nucleic Acids Res, 36, 5290–5296 (2008).

Garneau NL, Wilusz J, and Wilus CJ. *The highways and byways of mRNA decay.* Nat. Rev. Mol. Cell Biol. 2007; 8, 113-26.

Geng L, Chaudhuri A, Talmon G, Wisecarver JL, Are C, Brattain M, and Wang J. *MicroRNA-192 suppresses liver metastasis of colon cancer.* Oncogene 33, 5332-5340 (2014).

Gherzi R, Chen CY, Ramos A, and Briata P. *KSRP controls pleiotropic cellular functions.* Semin Cell Dev Biol. 2014 Oct; 34:2-8. doi: 10.1016/j.semcdb.2014.05.004.

Gherzi R, Chen CY, Trabucchi M, Ramos A, and Briata P. *The role of KHSRP in mRNA decay and microRNA precursor maturation.* Wiley Interdiscip. Rev. RNA 1 (2010) 230–239.

Gherzi R, Lee KY, Briata P, Wegmüller D, Moroni C, Karin M, and Chen CY. *A KH domain RNA binding protein, KSRP, promotes ARE-directed mRNA turnover by recruiting the degradation machinery.* Mol Cell. 2004 Jun 4;14(5):571-83.

Gherzi R, Trabucchi M, Ponassi M, et al. *The RNA-Binding Protein KSRP Promotes Decay of β-Catenin mRNA and Is Inactivated by PI3K-AKT Signaling.* PLoS Biology. 2006; 5(1):e5. doi:10.1371/journal.pbio.0050005. (Retracted)

Gibb EA, Brown CJ, and Lam WL. *The functional role of long non-coding RNA in human carcinomas.* Mol. Cancer 2011, 10, 38.

Giovarelli M, Bucci G, Ramos A, Bordo D, Wilusz CJ, Chen CY, Puppo M, Briata P, and Gherzi R. *H19 long noncoding RNA controls the mRNA decay promoting function of KHSRP.* Proc. Natl. Acad. Sci. U S A 111, E5023-5028 (2014).

Gonzalez DM & Medici D. *Signaling mechanisms of the epithelial-mesenchymal transition.* Science Signaling 2014, 7(344), re8. http://doi.org/10.1126/scisignal.2005189.

Grishin NV. *KH domain: one motif, two folds*. Nucleic Acids Res. (2001); Feb 1; 29(3):638-43.

Greenburg G & Hay ED. *Epithelia suspended in collagen gels can lose polarity and express characteristics of migrating mesenchymal cells*. J Cell Biol (1982) 95: 333–339

Grosse-Wilde A, Fouquier d'Hérouël A, McIntosh E, et al. *Stemness of the hybrid Epithelial/Mesenchymal State in Breast Cancer and Its Association with Poor Survival*. Ben-Jacob E, ed. *PLoS ONE*. 2015; 10(5):e0126522. doi:10.1371/journal.pone.0126522.

Guilford P, Hopkins J, Harraway J, McLeod M, McLeod N, Harawira P, et al. *E-cadherin germline mutations in familial gastric cancer*. Nature. 1998. doi:10.1038/32918.

Guo W, Keckesova Z, Donaher JL, et al. *Slug and Sox9 Cooperatively Determine the Mammary Stem Cell State*. Cell. 2012; 148(5):1015-1028. doi:10.1016/j.cell.2012.02.008.

Gutschner T & Diederichs, S. *The hallmarks of cancer: A long non-coding RNA point of view*. RNA Biol. 2012, 9, 703–719.

H

Ha M & Kim VN. *Regulation of microRNA biogenesis*. Nat Rev Mol Cell Biol, 2014 Aug; 15(8):509-24. doi: 10.1038/nrm3838.

Han GJ, Xia JG, Inagaki Y, Tang W, and Kokudo N. *Anti-tumor effects and cellular mechanisms of resveratrol*. Drug Discov. Ther. 9 (2015) 1–12. http://dx.doi.org/10.5582/ddt.2015.01007.

Hashimoto Y, Akiyama Y, and Yuasa Y. *Multiple-to-multiple relationships between microRNAs and target genes in gastric cancer*. PLoS One. 2013 May 8; 8(5):e62589. doi: 10.1371/journal.pone.0062589.

He Y & Smith R. *Nuclear functions of heterogeneous nuclear ribonucleoproteins A/B*. Cell Mol. Life Sci. 66,1239-1256 (2009).

Heery R, Finn SP, Cuffe S, and Gray SG. *Long Non-Coding RNAs: Key Regulators of Epithelial-Mesenchymal Transition, Tumour Drug Resistance and Cancer Stem Cells*. Cancers (2017); 9(4):38. doi:10.3390/cancers9040038.

Heo I, Joo C, Cho J, Ha M, Han J, and Kim VN. *Lin28 mediates the terminal uridylation of let-7 precursor MicroRNA*. Mol Cell (2008) 32: 276–284.

Hollingworth D, Candel AM, Nicastro G, Martin SR, Briata P, Gherzi R, and Ramos A. *KH domains with impaired nucleic acid binding as a tool for functional analysis*. Nucleic Acids Research. 2012; 40(14):6873-6886. doi:10.1093/nar/gks368.

Horiguchi K, Sakamoto K, Koinuma D et al. *TGF-β drives epithelial-mesenchymal transition through δEF1-mediated downregulation of ESRP*. Oncogene 2012; 31: 3190–201.

Houseley J & Tollervey D. *The Many Pathways of RNA Degradation*. Cell (2009). Volume 136, Issue 4 , 763 - 776.

Hsieh TC, Wong C, John Bennett D, Wu JM. *Regulation of p53 and cell proliferation by resveratrol and its derivatives in breast cancer cells: An in silico and biochemical approach targeting integrin v 3*. Int. J. Cancer 2011, 129, 2732–2743.

Huelga SC, Vu AQ, Arnold JD, Liang TY, Liu PP, Yan BY, Donohue JP, Shiue L, Hoon S, Brenner S, Ares MJ, and Yeo GW. *Integrative genome-wide analysis reveals cooperative regulation of alternative splicing by hnRNP proteins*. Cell Rep. 1, 167-178 (2012).

I

Ikenouchi J, Matsuda M, Furuse M, and Tsukita S. *Regulation of tight junctions during the epithelium-mesenchyme transition: direct repression of the gene expression of claudins/occludin by Snail*. Journal of Cell Science 2003 116: 1959-1967; doi: 10.1242/jcs.00389.

Ikushima H & Miyazono K. *TGFβ signalling: A complex web in cancer progression*. Nat. Rev. Cancer 2010, 10, 415–424.

Ingolia NT, Lareau LF, and Weissman JS. *Ribosome Profiling of Mouse Embryonic Stem Cells Reveals the Complexity of Mammalian Proteomes*. Cell (2011); 147(4):789-802. doi:10.1016/ j.cell.2011.10.002.

Ishikawa K, He S, Terasaki H, Nazari H, Zhang H, Spee C, and Hinton DR. *Resveratrol inhibits epithelial-mesenchymal transition of retinal pigment epithelium and development of proliferative vitreoretinopathy*. Scientific Reports, 5, 16386 (2015). http://doi.org/10.1038/ srep16386.

J

Jo MH, Song J-J, and Hohng S. *Single-molecule fluorescence measurements reveal the reaction mechanisms of the core-RISC, composed of human Argonaute 2 and a guide RNA*. BMB Reports 2015; 48(12):643-644. doi:10.5483/BMBRep.2015.48.12.235.

Jolly MK, Jia D, Boareto M, Mani SA, Pienta KJ, Ben-Jacob E, et al. *Coupling the modules of EMT and stemness: a tunable 'stemness window' model.* Oncotarget. 2015. doi:10.18632/oncotarget.4629.

Jolly MK, Ward C, Eapen MS, Myers S, Hallgren O, Levine H, and Sohal SS. *Epithelial mesenchymal transition (EMT), a spectrum of states: role in lung development, homeostasis and disease.* Dev. Dyn. Accepted Author Manuscript (2017). doi:10.1002/dvdy.24541.

Jolly MK, Boareto M, Huang B, Jia D, Lu M, Ben-Jacob E, Onuchic JN, and Levine H. *Implications of the Hybrid Epithelial/Mesenchymal Phenotype in Metastasis.* Front. Oncol. 5, 155 (2015).

K

Kalluri R & Neilson EG. *Epithelial mesenchymal transition and its implications for fibrosis.* J. Clin. Invest. 112:1776–1784 (2003).

Kalluri R & Weinberg RA. *The basics of epithelial-mesenchymal transition.* J. Clin. Invest. 119, 1420-1428 (2009).

Katsuno Y, Lamouille S, and Derynck R. *TGF-β signaling and epithelial-mesenchymal transition in cancer progression.* Curr. Opin. Oncol. 25, 76-84 (2013).

Kessenbrock K, Plaks V, and Werb Z. *Matrix metalloproteinases: regulators of the tumor microenvironment.* Cell. 2010. doi: 10.1016/j.cell.2010.03.015.

Kilchert C, Wittmann S, and Vasiljeva L. *The regulation and functions of the nuclear RNA exosome complex.* Nat Rev Mol Cell Biol. (2016); 17(4):227-39. doi:10.1038/nrm. 2015.15.

Kim HJ, Litzenburger BC, Cui X, Delgado DA, Grabiner BC, Lin X, Lewis MT, Gottardis MM, Wong TW, Attar RM, Carboni JM, and Lee AV. *Constitutively active type I insulin-like growth factor receptor causes transformation and xenograft growth of immortalized mammary epithelial cells and is accompanied by an epithelial-to-mesenchymal transition mediated by NF-kB and Snail.* Mol. Cell. Biol. (2007) 27, 3165–3175.

Kim N, Kim H, Jung I, Kim Y, Kim D, and Han YM. *Expression profiles of miRNAs in human embryonic stem cells during hepatocyte differentiation.* Hepatol Res. 2011 Feb; 41(2):170-83. doi: 10.1111/j.1872-034X.2010.00752.x.

Kouzarides T. *Chromatin modifications and their function*. Cell. 2007. doi:10.1016/ j.cell. 2007.11.005.

Krol J, Loedige I, and Filipowicz W. *The widespread regulation of microRNA biogenesis, function and decay*. Nat Rev Genet 2010 Sep; 11(9):597-610. doi: 10.1038/nrg2843.

Kurrey NK, Jalgaonkar SP, Joglekar AV, Ghanate AD, Chaskar PD, Doiphode RY, and Bapat SA. *Snail and slug mediate radioresistance and chemoresistance by antagonizing p53-mediated apoptosis and acquiring a stem-like phenotype in ovarian cancer cells*. Stem Cells. 2009 Sep; 27(9):2059-68.

L

Lamouille S, Subramanyam D, Blelloch R, and Derynck R. *Regulation of epithelial-mesenchymal and mesenchymal-epithelial transitions by microRNAs*. Curr. Opin. Cell Biol. (2013); 25, 200-207.

Langmead B & Salzberg, SL. *Fast gapped-read alignment with Bowtie 2*. Nat. Methods, 9, 357–359 (2012).

Latruffe N, Lançon A, Frazzi R, Aires V, Delmas D, Michaille JJ, Djouadi F, Bastin J, and Cherkaoui-Malki M. *Exploring new ways of regulation by resveratrol involving miRNAs, with emphasis on inflammation*. Ann. N. Y. Acad. Sci. 1348 (2015) 97–106. http://dx.doi.org/10.1111/nyas.12819.

Le XF, Almeida MI, Mao W, Spizzo R, Rossi S, Nicoloso MS, Zhang S, Wu Y, Calin GA, and Bast RC. Jr. *Modulation of MicroRNA-194 and cell migration by HER2-targeting trastuzumab in breast cancer*. PLoS One (2012) 7, e41170.

Lellek H, Kirsten R, Diehl I, Apostel F, Buck F, and Greeve J. *Purification and molecular cloning of a novel essential component of the apolipoprotein B mRNA editing enzyme-complex*. J. Biol. Chem. (2000); 275, 19848-19856.

Lewis HA, Musunuru K, Jensen KB, Edo C, Chen H, Darnell RB, and Burley SK. *Sequence-specific RNA binding by a Nova KH domain: implications for paraneoplastic disease and the fragile X syndrome*. Cell. 2000; 100:323–32.

Li H, Handsaker B, Wysoker A, Fennell T, Ruan J, Homer N, and Durbin R. *The Sequence Alignment/Map format and SAM tools*. Bioinformatics 25, 2078–2079 (2009).

Lim J & Thiery JP. *Epithelial-mesenchymal transitions: Insights from development*. Development 139, 3471–3486 (2012).

Lin HY, Tang HY, Davis FB, and Davis PJ. *Resveratrol and apoptosis*. Ann. N. Y. Acad. Sci. 2011, 1215, 79–88.

Liu Y & Liu Q. *ATM Signals miRNA Biogenesis Through KHSRP*. Molecular cell. 2011; 41(4):367-368. doi:10.1016/j.molcel.2011.01.027.

M

Mani SA, Guo W, Liao M-J, et al. *The epithelial-mesenchymal transition generates cells with properties of stem cells*. Cell. 2008; 133(4):704-715. doi:10.1016/j.cell.2008.03.027.

Marambaud P, Zhao H, and Davies P. *Resveratrol promotes clearance of Alzheimer's disease amyloid-beta peptides*. J Biol Chem 2005; 280:37377–37382.

Markus MA, Marques FZ, and Morris BJ. *Resveratrol, by modulating RNA processing factor levels, can influence the alternative splicing of pre-mRNAs*. PLoS One 6, e28926 (2011). doi: 10.1371/journal.pone.0028926.

Martinez-Estrada OM, Culleres A, Soriano FX, Peinado H, Bolos V, Martinez FO, et al. *The transcription factors Slug and Snail act as repressors of Claudin-1 expression in epithelial cells*. Biochem J. 2006. doi:10.1042/BJ20050591.

Matsuda Y, Hagio M, Seya T, and Ishiwata T. *Fibroblast growth factor receptor 2 IIIc as a therapeutic target for colorectal cancer cells*. Mol. Cancer Ther. 11, 2010-2020 (2012). doi: 10.1158/1535-7163.

Matter N, Marx M, Weg-Remers S, Ponta H, Herrlich P, and König H. *Heterogeneous ribonucleoprotein A1 is part of an exon-specific splice-silencing complex controlled by oncogenic signaling pathways*. J. Biol. Chem. 275, 35353-60 (2000).

McDonald OG, Wu H, Timp W, Doi A, and Feinberg AP. *Genome-scale epigenetic reprogramming during epithelial-to-mesenchymal transition*. Nat. Struct. Mol. Biol. 18, 867–874 (2011).

Michlewski G & Cáceres JF. *Antagonistic role of hnRNP A1 and KHSRP in the regulation of let-7a biogenesis*. Nat. Struct. Mol. Biol. 17, 1011-1018 (2010).

Min H, Turck CW, Nikolic JM, and Black DL. *A new regulatory protein, KHSRP, mediates exon inclusion through an intronic splicing enhancer.* Genes Dev. 11, 1023-1036 (1997).

Morel A-P, Lièvre M, Thomas C, Hinkal G, Ansieau S, and Puisieux A. *Generation of Breast Cancer Stem Cells through Epithelial-Mesenchymal Transition*. Klefstrom J, ed. PLoS ONE. 2008; 3(8): e2888. doi:10.1371/journal.pone.0002888.

Moshiri A, Puppo M, Rossi M, Gherzi R, and Briata P. *Resveratrol limits epithelial to mesenchymal transition through modulation of KHSRP/hnRNPA1-dependent alternative splicing in mammary gland cells.* Biochim Biophys Acta (2017) Mar; 1860(3):291-298. doi: 10.1016/j.bbagrm.2017.01.001.

Moustakas A & Heldin CH. *Induction of epithelial-mesenchymal transition by transforming growth factor β.* Semin.Cancer Biol. 22, 446-454 (2012).

Nakanishi K. *Anatomy of RISC: how do small RNAs and chaperones activate Argonaute proteins?* Wiley Interdisciplinary Reviews RNA. 2016; 7(5):637-660. doi:10.1002/wrna.1356.

N

Nicastro G, García-Mayoral MF, Hollingworth D, et al. *Non-canonical Guanine recognition mediates KSRP regulation of Let-7 biogenesis.* Nature structural & molecular biology (2012); 19(12):1282-1286. doi:10.1038/nsmb.2427.

Nieto MA, Huang RY, Jackson RA, and Thiery JP. *EMT: 2016*. Cell 166, 21-45 (2016). doi: 10.1016/j.cell.2016.06.028.

O

Orallo F. *Comparative studies of the antioxidant effects of cis- and trans-resveratrol.* Curr Med Chem 2006; 13:87–98.

P

Palumbo MO, Kavan P, Miller WH, et al. *Systemic cancer therapy: achievements and challenges that lie ahead.* Frontiers in Pharmacology (2013), 4:57. doi:10.3389/fphar.2013.00057.

Pan Q, Shai O, Lee LJ, Frey BJ, and Blencowe BJ. *Deep surveying of alternative splicing complexity in the human transcriptome by high-throughput sequencing.* Nat. Genet. 2008; 40:1413–1415. doi: 10.1038/ng.259.

Pardali K & Moustakas A. *Actions of TGF-beta as tumor suppressor and pro-metastatic factor in human cancer*. Biochim Biophys Acta.1775, 21-62 (2007).

Pasero M, Giovarelli M, Bucci G, Gherzi R, and Briata P. *Bone morphogenetic protein/SMAD signaling orients cell fate decision by impairing KHSRP-dependent microRNA maturation*. Cell Rep. 2, 1159-1168 (2012). doi: 10.1016/j.celrep.2012.10.020.

Pattabiraman DR & Weinberg RA. *Targeting the Epithelial-to-Mesenchymal Transition: The Case for Differentiation-Based Therapy*. Cold Spring Harb Symp Quant Biol. (2016); 81:11-19. doi: 10.1101/sqb.2016.81.030957.

Pharoah PD, Guilford P, and Caldas C. *International gastric cancer linkage C. Incidence of gastric cancer and breast cancer in CDH1 cancer families*. Gastroenterology (2001); 121:1348–53.

Polyak K & Weinberg RA. *Transitions between epithelial and mesenchymal states: acquisition of malignant and stem cell traits*. Nat. Rev. Cancer (2009); 9, 265-273.

Ponting CP, Oliver PL, and Reik W. *Evolution and functions of long noncoding RNAs*. Cell (2009); 136, 629–641.

Prensner JR & Chinnaiyan AM. *The emergence of lncRNAs in cancer biology*. Cancer Discov (2011); 1, 391–407.

Prieto-García E, Díaz-García CV, García-Ruiz I et al. *Epithelial-to-mesenchymal transition in tumor progression*. Med Oncol. 34:122 (2017). doi:10.1007/s12032-017-0980-8.

Puppo M, Bucci G, Rossi M, Giovarelli M, Bordo D, Moshiri A, Gorlero F, Gherzi R, and Briata P. *miRNA-Mediated KHSRP Silencing Rewires Distinct Post-Transcriptional Programs during TGF-β-Induced Epithelial-to-Mesenchymal Transition*. Cell Rep. 16, 967-978 (2016). doi: 10.1016/j.celrep.2016.06.055.

Q

Qi X, Zhang L, and Lu X. *New Insights into the Epithelial-to-Mesenchymal Transition in Cancer*. Trends Pharmacol. Sci (2016).

Quinlan AR & Hall IM. *BEDTools: A flexible suite of utilities for comparing genomic features*. Bioinformatics 26, 841–842 (2010).

Quinn JJ & Chang HY. *Unique features of long non-coding RNA biogenesis and function*. Nat Rev Genet. 2016 Jan;17(1):47-62. doi: 10.1038/nrg.2015.10.

R

Repetto E, Briata P, Kuziner N, Harfe BD, McManus MT Gherzi R, Rosenfeld MG and Trabucchi M. *Let-7b/c Enhance the Stability of a Tissue-Specific mRNA During Mammalian Organogenesis as Part of a Feedback Loop Involving KHSRP*. PLoS Genet 8 (7), e1002823. 2012 Jul 26.

Ring HZ, Vameghi-Meyers V, Nikolic JM, et al. *Mapping of the KHSRP gene to a region of conserved synteny on human chromosome 19p13.3 and mouse chromosome 17*. Genomics (1999); 56 (3): 350–2. doi:10.1006/geno.1998.5725.

Rinn JL & Chang HY. *Genome regulation by long noncoding RNAs*. Annu. Rev. Biochem. 81, 145–166 (2012).

Rocha-González HI, Ambriz-Tututi M, and Granados-Soto V. *Resveratrol: a natural compound with pharmacological potential in neurodegenerative diseases*. CNS Neurosci Ther (2008) Fall; 14(3):234-47. doi: 10.1111/j.1755-5949.2008.00045.x.

Rüegger S & Großhans H. *MicroRNA turnover: when, how, and why*. Trends Biochem Sci. 2012 Oct; 37(10):436-46. doi: 10.1016/j.tibs.2012.07.002.

Ruggiero T, Trabucchi, M, Ponassi, M, Corte G, Chen CY, al-Haj L, Khabar KS, Briata P, and Gherzi R. *Identification of a set of KHSRP target transcripts upregulated by PI3K-AKT signaling*. BMC Mol Biol. 16, 8:28 (2007).

Russo A, Catillo M, Esposito D, Briata P, Pietropaolo C, and Russo G. *Autoregulatory circuit of human rpL3 expression requires hnRNP H1, NPM and KHSRP*. Nucleic Acids Res. 2011; 39:7576–7585. doi: 10.1093/nar/gkr461.

S

Saitoh M. *Epithelial–mesenchymal transition is regulated at posttranscriptional levels by transforming growth factor-beta signaling during tumor progression*. Cancer Sci. 2015. doi:10.1111/cas.12630.

Sandler H & Stoecklin G. *Control of mRNA decay by phosphorylation of tristetraprolin*. Biochem Soc Trans (2008), Jun; 36(Pt 3):491-6. doi: 10.1042/BST0360491.

Sarrió D, Socorro MP, Hardisson D, Cano S, Moreno-Bueno G, and Palacios J. *Epithelial-Mesenchymal Transition in Breast Cancer Relates to the Basal-like Phenotype*. Cancer Res February (2008) 15 (68) (4) 989-997; doi: 10.1158/0008-5472.CAN-07-2017

Savagner P, Vallés AM, Jouanneau J, Yamada KM, and Thiery JP. *Alternative splicing in fibroblast growth factor receptor 2 is associated with induced epithelial-mesenchymal transition in rat bladder carcinoma cells*. Mol. Biol. Cell. 5, 851-862 (1994).

Scanlon CS, Van Tubergen EA, Inglehart RC, and D'Silva NJ. *Biomarkers of Epithelial-Mesenchymal Transition in Squamous Cell Carcinoma*. Journal of Dental Research, 92(2), 114–121 (2013). http://doi.org/10.1177/0022034512467352.

Schmidlin M, Lu M, Leuenberger SA, Stoecklin G, Mallaun M, Gross B, Gherzi R, Hess D, Hemmings BA, and Moroni C. *The ARE-dependent mRNA-destabilizing activity of BRF1 is regulated by protein kinase B*. EMBO J. 2004 Dec.

Schoenberg DR & Maquat LE. *Regulation of cytoplasmic mRNA decay*. Nature Reviews. Genetics, 13(4), 246–259 (2012). http://doi.org/10.1038/nrg3160.

Senfter D, Madlener S, Krupitza G, et al. *The microRNA-200 family: still much to discover*. Biomolecular Concepts (2016), 7(5-6), pp. 311-319. Retrieved 17 Jul. 2017, from doi:10.1515/bmc-2016-0020

Serrano-Gomez SJ, Maziveyi M, and Alahari SK. *Regulation of epithelial–mesenchymal transition through epigenetic and posttranslational modifications*. Mol Cancer. 2016. doi:10.1186/s12943-016-0502-x.

Serrano-Gomez SJ, Maziveyi M, and Alahari SK. *Regulation of epithelial-mesenchymal transition through epigenetic and post-translational modifications*. Molecular Cancer, 15, 18 (2016). http://doi.org/10.1186/s12943-016-0502-x.

Shannon P, Markiel A, Ozier O, Baliga NS, Wang JT, Ramage D, Amin N, Schwikowski B, and Ideker T. *Cytoscape: a software environment for integrated models of biomolecular interaction networks*. Genome Res. 2003 Nov;13(11):2498-504.

Shapiro IM, Cheng AW, Flytzanis NC, et al. *An EMT–Driven Alternative Splicing Program Occurs in Human Breast Cancer and Modulates Cellular Phenotype*. PLoS Genetics. 2011; 7(8):e1002218. doi:10.1371/journal.pgen.1002218.

She QB, Bode AM, Ma WY, Chen NY, and Dong Z. *Resveratrol-induced activation of p53 and apoptosis is mediated by extracellular-signal-regulated protein kinases and p38 kinase*. Cancer Res. 2001, 61, 1604–1610.

Shi Y & Massagué J. *Mechanisms of TGF-beta signaling from cell membrane to the nucleus*. Cell 113, 685-700 (2003).

T

Tam WL & Weinberg RA. *The epigenetics of epithelial-mesenchymal plasticity in cancer*. Nature medicine (2013); 19(11):1438-1449. doi:10.1038/nm.3336.

Tan S, Li R, Ding K, Lobie PE, and Zhu T. *mi*R-*198 inhibitsmigration and invasion of hepatocellular carcinoma cells by targeting the HGF/c-MET pathway*. FEBS Lett. 585, 2229–2234 (2011).

Thiery JP. *Epithelial–mesenchymal transitions in development and pathologies*. Curr. Opin. Cell Biol. 15, 740–746 (2003).

Trabucchi M, Briata P, García-Mayoral M, Haase AD, Filipowicz W, Ramos A, Gherzi R, and Rosenfeld MG. *The RNA-binding protein KHSRP promotes the biogenesis of a subset of microRNAs*. Nature 2009; 459, 1010-14.

Trimboli AJ, Fukino K, De Bruin A, Wei G, Shen L, Tanner SM, Creasap N, Rosol TJ, Robinson ML, Eng C, Ostrowski MC, and Leone G. *Direct evidence for epithelial–mesenchymal transitions in breast cancer*. Cancer Res. (2008); 68, 937-945.

Tripathi V, Sixt KM, Gao S, Xu X, Huang J, Weigert R, Zhou M, and Zhang YE. *Direct Regulation of Alternative Splicing by SMAD3 through PCBP1 Is Essential to the Tumor-Promoting Role of TGF-β*. Molecular Cell (2016) Volume 64, Issue 3, 549 – 564.

Tupy JL, Bailey AM, Dailey G, et al. *Identification of putative noncoding polyadenylated transcripts in Drosophila melanogaster*. PNAS (2005); 102(15):5495-5500. doi:10.1073/pnas.05014 22102.

U

Ulitsky I & Bartel DP. *lincRNAs: genomics, evolution, and mechanisms*. Cell 154, 26–46 (2013).

Usha S, Johnson IM, and Malathi R. *Interaction of resveratrol and genistein with nucleic acids*. J Biochem Mol Biol. 2005 Mar 31;38(2):198-205.

V

Valverde R, Edwards L, and Regan L. *Structure and function of KH domains*. FEBS J. (2008); Jun; 275(11):2712-26. doi: 10.1111/j.1742-4658.2008.06411.x.

Visone R & Croce CM. *MiRNAs and cancer.* Am J Pathol. 2009 Apr; 174(4):1131-8. doi: 10.2353/ajpath.2009.080794.

Viswanathan SR & Daley GQ. *Lin28: A microRNA regulator with a macro role.* Cell (2010) 140: 445–449.

Vlasova-St. Louis I & Bohjanen PR. *Post-transcriptional regulation of cytokine and growth factor signaling in cancer.* Cytokine and Growth Factor Reviews (2017) , Volume 33 , 83 – 93.

Volinia S, Calin, GA, Liu CG, Ambs S, Cimmino A, Petrocca F, Visone R, Iorio M, Roldo C, Ferracin M et al. *A microRNA expression signature of human solid tumors defines cancer gene targets*. Proc. Natl. Acad. Sci. USA 2006, 103, 2257–2261.

W

Waldmeier L, Meyer-Schaller N, Diepenbruck M, and Christofori G. *Py2T murine breast cancer cells, a versatile model of TGF-β-induced EMT in vitro and in vivo.* PLoS One 7, e48651 (2012). doi: 10.1371/journal.pone.0048651.

Wang Y, Shi J, Chai K, Ying X, and Zhou BP. *The Role of Snail in EMT and Tumorigenesis*. Current Cancer Drug Targets, 13(9), 963–972 (2013).

Warzecha CC, Sato TK, Nabet B, Hogenesch JB, and Carstens RP. *ESRP1 and ESRP2 are epithelial cell-type-specific regulators of FGFR2 splicing.* Mol. Cell. 33, 591-601(2009).

Warzecha CC & Carstens RP. *Complex changes in alternative pre-mRNA splicing play a central role in the epithelial-to-mesenchymal transition (EMT).* Semin. Cancer Biol. 22, 417-427 (2012). doi: 10.1016/j.semcancer.2012.04.003.

Weiskirchen S & Weiskirchen R. *Resveratrol: How Much Wine Do You Have to Drink to Stay Healthy?* Advances in Nutrition (2016); 7(4):706-718. doi:10.3945/an.115.011627.

Wilson GM, Lu J, Sutphen K, Suarez Y, Sinha S, Brewer B, Villanueva-Feliciano EC, Ysla RM, Charles S, and Brewer G. *Phosphorylation of p40AUF1 regulates binding to A+U-rich mRNA-destabilizing elements and protein-induced changes in ribonucleoprotein structure.* J Biol Chem (2003), Aug 29;278(35):33039-48.

Winter J, Jung S, Keller S, Gregory RI, and Diederichs S. *Many roads to maturity: microRNA biogenesis pathways and their regulation.* Nature Cell Biology 11, 228 – 234 (2009) doi:10.1038/ncb0309-228.

X

Xi Q, Wang Z, Zaromytidou AI, Zhang XH, Chow-Tsang LF, Liu JX, Kim H, Barlas A, Manova-Todorova K, Kaartinen V, Studer L, Mark W, Patel DJ, and Massagué J. *A poised chromatin platform for TGF-β access to master regulators.* Cell 147, 1511–1524 (2011).

Xu J, Lamouille S, and Derynck R. *TGF-beta-induced epithelial to mesenchymal transition.* Cell Res. (2009); 19, 156-172.

Xu Y, Gao XD, Lee JH, Huang H, Tan H, Ahn J, Reinke LM, Peter ME, Feng Y, Gius D, Siziopikou KP, Peng J, Xiao X, and Cheng C. *Cell type-restricted activity of hnRNPM promotes breast cancer metastasis via regulating alternative splicing.* Genes Dev. 28, 1191-1203 (2014). doi: 10.1101/gad.241968.114.

Xu H, Xiong C, He L, Wu B, Peng L, Cheng Y, Jiang F, Tan L, Tang L, Tu Y, Yang Y, Liu C, Gao Y, Li G, Zhang C, Liu S, Xu C, Wu H, Li G, and Liang S. *Trans-resveratrol attenuates high fatty acid-induced P2X7 receptor expression and IL-6 release in PC12 cells: possible role of P38 MAPK pathway.* Inflammation (2015) Feb; 38(1):327-37. doi: 10.1007/s10753-014-0036-6.

Y

Yang J, Bennett BD, Luo S, Inoue K, Grimm SA, Schroth GP, Bushel PR, Kinyamu HK, and Archer TK. *LIN28A Modulates Splicing and Gene Expression Programs in Breast Cancer Cells.* Mol. Cell. Biol. 35, 3225-3243 (2015).

Ye X & Weinberg RA. *Epithelial-Mesenchymal Plasticity: A Central Regulator of Cancer Progression.* Trends Cell Biol. 25, 675-686 (2015).

Z

Zhang X, Devany E, Murphy MR, Glazman G, Persaud M, and Kleiman FE. *PARN deadenylase is involved in miRNA-dependent degradation of TP53 mRNA in mammalian cells.* Nucleic Acids Research. (2015); 43(22):10925-10938. doi:10.1093/nar/ gkv959.

Zhang Y, Yang P, and Wang XF. *Microenvironmental regulation of cancer metastasis by miRNAs*. Trends Cell Biol. 24, 153-160 (2014).

Zhang YY, Wu JW, and Wang ZX. *Mitogen-activated protein kinase (MAPK) phosphatase 3-mediated cross-talk between MAPKs ERK2 and p38alpha*. J Biol Chem (2011) May 6; 286(18): 16150-62. doi: 10.1074/jbc.M110.203786.

Zheng X, Carstens JL, Kim J, Scheible M, Kaye J, Sugimoto H, Wu CC, LeBleu VS, and Kalluri R. *Epithelial-to-mesenchymal transition is dispensable for metastasis but induces chemoresistance in pancreatic cancer*. Nature 527, 525-530 (2015).

Zhou BP, Deng J, Xia W, Xu J, Li YM, Gunduz M, et al. *Dual regulation of Snail by GSK-3beta-mediated phosphorylation in control of epithelial–mesenchymal transition*. Nat Cell Biol. 2004. doi:10.1038/ncb1173.

Zhou R, Gong AY, Eischeid AN, and Chen XM. *miR-27b targets KHSRP to coordinate TLR4-mediated epithelial defense against Cryptosporidium parvum infection*. PLoS Pathog. 8, e1002702 (2012).

Zinder JC & Lima CD. *Targeting RNA for processing or destruction by the eukaryotic RNA exosome and its cofactors*. Genes & Development. 2017; 31(2):88-100. doi:10.1101/gad.294769.116.

Web sites

http://www.rcsb.org/pdb/protein/Q92945

http://imagej.nih.gov/ij/index.html

http://www.ncbi.nlm.nih.gov/bioproject/312753

http://www.ncbi.nlm.nih.gov/bioproject/312702

http://www.bioinformatics.bbsrc.ac.uk/projects/fastqc

http://hannonlab.cshl.edu/fastx_toolkit

http://broadinstitute.github.io/picard

https://github.com/broadinstitute/picard

http://www.ensembl.org